



5-2019

**DETERMINING GRID SECURITY THROUGH DYNAMIC STABILITY
ANALYSIS OF MAJOR CONTINGENCIES AND INCREASED
RENEWABLE PENETRATION**

Summer Francesca Fabus
University of Tennessee, sfabus@vols.utk.edu

Follow this and additional works at: https://trace.tennessee.edu/utk_gradthes

Recommended Citation

Fabus, Summer Francesca, "DETERMINING GRID SECURITY THROUGH DYNAMIC STABILITY ANALYSIS OF MAJOR CONTINGENCIES AND INCREASED RENEWABLE PENETRATION. " Master's Thesis, University of Tennessee, 2019.
https://trace.tennessee.edu/utk_gradthes/5411

This Thesis is brought to you for free and open access by the Graduate School at TRACE: Tennessee Research and Creative Exchange. It has been accepted for inclusion in Masters Theses by an authorized administrator of TRACE: Tennessee Research and Creative Exchange. For more information, please contact trace@utk.edu.

To the Graduate Council:

I am submitting herewith a thesis written by Summer Francesca Fabus entitled "DETERMINING GRID SECURITY THROUGH DYNAMIC STABILITY ANALYSIS OF MAJOR CONTINGENCIES AND INCREASED RENEWABLE PENETRATION." I have examined the final electronic copy of this thesis for form and content and recommend that it be accepted in partial fulfillment of the requirements for the degree of Master of Science, with a major in Electrical Engineering.

Yilu Liu, Major Professor

We have read this thesis and recommend its acceptance:

Leon Tolbert, Hector Pulgar

Accepted for the Council:

Dixie L. Thompson

Vice Provost and Dean of the Graduate School

(Original signatures are on file with official student records.)

**DETERMINING GRID SECURITY THROUGH
DYNAMIC STABILITY ANALYSIS OF MAJOR
CONTINGENCIES AND INCREASED RENEWABLE
PENETRATION**

A Thesis Presented for the
Master of Science
Degree
The University of Tennessee, Knoxville

Summer Francesca Fabus
May 2019

Copyright © 2019 by Summer Fabus.
All rights reserved.

ACKNOWLEDGEMENTS

I would like to thank my research advisor, Dr. Yilu Liu, for encouraging me to be a part of her group and helping to fund my graduate education. Through her leadership, I have strengthened my education in the field of power systems. Her dedication to research inspires me to continuously innovate and to solve new problems. I would also like to thank Dr. Shutang You and others I have worked with on Dr. Liu's team. As my mentor, Dr. You was always patient, knowledgeable, and helpful in any project we worked on together. I am highly appreciative of the opportunities the University of Tennessee, Knoxville has given me. Specifically, I want to acknowledge the Bodenheimer Fellowship committee for believing in me and providing funding towards my MS degree. Additionally, I am thankful for the Center for Resilient Electric Energy Transmission Networks (CURENT) research center for providing me with research, outreach, and industry opportunities that motivated me to pursue a graduate degree and career in the power industry. Lastly, I would like to thank my husband and parents for their continuous love and support throughout my education.

ABSTRACT

The challenge of ensuring grid security becomes more complex with the advancement of new technology and major events causing widespread damage in the system. Threats of cyber-attacks create permutations of possible contingencies that may have never been considered in typical operations and planning. Natural disasters have caused devastating effects, taking out entire power systems and leaving thousands of customers without service for extended periods. The integration of more renewables into the grid creates dynamic stability concerns due to the replacement of large, rotating machines. In these examples, security can be assessed by studying dynamic stability, while also considering the consequences of each contingency or modification in the system.

Security has been analyzed in three separate projects using various systems. The first project is Multi-Timescale Integrated Dynamics and Scheduling for Solar (MIDAS). In this project, a machine learning tool was used to determine security criteria for frequency, transient, and small-signal stability of a power system integrated with renewables. Security assessment is a fundamental function for both short-term and long-term power system operation. The developed data-driven security assessment (DSA) criteria uses machine learning to determine when it is necessary to trigger dynamic simulation by linking traditional isolated dynamic simulation with long-term scheduling. In the second project, a model of Puerto Rico's 2018 transmission system was created. Simulations of major contingencies were performed on the Puerto Rico system, including the trip of main transmission corridors along the path of destructive Hurricane Maria. In the future, higher renewable penetration in the Puerto Rico system is expected. Therefore, studies were run at high solar penetration levels to assess dynamic stability under these conditions. Lastly, a cybersecurity study of a large system was also performed. Several scenarios were analyzed to determine stability boundaries and effects of possible targeted attacks. The goal was to determine critical contingencies that would cause system collapse.

TABLE OF CONTENTS

1	Introduction and General Information	1
1.1	Dynamic Security Assessment (DSA) for Multi-Timescale Integrated Dynamics and Scheduling for Solar (MIDAS).....	1
1.2	Assessing Security During Natural Disasters and Increased Renewable Penetration in Puerto Rico	3
1.3	Assessing Security During Cyber-Attacks and Wide-Area Physical Attacks on Bulk Electric System Assets	5
2	Dynamic Security Assessment (DSA) for Multi-Timescale Integrated Dynamics and Scheduling for Solar (MIDAS)	6
2.1	Literature Review.....	6
2.2	Machine-Learning Based Stability Analysis to Determine DSA Criteria	13
2.2.1	Creation of Steady-State Cases: The 23-Bus System Example....	13
2.2.2	Creation of Steady-State Cases: The 18-Bus System.....	21
2.2.3	Data-Driven Frequency Stability Margin Prediction	21
2.2.4	Data-Driven Transient Stability Margin Prediction	26
2.2.5	Data-Driven Small-Signal Stability Margin Prediction	29
2.3	Summary	30
3	Assessing Security During Natural Disasters and Increased Renewable Penetration in Puerto Rico	35
3.1	Development of the 2018 Puerto Rico Power Transmission System Study Model	35
3.1.1	The Power Flow Model of the Puerto Rico Power Transmission System.....	35
3.1.2	The Power Flow Solution.....	38
3.1.3	Overview of the Dynamics of the Puerto Rico Power Transmission System.....	42
3.1.4	Dynamic Simulations Performed on the Developed 2018 PREPA Transmission Model.....	42
3.1.5	PPREPA Transmission System Mapping	64
3.2	Placement of Universal Grid Analyzer (UGA) Measurements for Dynamic Model Validation	64
3.3	Dynamic Simulations Performed on the 2022 PREPA-Developed Model	71
3.4	Summary	75
4	Assessing Security During Cyber-Attacks and Wide-Area Physical Attacks on Bulk Electric System Assets.....	80
4.1	Literature Review.....	80
4.2	Development of the Atlantis 9000 Model Mapping for the Purpose of Cyber-Security System Study	81
4.2.1	Introduction of Atlantis 9000 Model	81
4.2.2	Programmatic Conversion of PSS®E Cartesian Coordinates to GPS Coordinates.....	82

4.2.3	Mapping the System Using PSGT	82
4.3	Modeling Dynamic Effects of Possible Cyber-Attack Scenarios	85
4.3.1	Scenario #1: Tripping Largest Generation Facilities within a Given Zone.....	85
4.3.2	Scenario #2: Tripping Multiple High-Voltage Substations in a Given Zone.....	90
4.3.3	Scenario #3: Radial Area Attack Created by Tripping N-Levels from the Largest Generator in a Given Zone	94
4.3.4	Scenario #4: Radial Area Attack Tripping N-Levels from the Largest Load in a Given Zone	102
4.3.5	Adding Generator and Load Relays into the Model During Radial Area Simulations.....	106
4.3.6	Scenario #5: Tripping Buses in Multiple Areas Simultaneously ...	111
4.4	Summary	111
5	Conclusions and Recommendations for Future Work.....	116
5.1	Dynamic Security Assessment (DSA) for Multi-Timescale Integrated Dynamics and Scheduling for Solar (MIDAS) Future Work	116
5.2	Assessing Security During Natural Disasters and Increased Renewable Penetration in Puerto Rico Future Work.....	117
5.3	Assessing Security During Cyber-Attacks and Wide-Area Physical Attacks on Bulk Electric System Assets Future Work.....	117
	List of References	118
	Appendix.....	124
A.1	Python and MATLAB Scripts Used to Generate Test Cases in Machine Learning Project	125
A.1.1	Python Scripts for 23-Bus System.....	125
A.1.2	Python Scripts for 18-Bus System.....	129
A.2	Power Plant and Machine Modeling Consideration for PREPA Transmission Model	136
A.3	Development of High PV Models of PREPA System Using 2019 Day-Peak Model	136
A.4	How to Use the PGST Tool.....	143
	Vita.....	147

LIST OF TABLES

Table 2.1. Support vector machine (SVM) based method for transient stability assessment.....	7
Table 2.2. Neural network (NN) based methods for transient stability assessment	8
Table 2.3. Decision tree (DT) based methods for transient stability assessment	10
Table 2.4. Other methods for transient stability assessment	10
Table 2.5. Data-driven frequency stability assessment.....	12
Table 2.6. Data-driven small-signal stability assessment.....	12
Table 2.7. Overview of security assessment approaches for frequency, transient, and small-signal stability	14
Table 2.8. Participation factor of generators in Mode 1.....	31
Table 2.9. Participation factor of generators in Mode 2.....	32
Table 2.10. Participation factor of generators in Mode 3.....	33
Table 2.11. Damping ratio change of three selected modes compared to individual and total generator output.....	34
Table 3.1. PREPA transmission system study model overview	37
Table 3.2. Generator types and capacities	37
Table 3.3. Transmission line resistance, reactance, and susceptance per mile	39
Table 3.4. Load values for each bus derived from population distribution in Puerto Rico.....	39
Table 3.5. Generator dynamic models in the Puerto Rico power system model	45
Table 3.6. Branch overload and out-of-limit voltage report from corridor trip simulations.....	63
Table 3.7. Existing Puerto Rico UGA Locations.....	67
Table 3.8. Proposed Puerto Rico UGA Locations	67
Table 3.9. Typical parameters for GEPVG model	73
Table 3.10. Typical parameters for GEPVE model	74
Table 3.11. Parameters for DLSHBL load under-frequency protection model	77
Table 4.1. Summary of simulations results from tripping generator buses with output greater than 570 MW in Zone 6	87
Table 4.2. Summary of simulations results from tripping generator buses with output greater than 565 MW in Zone 6	88
Table 4.3. Frequency response of tripping 1 level from largest generator in Zone 20.....	98
Table 4.4. Frequency response of tripping 2 levels from largest generator in Zone 20.....	98
Table 4.5. Frequency response of tripping 3 levels from largest generator in Zone 20.....	99
Table 4.6. Frequency response of tripping 4 levels from largest generator in Zone 20.....	99

Table 4.7. Frequency response of tripping 5 levels from largest generator in Zone 20.....	100
Table 4.8. Frequency response of tripping 1 level from largest load in Zone 14	104
Table 4.9. Frequency response of tripping 2 levels from largest load in Zone 14	104
Table 4.10. LDSHAL relay model parameter settings	107
Table 4.11. FRGDCAT relay model parameter settings.....	108
Table 4.12. Frequency response of tripping 1 level from largest generator in Zones 5 and 21	112
Table 4.13. Frequency response of tripping 2 levels from largest generator in Zones 5 and 21	113
Table 4.14. Frequency response of tripping 3 levels from largest generator in Zones 5 and 21	113
Table A.1. Online non-renewable machines	139

LIST OF FIGURES

Figure 1.1. Pyramid showing relationship of definitions between stability, security, and reliability definitions from [1].....	2
Figure 1.2. Diagram of the quasi-dynamic multiple timescales power system simulation framework [2].....	4
Figure 1.3. Major generation and transmission assets of PREPA system [5]	4
Figure 2.1. Accuracy comparison of machine learning methods.....	12
Figure 2.2. Diagram of 23-bus system	15
Figure 2.3. Map of selected balancing authorities and corresponding areas of 23-bus system [36].....	17
Figure 2.4. Total load curve for PACW	18
Figure 2.5. Total load curve for Area 1 of 23-bus system	18
Figure 2.6. Total load curve for AESO	19
Figure 2.7. Total load curve for Area 2 of the 23-bus system	19
Figure 2.8. Total load curve for TEP	20
Figure 2.9. Total load curve for Area 5 of the 23-bus system	20
Figure 2.10. Diagram of the 18-bus system provided by NREL	22
Figure 2.11. Total system generation curve for 18-bus system over 24-hour period.....	24
Figure 2.12. Inertia level of machines as a percent of the base inertia over 24-hour period.....	24
Figure 2.13. Minimum frequency nadir of all machines (with forced inertia change) over 24-hour period.....	25
Figure 2.14. Estimation error of frequency nadir of generators.....	25
Figure 2.15. Correlation between critical clearing time and total power generation over 24 hours.....	27
Figure 2.16. Modelled and estimated critical clearing time in testing dataset	27
Figure 2.17. Critical clearing time estimation error distribution	28
Figure 2.18. Mode 1 modeled vs. estimated damping ratio over 24-hour period	31
Figure 2.19. Mode 1 damping ratio estimation error distribution	31
Figure 2.20. Mode 2 modeled vs. estimated damping ratio over 24-hour period	32
Figure 2.21. Mode 2 damping ratio estimation error distribution	32
Figure 2.22. Mode 3 modeled vs. estimated damping ratio over 24-hour period	33
Figure 2.23. Mode 3 damping ratio estimation error distribution	33
Figure 3.1. PREPA's 2018 transmission system [38].....	36
Figure 3.2. Power flow solution of the Puerto Rico system using Newton-Raphson method	41
Figure 3.3. Contour map of real power at each bus in the PREPA system.....	43
Figure 3.4. Contour map of reactive power at each bus in the PREPA system ..	43
Figure 3.5. Contour map of line MW flow in the PREPA system.....	44
Figure 3.6. Contour map of line MVar flow in the PREPA system	44
Figure 3.7. Frequency response in no-contingency simulation	45

Figure 3.8. Map of Puerto Rico indicating Guayanilla [43]	46
Figure 3.9. Frequency response after tripping the Costa Sur Steam Plant (681 MW)	46
Figure 3.10. Map of Puerto Rico indicating Caguas [43].....	48
Figure 3.11. Frequency response after 198MW load shedding in Caguas	48
Figure 3.12. Map of Puerto Rico indicating the Hato Rey substation [43]	49
Figure 3.13. Frequency response after a fault on the 115kV bus at the Hato Rey substation (Bus 21).....	49
Figure 3.14. System voltage after a fault on the 115kV bus at the Hato Rey substation (Bus 21).....	50
Figure 3.15. Map of Puerto Rico indicating approximate 230kV transmission path from Guayanilla to Manatí [43].....	50
Figure 3.16. Frequency response after a three-phase short-circuit fault on the Guayanilla- Manatí 230kV transmission line	51
Figure 3.17. System voltage after a three-phase short-circuit fault on the Guayanilla-Manati 230kV transmission line	51
Figure 3.18. Map of Puerto Rico indicating the Santa Isabel substation [43]	52
Figure 3.19. Frequency response after tripping Santa Isabel substation	52
Figure 3.20. Transmission map indicating Cluster 1 with annotations added to map from [38].....	53
Figure 3.21. Frequency response after tripping Cluster 1	54
Figure 3.22. Transmission map indicating Cluster 2 with annotations added to map from [38].....	55
Figure 3.23. Frequency response after tripping Cluster 2	56
Figure 3.24. Transmission map indicating Cluster 3 with annotations added to map from [38].....	57
Figure 3.25. Frequency response after tripping Cluster 3	58
Figure 3.26. Transmission map indicating Cluster 4 with annotations added to map from [38].....	59
Figure 3.27. Frequency response after tripping Cluster 4	60
Figure 3.28. Frequency response after tripping Cluster 1 and Cluster 4.....	60
Figure 3.29. Frequency response after tripping Cluster 1 and Cluster 2.....	61
Figure 3.30. Frequency response after tripping Cluster 2 and Cluster 3.....	61
Figure 3.31. Frequency response after tripping Cluster 3 and Cluster 4.....	62
Figure 3.32. PREPA transmission system generated in ArcMap (red - 115kV; blue - 230kV)	65
Figure 3.33. Map of existing and proposed UGA locations in Puerto Rico with annotations added to map from [38]	68
Figure 3.34. Frequency measured by UGAs during generation trip event followed by power swings detected on 08/02/2018 at 04:51:02 UTC	69
Figure 3.35. Frequency measured by UGAs during fast frequency ramp up or possible load drop detected on 09/03/2018 at 12:17:20 UTC	69
Figure 3.36. Frequency measured by UGAs during local oscillation detected on 08/02/2018 at 19:00:42 UTC.....	70

Figure 3.37. Worst-case corridor trip combination for 2022 PREPA-developed model with annotations added to map from [38]	72
Figure 3.38. Frequency response of tripping worst-case corridor trip combination for 2022 PREPA-developed model	73
Figure 3.39. Frequency response of tripping 98.5 MW in 2022 PREPA-developed system with 29% renewable penetration	76
Figure 3.40. Frequency response of tripping 98.5 MW in 2022 PREPA-developed system with 52% renewable penetration	76
Figure 3.41. Frequency response of tripping 98.5 MW in 2022 PREPA-developed system with 72% renewable penetration	77
Figure 3.42. Frequency response of tripping 98.5 MW in 2022 PREPA-developed system with 29% renewable penetration and load and line relays	78
Figure 3.43. Frequency response of tripping 98.5 MW in 2022 PREPA-developed system with 52% renewable penetration and load and line relays	78
Figure 3.44. Frequency response of tripping 98.5 MW in 2022 PREPA-developed system with 72% renewable penetration and load and line relays	79
Figure 4.1. Atlantis 9000 system diagram showing buses and branches	83
Figure 4.2. Google Earth view of Atlantis 9000 system	84
Figure 4.3. Zone view in PSGT	86
Figure 4.4. Voltage level view in PSGT	86
Figure 4.5. Frequency response of tripping generators with output greater than 570 MW in Zone 6	87
Figure 4.6. System voltage while tripping generators with output greater than 570 MW in Zone 6	88
Figure 4.7. Frequency response of tripping generators with output greater than 565 MW in Zone 6	89
Figure 4.8. System voltage while tripping generators with output greater than 565 MW in Zone 6	89
Figure 4.9. Frequency response of tripping 20 400kV buses in Zone 1	91
Figure 4.10. System voltage while tripping 20 400kV buses in Zone 1	91
Figure 4.11. Frequency response of tripping 21 400kV buses in Zone 1	92
Figure 4.12. Frequency response of tripping 21 400kV buses in Zone 1 zoomed in view	92
Figure 4.13. System voltage while tripping 21 400kV buses in Zone 1	93
Figure 4.14. Frequency response while tripping the largest generator in Zone 20	95
Figure 4.15. Frequency response while tripping the largest generator in Zone 20 zoomed in view	95
Figure 4.16. Atlantis 9000 model generator bus 7979	96
Figure 4.17. Atlantis 9000 Stage 1 connections to bus 7979	96
Figure 4.18. Atlantis 9000 Stage 2 connections to bus 7979	97
Figure 4.19. System voltage while tripping 4 levels from largest generator in Zone 20	100

Figure 4.20. System voltage while tripping 5 levels from largest generator in Zone 20.....	101
Figure 4.21. Google Earth image of entire Atlantis 9000 system buses (yellow) and buses tripped in Stage 5 (red) from tripping largest generator in Zone 20	101
Figure 4.22. Frequency response while tripping the largest load in Zone 14	103
Figure 4.23. Frequency response while tripping the largest load in Zone 14 zoomed in view	103
Figure 4.24. System voltage while tripping 1 stage from largest load in Zone 14	105
Figure 4.25. System voltage while tripping 2 stages from largest load in Zone 14	105
Figure 4.26. Google Earth image of entire Atlantis 9000 system buses (yellow) and buses tripped in Stage 2 (red) from tripping largest load in Zone 14 ..	107
Figure 4.27. Frequency response of tripping 5 stages from largest generator in Zone 20 with relays.....	108
Figure 4.28. System voltage while tripping 5 stages from largest generator in Zone 20 with relays.....	109
Figure 4.29. Frequency response of tripping 2 stages from largest load in Zone 14 with relays.....	109
Figure 4.30. System voltage while tripping 2 stages from largest load in Zone 14 with relays.....	110
Figure 4.31. Tripping multiple areas.....	112
Figure 4.32. Google Earth image of entire Atlantis 9000 system buses (yellow) and buses tripped in Stage 2 (red) from tripping largest generators in Zones 5 and 21	114
Figure A.1. Frequency response of tripping 80 MW of generation in 15% renewable case.....	137
Figure A.2. Frequency response of tripping 80 MW of generation in 30% renewable case.....	139
Figure A.3. Frequency response of tripping 80 MW of generation in 50% renewable case.....	140
Figure A.4. Frequency response of tripping 80 MW of generation in 70% renewable case.....	140
Figure A.5. Frequency response of tripping 80 MW of generation in 80% renewable case.....	141
Figure A.6. Frequency response of tripping 80 MW of generation in 80% renewable case without relays included	141
Figure A.7. Frequency response of tripping 80 MW of generation in 90% renewable case.....	142
Figure A.8. Frequency response of tripping 80 MW of generation in 90% renewable case without relays included	142
Figure A.9. PSSE_Data_Interface software user interface	144

Figure A.10. PSSE_Data_Interface software user interface with PSS®E raw file import buttons highlighted.....	144
Figure A.11. Example of PSS®E model bus data imported into PSGT software	145
Figure A.12. Example of PSS®E model bus and branch data imported into PSGT software	145
Figure A.13. Example of PSS®E model imported into PSGT software with bus, branch, and GPS data	146

INTRODUCTION AND GENERAL INFORMATION

A task force set up jointly between International Council on Large Electric Systems (CIGRE) and Institute of Electrical and Electronics Engineers (IEEE) defines power system security as the degree of risk in the system's ability to survive imminent disturbances without interruption of customer service, which depends on the system operating condition as well as the contingent probability of disturbances [1]. This task force defines stability of a power system as the continuance of intact operation following a disturbance [1]. Security is distinguished from stability in terms of contingency effects, in that two systems can have identical stability margins but vary in security due to instability consequences [1]. In order for a system to be reliable, it must be secure most of the time. The pyramid in Figure 1.1 illustrates how a system must be stable to be secure and secure to be reliable.

Stability analysis is an essential part of dynamic security assessment. Along with determining whether or not a system will be stable after a given disturbance, the probability and consequences of instability should be considered, which incorporates security assessment. This thesis covers research performed on three projects that involve dynamic security assessments through stability analysis using various approaches.

Dynamic Security Assessment (DSA) for Multi-Timescale Integrated Dynamics and Scheduling for Solar (MIDAS)

Multi-Timescale Integrated Dynamics and Scheduling for Solar (MIDAS) is part of the Department of Energy (DOE) Solar Energy Technologies Office (SETO) program, which focuses on addressing the affordability, flexibility, and performance of solar technologies on the grid. Members of the MIDAS team are from NREL (National Renewable Energy Laboratory), Electric Power Research Institute (EPRI), Southern Methodist University (SMU), California Independent Service Organization (CAISO), Electric Reliability Council of Texas (ERCOT), and the University of Tennessee, Knoxville (UTK).

The goal of MIDAS is to simulate the interaction between market scheduling and dynamic responses. This is done by developing temporally comprehensive, closed-loop simulation models that seamlessly simulate solar photovoltaic (PV) variability and its impact on power systems operations from economic scheduling timescales (day-ahead to hours) to dynamic response analysis (seconds to sub-seconds). A quasi-dynamic method integrates short-term dynamics, mid-term scheduling, and long-term unit commitment into a single simulation framework to realize the multi-timescale simulation.

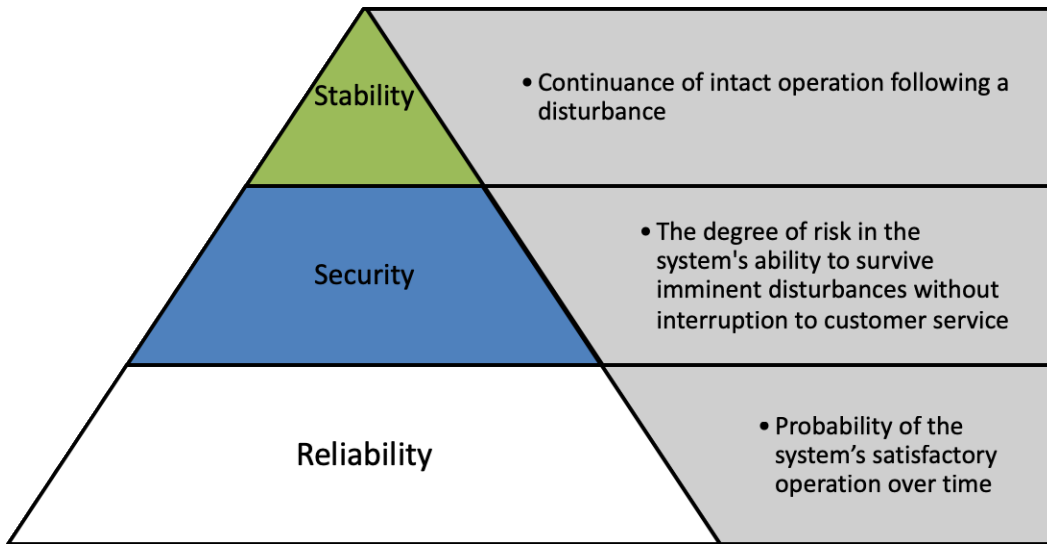


Figure 1.1. Pyramid showing relationship of definitions between stability, security, and reliability definitions from [1]

To assist the quasi-dynamic simulation framework, data-driven security assessment (DSA) criteria was used to significantly reduce the computational burden. The DSA criteria provides a key indicator to switch the simulation method by determining when it is necessary to trigger dynamic simulation. The DSA uses machine learning to decide when and to what extent to activate the dynamic model during simulation, using dispatch scheduling data as input. The stability margins associated with the dynamic security assessment include small-signal stability, frequency stability, and transient stability. As part of the DSA team, UTK was tasked with determining the data-driven-based security assessment criteria using model integration.

The concept of this framework presented in Figure 1.2. As presented in this diagram, a trigger, or the data-driven-based security assessment, integrates power scheduling data with power system dynamics. When incorporating solar into the system generation, PV and inverter models become a part of power system dynamics, and solar scheduling is included in the system scheduling model.

Assessing Security During Natural Disasters and Increased Renewable Penetration in Puerto Rico

In fall 2017, Hurricane Maria became the largest blackout in U.S. history, by customer-hours of lost electricity service [3]. Electricity was cut off to 100% of the island, with many households going at least 84 days without power [4]. A year after the storm, all customers were finally restored. Hurricane Maria also caused as much as \$94.4 billion in damages and a death toll of almost 3,000 people [4].

The path of Hurricane Maria, along with main transmission and generation assets of the Puerto Rico Electric Power Authority (PREPA) system, is presented in Figure 1.3. According to 2019 census data, about 40% Puerto Rico's population lives in the metropolitan area of San Juan in the northeast corner of the territory [5]. The transmission lines carrying electricity from south to north, shown in Figure 1.3, are vulnerable since the majority of generation capacity is in the south. Although 847 transmission structures fell during the hurricane, the complete outage was a result of two main 230kV lines failing after a fire at a circuit breaker at the Aguirre plant [5]. Several plants and distribution lines were also destroyed due to flooding and strong winds.

After the hurricane, DOE wanted to further analyze Puerto Rico's grid. DOE's Office of Electricity asked the national laboratories to perform near-term modeling activities for Puerto Rico. The request was part of the federal effort to support the rebuilding of a more resilient and secure electric power grid system after devastation caused by Hurricane Maria.

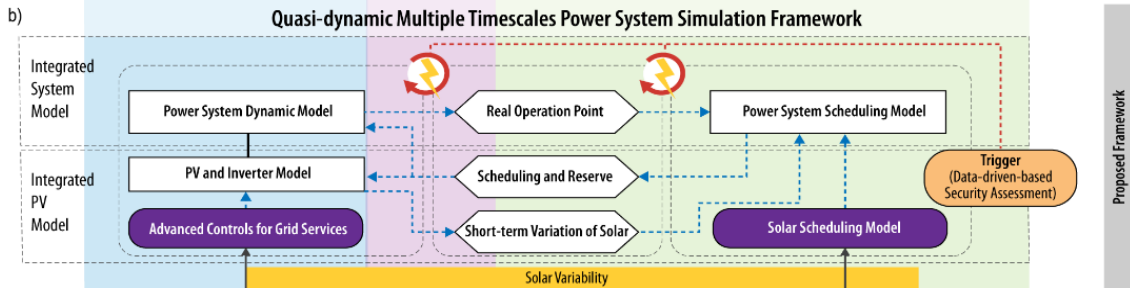


Figure 1.2. Diagram of the quasi-dynamic multiple timescales power system simulation framework [2]

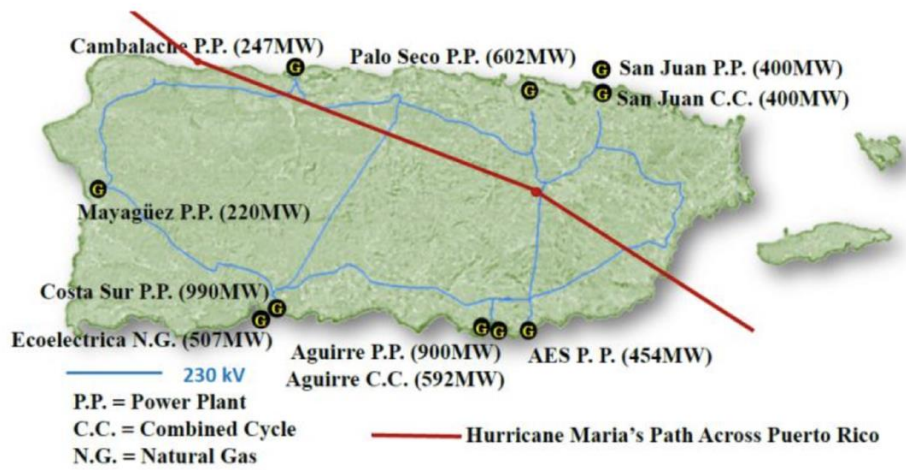


Figure 1.3. Major generation and transmission assets of PREPA system [5]

Recommendations to DOE included protection and prevention against future natural disasters and weather-related events, along with understanding the effects of increased renewable penetration throughout the system. Recommendations were developed by creating and analyzing transmission system models of the PREPA grid. Additionally, sensors were requested to be placed throughout the Puerto Rico system to provide enhanced situational awareness and refine developed transmission models by comparing actual measurements to modeled power flow and dynamic response.

Assessing Security During Cyber-Attacks and Wide-Area Physical Attacks on Bulk Electric System Assets

The motivation for the cyber-security project was to simulate and evaluate dynamic effects of a strategic wide-area cyber-attack, electromagnetic pulse (EMP), or geomagnetic disturbance (GMD) in the U.S power grid and other large systems. To do this, load flow and dynamic simulations were conducted to investigate impacts of hackers shutting down multiple substations or generation facilities within an electric utility.

Critical substations, connecting large generation plants and loads to the system, were determined as origins of the attacks. For the initial security assessment, dynamic frequency stability and voltage stability were analyzed following a major attack. Though the probability of the studied scenarios occurring is small, their effects were devastating, taking out an entire large system. The purpose of this project was to submit cyber-attack simulation results for a proposal to DOE. This proposal would then request additional funding in this cybersecurity research effort.

DYNAMIC SECURITY ASSESSMENT (DSA) FOR MULTI-TIMESCALE INTEGRATED DYNAMICS AND SCHEDULING FOR SOLAR (MIDAS)

This chapter discusses the creation of cases to train and test a UTK-developed machine learning tool. Dynamic stability margin was determined using results of generated test cases, and the machine learning tool was trained to recognize dynamic frequency, transient, and small-signal instability using power flow data as input.

Literature Review

The determination of the security assessment margin can be performed using model-based methods (e.g. full simulations) or data-driven methods. Full simulations rely on dynamic models and simulations to assess stability. In contrast, data-driven methods use datasets to train machine learning models to classify stable and unstable cases. The following review of existing methods for data-driven security assessment was part of a collaborative literature review with Dr. Shutang You and Dr. Yi Cui on the UTK team:

Existing methods for data-driven security assessment primarily focus on transient stability. Transient stability is concerned with the ability of the power system to maintain synchronism when subjected to a severe disturbance, such as a short circuit on a transmission line [1]. The existing literature that applies machine learning to determine transient stability mainly uses three categories of methods: support vector machine (SVM), neural network (NN), and decision tree (DT). Most of these studies used the New England 10-machine system as the test system. These methods have reached high accuracy in classifying stable and unstable cases.

Table 2.1 to Table 2.4 summarize the machine learning model, along with the power system model used in previous studies. The number of total samples, or waveforms, analyzed by the model are listed. A portion of these samples were used for training and the others for testing. The number of features refers to the number of parameters serving as input to the machine learning tool, such as individual voltage, angle, or frequency measurements. The percent accuracy identifies how results computed during testing compare with actual solutions.

Table 2.1. Support vector machine (SVM) based method for transient stability assessment

Ref	Model	Test System	Samples	Training	Testing	# Features	Accuracy (%)
[6]	SVM + transient energy function (TEF)	New England 10-machine	700	500	200	36, 18	97.5 – 100
[7]	Ball vector machine (BVM)	New England 10-machine	5500	4000	1500	200	97.1
[8]	SVM	Priiba system : 2484 buses	1242	994	248	224, 150, 100, 50	94.4
[8]	SVM + DT + rotor angles trajectory clustering	New England 10-machine and IEEE 145-bus	3672	1099	2573	19	90.74 – 98.15 94.75 – 95.41
[9]	SVM, Naïve Bayes, decision tree	IEEE 14-bus	8000	N/A	N/A	23	88.2 – 98.8
[10]	SVM + Cost-sensitive ensemble learning classifier	New England 10-machine	4290	4000	290	23	96.4 – 99.4
[12]	Least Square Support Vector Machine (LS-SVM)	New England 10-machine	6600	4620	1980	39	100
[13]	Reformed support vector machines + sequential minimal optimization (SMO)	New England 10-machine	20000	16000	4000	15	96.9
[14]	Fuzzy C-means clustering algorithm + SVM	IEEE 39-bus system	726	556	170	10	100

Table 2.2. Neural network (NN) based methods for transient stability assessment

Ref	Model	Test System	Samples	Training	Testing	# Features	Accuracy (%)
[15]	Extreme learning machines (ELM)	IEEE 50-bus system	6345	5076	1269	50	100
[16]	Extreme learning machine (ELM) + trajectory fitting (TF)	New England 10-machine	10000	N/A	N/A	100 (269)	99.1
[17]	Extreme learning machine (ELM) + a decision-making process	New England 10-machine	4000	2000	2000	N/A	97.92 – 98.38
[18]	An array of neural networks (NN) + an interpreter	PSB4 system + New England 10-machine	248/300	208/250	40/50	N/A	99.85/100
[19]	Probabilistic neural network (PNN)	IEEE 68-bus, 16-generator system + three wind generation units	190 operation conditions and three-phase faults	N/A	N/A	244, 150, 100, 50	> 99
[20]	Recurrent neural network (RNN) + long short-term memory network (LSTM)	New England 10-machine	5000	3750	1250	N/A	100
[21]	Long-short Term Memory (LSTM) ensemble neural network + decision machine	New England 10-machine	4058	3044	1014	N/A	100

Table 2.2. Continued

Ref	Model	Test System	Samples	Training	Testing	# Features	Accuracy (%)
[22]	Extreme learning machine(ELM) + Boosting learning	New England 10-machine	68640	N/A	N/A	50 (183)	100
[23]	Extreme learning machine(ELM)	New England 10-machine	1240	864	376	62	98
[24]	Convolutional neural network (CNN) + stacked auto-encoders (SAEs)	New England 10-machine	4014	2689	1325	22	96.78 – 98.68
[25]	Neural network (NN) + incremental learning	Shandong power system- 362 buses	945	540	405	N/A	96.6

Table 2.3. Decision tree (DT) based methods for transient stability assessment

Ref	Model	Test System	Samples	Training	Testing	# Features	Accuracy (%)
[26]	Decision tree (DT) + regression tree (RT)	Salt River Project (SRP) power system	41412	33130	8282	N/A	99.13
[27]	Weighted random forest (WRF)	New England 10-machine	2000	1300	700	263	98.79
[28]	Random forest (RF)	New England 10-machine	2000	1300	700	45	99.1
[29]	Decision tree (DT)	9-bus dynamic network and 1696-bus Iran national grid	513/1080	N/A	N/A	5	79.92 – 100 94.91 – 99.91

Table 2.4. Other methods for transient stability assessment

Ref	Model	Test System	Samples	Training	Testing	# Features	Accuracy (%)
[30]	Deep belief network (DBN)	A real regional power system in China, consisting of 1300 buses, 3215 transmission lines	10000	8330	1670	1762	98.02
[31]	Least Absolute Selection and Shrinkage Operator (LASSO)	A practical 470-bus system	1199	800	399	939	99.75
[32]	Type-2 fuzzy neural network	New England 10-machine	2000	1500	500	56	97.51 – 98.31

Existing machine-learning methods for data-driven security assessment primarily focus on transient stability. Very few studies have investigated frequency and small-signal stability assessment using machine-learning approaches. The studies found for frequency and small-signal stability are included in Table 2.5 and Table 2.6.

According to the Institute of Electrical and Electronics Engineers (IEEE) and International Council on Large Electric Systems (CIGRE) definition, frequency stability refers to the ability of a power system to maintain steady frequency following a severe system upset resulting in a significant imbalance between generation and load [1]. Instability that may result occurs in the form of sustained frequency swings leading to tripping of generating units and/or loads [1]. Very few studies have investigated frequency stability assessment using a data-driven approach. In [29], an artificial neural network (ANN) was used to predict the frequency stability using power flow information. However, this study does not consider the headroom reserve of each generator, which can increase the error of the model.

Small-disturbance (or small-signal) rotor angle stability is concerned with the ability of the power system to maintain synchronism under small disturbances. The disturbances are considered to be sufficiently small. Linearization of a system of equations is permissible for the purpose of analysis [1]. Reference [34] studied the small-signal stability of a single machine infinite bus system under different power and power factor conditions, as well as power system stabilizer settings. Reference [35] used a decision tree to predict the eigenvalue region of critical modes.

Comparing the accuracy of common machine learning methods, neural network models tend to have the highest accuracy, followed by decision tree models and support vector machine models, as shown in Figure 2.1. Although not used as frequently, the random forest method also has high accuracy. Therefore, the neural network and random forest models were selected for the machine-learning tool. Only the random forest model has been implemented in the tool, but the neural network model will later be integrated as well.

Though previous studies have used machine learning to predict stability, there are a few characteristics that make this model novel. Previous studies used specific power flow solution parameters as input to a machine learning tool, such as voltage and angle at particular buses, power flow of individual branches, along with individual machine and load data. Since the developed quasi-dynamic model is supposed to integrate long-term scheduling with short-term dynamics, only scheduling data, or generator dispatch, is used as an input into the tool. Additionally, other previously developed tools do not use models with high PV levels. The variability of PV makes long-term scheduling more complex.

Table 2.5. Data-driven frequency stability assessment

Ref	Model	Test System	Samples	Training	Testing	# Features	Accuracy (%)
[33]	Single-hidden layer feedforward network (SLFN)	IEEE 14-Bus System; New England 39-bus system	600	480	120	N/A	97.5%

Table 2.6. Data-driven small-signal stability assessment

Ref	Model	Test System	Samples	Training	Testing	# Features	Accuracy (%)
[34]	Artificial neural network	Single machine infinite bus system	N/A	N/A	N/A	4	~90%
[35]	Decision tree	PST 16-machine test system	2500	N/A	N/A	252	99.77%

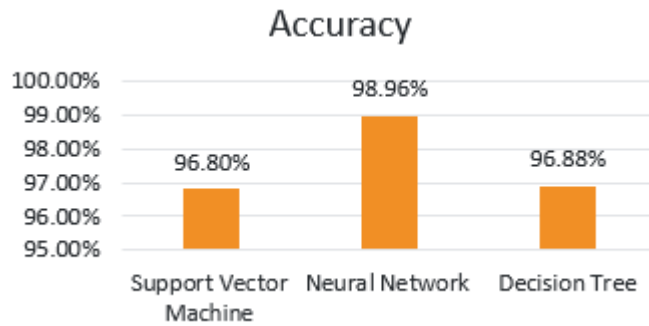


Figure 2.1. Accuracy comparison of machine learning methods

The machine learning tool created in the DSA project is designed to accurately assess the dynamic stability margin in cases with large amounts of solar generation. Lastly, each of the past studies mentioned only analyze a single stability issue, most often transient stability. This tool analyzes three stability issues: frequency, transient, and small-signal.

Machine-Learning Based Stability Analysis to Determine DSA Criteria

A machine learning tool, created by Dr. Yi Cui in MATLAB, was used to determine DSA criteria. The machine learning steps include database or data file extraction, training, classification, and testing. First, the tool extracts feature data from a database of real-time data points, directly from PSS®E dynamic simulation output files (.out) files, or from other power system simulation software files. Before the tool can classify whether or not a case is stable, it is trained by sets of stable and unstable cases. The tool then learns what criteria must be set based upon feature values from these cases.

Stability of a system was determined by assessing frequency stability, transient stability, and small-signal stability. For each stability problem, neural network based methods were to be used to develop the data-driven approach for security assessment. To train and test the machine learning tool, a number of steady-state cases were produced in PSS®E, each with varying generation dispatch. After steady-state cases were created, dynamic simulations were performed on each steady-state case and corresponding dynamic file, with the contingency and monitored parameters dependent upon the stability problem assessed. From dynamic simulation results, criteria for the security assessment was derived. Criteria was verified by inputting only generation dispatch results into the machine learning tool. The tool then determined whether or not the stability margin was met. These results were confirmed using other cases of simulated results. The data-driven assessment approaches developed for each stability type are summarized in Table 2.7.

2.1.1 Creation of Steady-State Cases: The 23-Bus System Example

The first set of steady-state cases were generated using a 23-bus system. The 23-bus system was provided as an example case with the installation of PSS®E 33. A diagram of the system is shown in Figure 2.2 was generated from the savnw.sld file provided by PSS®E. There are three main areas of the system, with Area 1 in the middle and Areas 2 and 5 on each side of Area 1. The total generation capacity of the system is 4,153.25 MW.

Table 2.7. Overview of security assessment approaches for frequency, transient, and small-signal stability

Stability Type	Machine Learning Training		Machine Learning Testing		Assessment Approach
	Contingency	Feature Monitored	Input	Output	
Frequency	Generation trip	System frequency	Generation dispatch results	Frequency nadir to determine frequency stability margin	<p>Generate a batch of cases with different dispatch and inertia levels.</p> <p>Evaluate frequency response using dynamic simulation.</p>
Transient	Three-phase fault on transmission line	Machine rotor angle	Generation dispatch results	Transient stability margin	<p>Generate a batch of cases with different dispatch and unit commitment.</p> <p>Evaluate transient stability using standard TPL-001-4 and dynamic simulation.</p>
Small-Signal	Linearization, small disturbance	Mode frequency and damping ratio computed by eigenvalue analysis	Generation dispatch results	Small-signal stability margin	<p>Generate a batch of cases with different dispatch and unit commitment.</p> <p>Evaluate small-signal stability using small-signal analysis and dynamic simulation.</p>

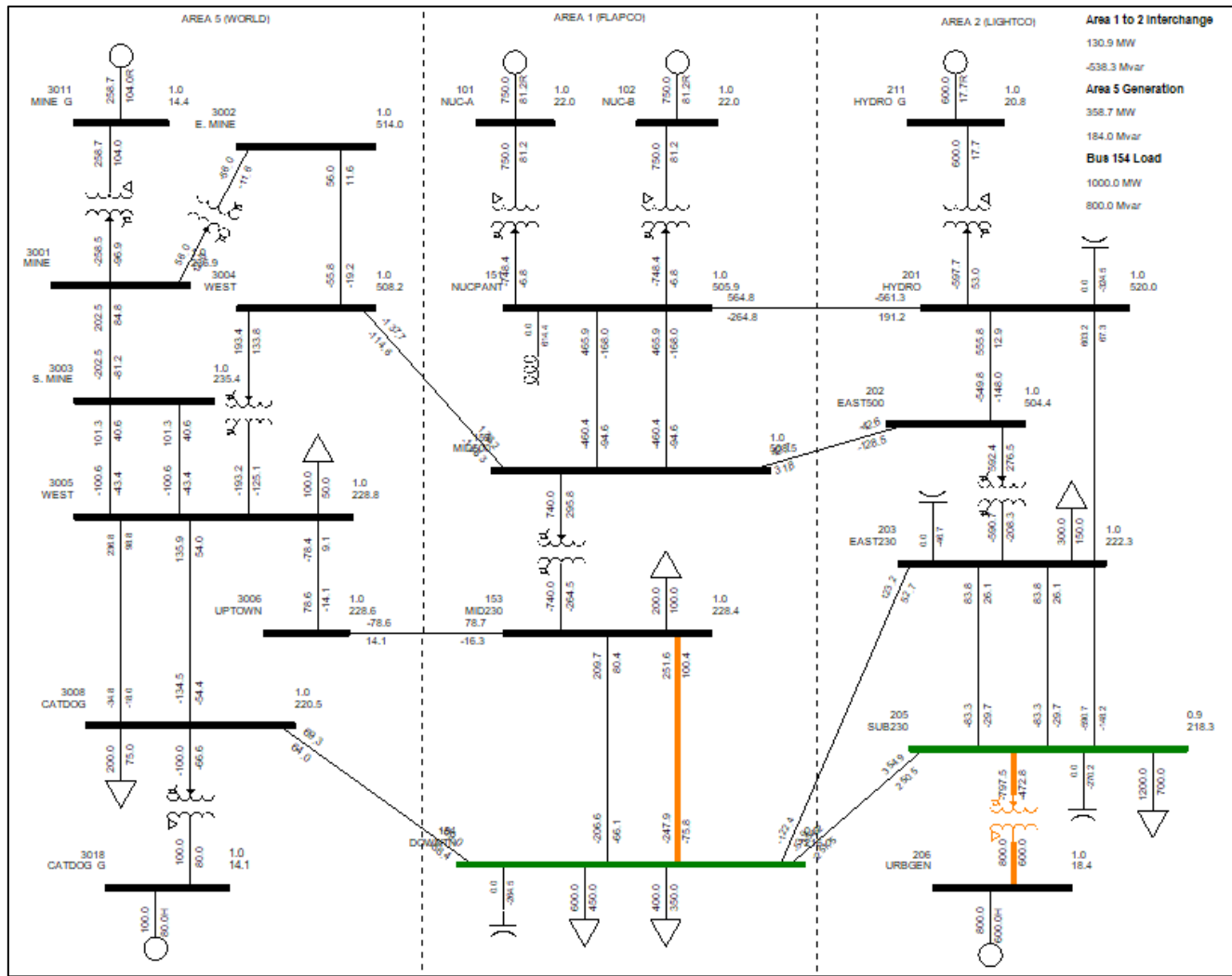


Figure 2.2. Diagram of 23-bus system

Each area of the system was assigned a different load curve, based on geographic diversity, as indicated in Figure 4.3. Load data was taken from three balancing authorities in the Western Interconnection, each at varying longitudes: Alberta Electric System Operator (AESO), PacifiCorp West (PACW), and Tucson Electric Power Authority (TEPC). Load data was predicted every hour over a period of 13 months, from 1/1/2020 0:00 to 1/31/2021 0:00. The 23-bus system load was adjusted by taking the total load of each area and scaling it by the percent deviation of the corresponding balancing authority's load data at each time. Comparisons of the 23-bus system areas' total loads and the balancing authorities' total loads over time are shown in Figure 2.4 to Figure 2.9.

An automated scheduling process was used to assign machine maintenance. Generator maintenance was scheduled during low-load periods. This process considered the system total load curve, machines currently offline or previously scheduled to be offline, along with each machine's capacity. Machine outages were scheduled in order from largest to smallest capacity. After each machine's maintenance was scheduled, an equivalent total system load curve was updated so the algorithm could account for previously scheduled service periods. Once a machine was taken out-of-service, the machine had an out-of-service duration of four weeks.

Transmission lines were also taken out of service depending on the probability of an outage occurring. Line outage probability was determined using the system's Reliability Outage Statistics Data file (.prb) in PSS®E. This file contains information, such as the branch reactance per mile, branch charging susceptance per mile, outage frequency for terminal caused single circuit outages, outage duration for terminal caused single circuit outages, outage frequency for single circuit outages per mile, and outage duration for single circuit outages. To calculate frequency and duration of each branch's outage over 13-month period, the following computations in (1) were implemented.

$$\begin{aligned}
 xm &= \text{branch reactance per mile} \\
 bm &= \text{branch charging susceptance per mile} \\
 ft &= \text{outage frequency for terminal caused single circuit outages} \\
 dt &= \text{outage duration for terminal caused single circuit outages} \\
 fmt &= \text{outage frequency for single circuit outages per mile} \\
 dmt &= \text{outage duration for single circuit outages}
 \end{aligned}
 \tag{1}$$

$$\begin{aligned}
 len &= \text{branch } x/xm \text{ (miles)} \\
 F &= len * fmt + ft \\
 D &= (fmt * dmt * len + ft * dt) / F \\
 \text{Failure Time} &= F * D / 9528 \\
 *9528 &= \text{total number of hours from 1/1/2020 to 1/31/2021}
 \end{aligned}$$

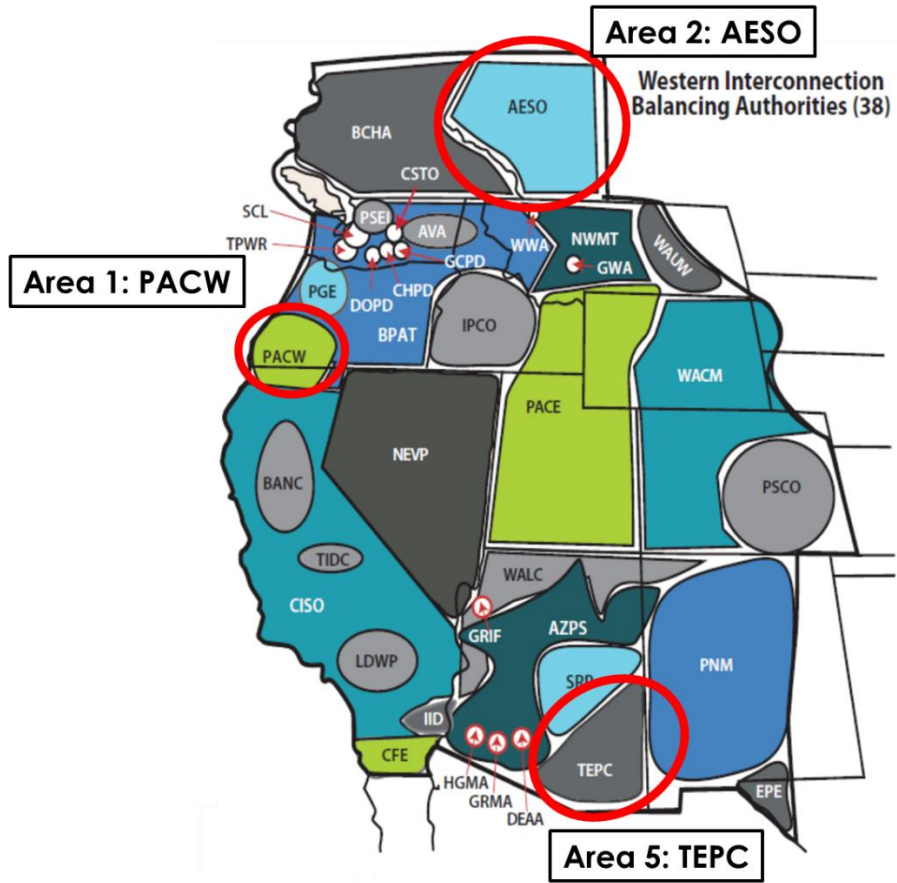


Figure 2.3. Map of selected balancing authorities and corresponding areas of 23-bus system [36]

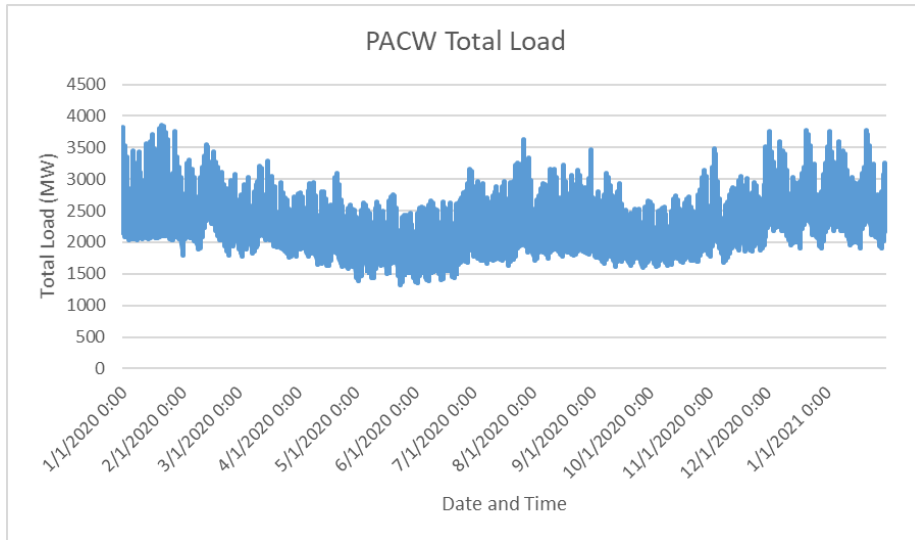


Figure 2.4. Total load curve for PACW

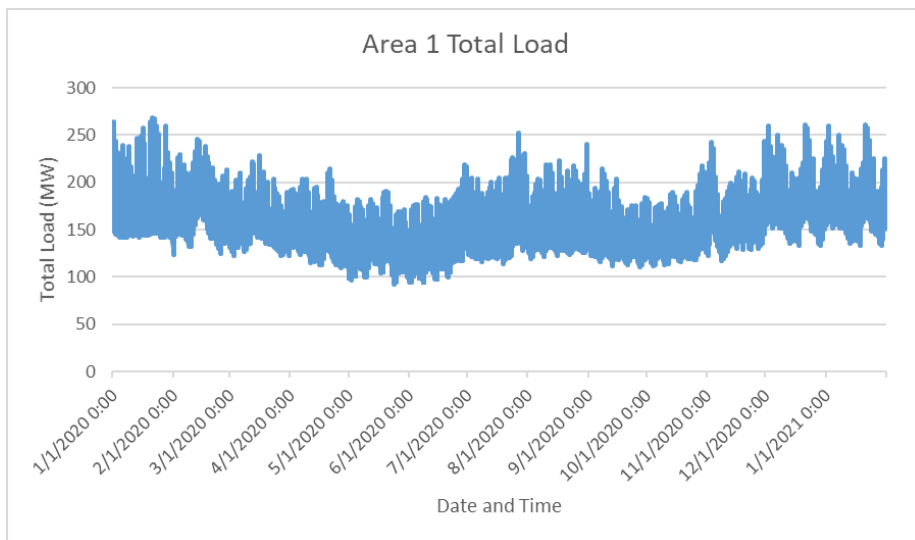


Figure 2.5. Total load curve for Area 1 of 23-bus system

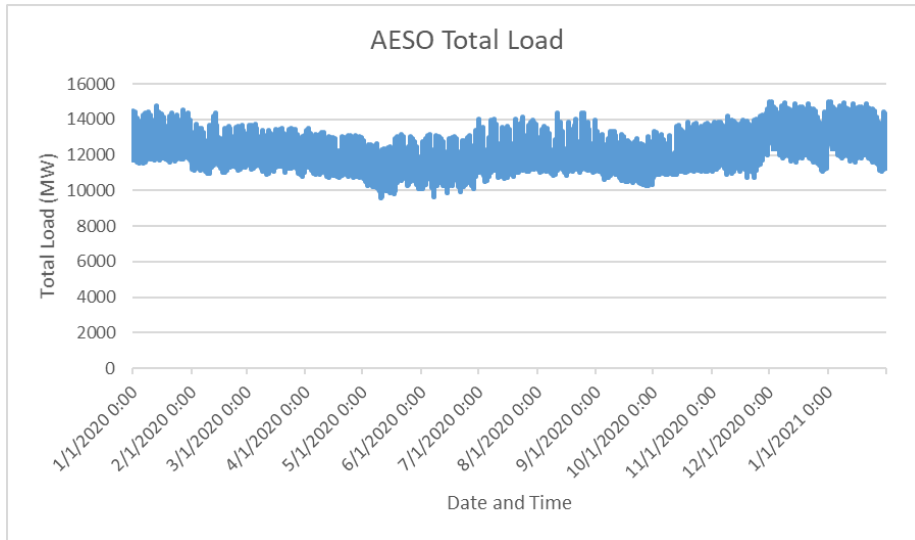


Figure 2.6. Total load curve for AESO

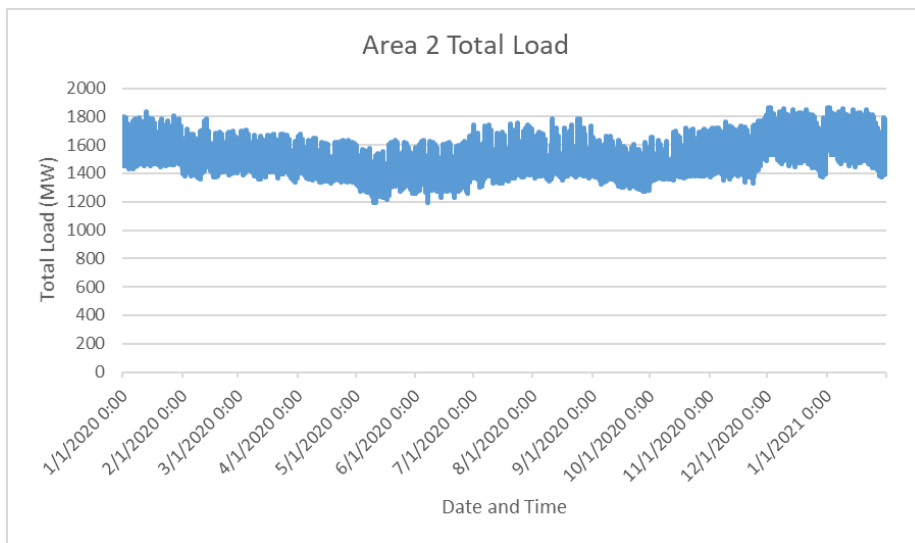


Figure 2.7. Total load curve for Area 2 of the 23-bus system

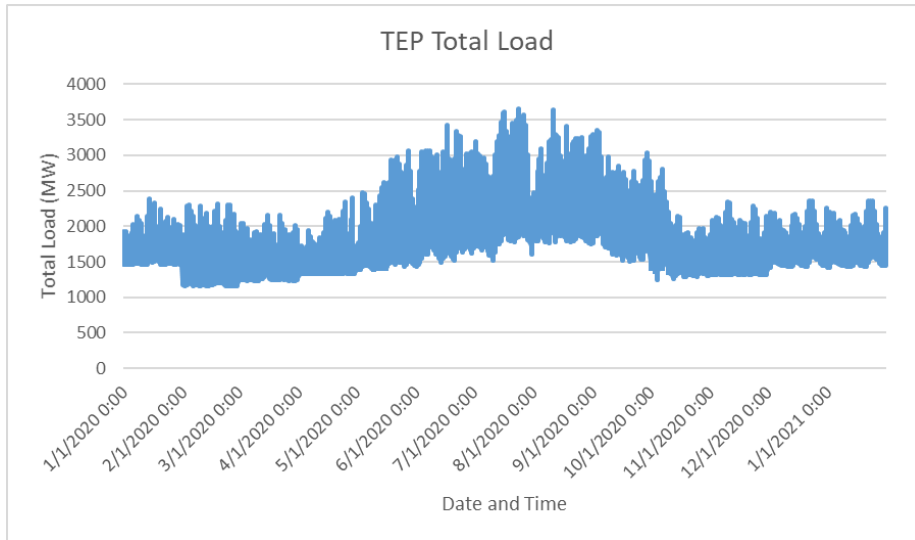


Figure 2.8. Total load curve for TEP

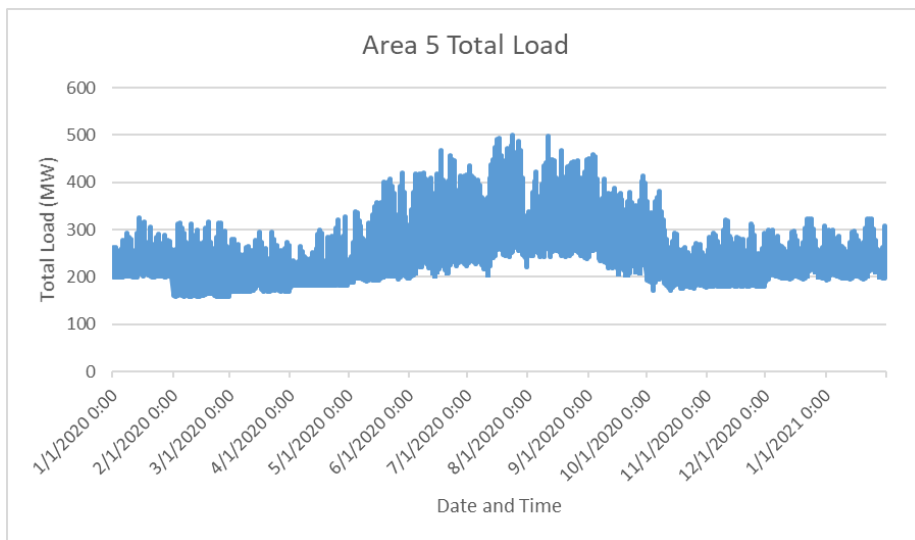


Figure 2.9. Total load curve for Area 5 of the 23-bus system

The results of a random number generator, with uniform distribution, determined whether or not a transmission line was out of service or not at each hour. Because transmission line outages were scheduled based on chance, the probability of a transmission line being out at a given hour was not dependent upon if the line had been previously scheduled to be out-of-service. Examples of events causing these types of outages include inclement weather, operator error, or other physical disturbances. An outage duration of 10 hours was set for each line out-of-service. The Python script used to generate saved cases for the 23-bus system is included in the Appendix in Section A.1.1.

2.1.2 Creation of Steady-State Cases: The 18-Bus System

The 18-bus system was provided by NREL and was originally converted from PSLF software to PSS®E. Similar to the 23-bus system, the 18-bus system has three areas. It was determined to use the 18-bus system instead of the 23-bus system because there is loop flow between four areas, where each area is directly connected to at least two other areas. In the 23-bus system, only Area 1 is connected to each of the other two areas. A diagram of the 18-bus system can be found in Figure 2.10. In the 18-bus system, there are 6 machines, with a system total capacity of 4,270 MW, 18 branches, 7 transformers, and 8 loads totaling 2,130 MW in the base case.

NREL provided load and generation data for the 18-bus system over a 24-hour period. Although individual load and machine data was given for every 4 seconds of the 24-hour period, saved cases were only generated for every 5 minutes. Therefore, 288 PSS®E saved cases were created. The developed saved cases were used in frequency, transient, and small-signal analysis. A Python script extracted generation and load data from input comma-separated values (CSV) files, scaled each machine's and load's real power, and saved the results in individual PSS®E saved case files for each 5-minute period. The Python script used to generate saved cases for the 18-bus system is included in the Appendix in Section A.1.2.1.

2.1.3 Data-Driven Frequency Stability Margin Prediction

To predict the frequency stability margin, the same contingency, a generation trip, was run on each file in the batch of generated steady-state cases. Since the steady-state cases had various levels of generation dispatch, inertia levels were modified in the PSS®E dynamic files accordingly, depending on total generation output. The contingency was selected by tripping the maximum amount of generation the system could handle, while still converging. After each dynamic simulation was run, the frequency response was evaluated.

A curve of the 18-bus system's total generation is shown in Figure 2.11. The inertia level was forced to be a percentage of the base inertia depending on total generation output. The purpose of adjusting the inertia at each generation level was to create a sufficient number of stable and unstable cases to train and test the machine learning tool. Though the total generation output over the 24-hour period did not change enough to alter unit commitment and dispatch by large amounts, the inertia was forced to change linearly, even with a smaller range of generation output variation. A linear function was created to correlate generator output and inertia level. The percentages ranged from 20% to 100% of the base inertia, corresponding to the minimum and maximum total generation output. Another Python script was written to extract total generation at each time period from a file, scale each machine's inertia parameter based on the total generation value, and save the results to individual PSS®E dynamic files. A curve of the total inertia level at each time step, given as a percentage of the base case inertia, is shown in Figure 2.12. The Python script used to create the set of dynamic files is in the Appendix in Section A.1.2.2.

PSS®E simulations were run on each set of saved cases and dynamic cases. While tripping 70 MW of generation on each case, the speed deviations of all machines were monitored. To trip exactly 70 MW, machine West G1 was split into two machines, with one machine having a constant output of 70 MW and the other machine's output adjusting according to changes in dispatch. Using MATLAB, the speed deviations were converted to frequency, and the minimum frequency nadirs of all machines for each case were computed and graphed. As expected, the frequency nadir follows the pattern of both the inertia and generation curves, indicated by Figure 2.13. The Python script used to simulate the generation trip on each set of saved cases and dynamic cases is in the Appendix in Section A.1.2.3.

For machine learning model development, or training and testing the model, stability was determined by examining the frequency nadir of each simulation output. Real power dispatch of all generators was provided as input to the machine learning tool. The frequency nadir of each generator was estimated, subjected to the generation trip. Among 288 generated cases, 70% of cases were randomly selected for training, and the remaining cases were used for testing.

The capability of the machine learning model in predicting the frequency stability margin was then validated by using the power flow solution. During testing, the input to the machine learning tool was the real power output of all machines. The output was frequency stability margin prediction, based on estimated frequency nadir. The distribution of frequency nadir estimation errors was plotted for each generator. As seen in Figure 2.14, the estimation error of frequency nadir of generators is less than 20 mHz.

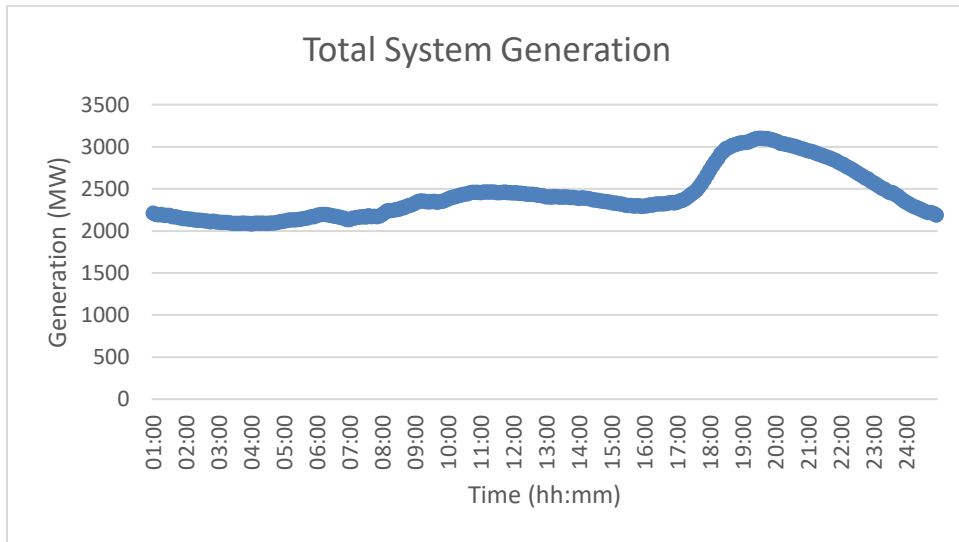


Figure 2.11. Total system generation curve for 18-bus system over 24-hour period

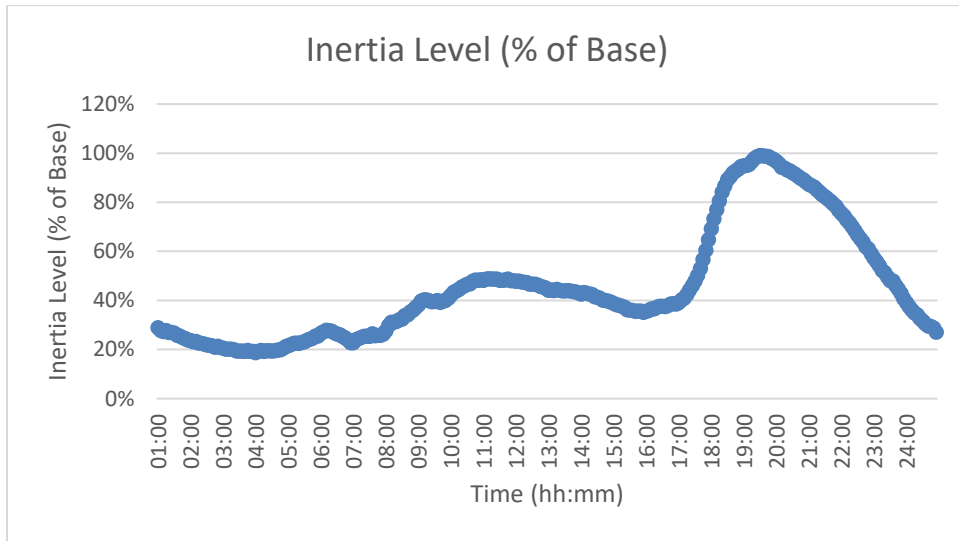


Figure 2.12. Inertia level of machines as a percent of the base inertia over 24-hour period

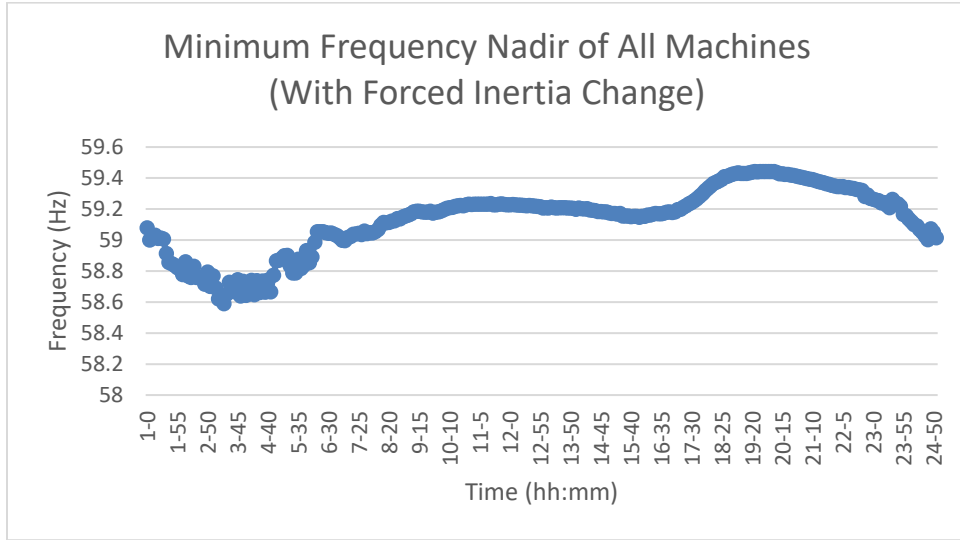


Figure 2.13. Minimum frequency nadir of all machines (with forced inertia change) over 24-hour period

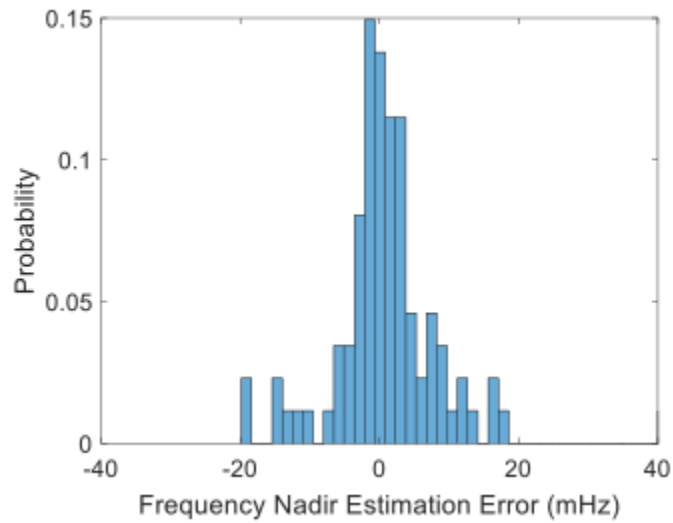


Figure 2.14. Estimation error of frequency nadir of generators

2.1.4 Data-Driven Transient Stability Margin Prediction

To predict the transient stability margin, a three-phase fault on transmission line, was introduced in the system. Although the location of the fault was fixed during all simulations, fault clearing time was varied. In this example, the fault was on the branch between North-01 (Bus 1) and North-02 (Bus 2) in the 18-bus system. The same set of fault clearing times were tested at each time step, or every 5 minutes of the 24-hour data period. At each 5-minute time step, fault clearing time was adjusted from 60 ms-720 ms in intervals of 20 ms. Therefore, 9,792 total test cases were created. Critical clearing time (CCT) was selected as the metric of transient stability. CCT is defined as the maximum time allowed to remove the disturbance without interrupting the system's performance. The system will be stable if the disturbance can be cleared before the time allowed. The purpose of adjusting the fault clearing time in small intervals was to create a sufficient number of stable and unstable cases to determine a more exact critical clearing time. During each simulation, rotor angles of all machines were monitored. If the rotor angle deviation of any two generators exceeded 180 degrees, the case was considered unstable. The Python script used to simulate the three-phase fault on the set of saved cases for different clearing times is in the Appendix in Section A.1.2.4.

The critical clearing time at each dispatch level, or five minutes of data, was determined by finding the maximum clearing time where the system still converged at each time step. In general, total system generation and fault critical clearing time had an inverse relationship. The system was considered more stable during time steps when the fault required a higher critical clearing time and less stable when it had a lower critical clearing time. Therefore, greater transient stability was observed at lower system generation levels. A graph is provided in Figure 2.15 that shows the relationship of total system generation over time to critical clearing time of a three-phase fault at a given location.

The capability of the machine learning model in predicting the transient stability margin was then validated by using the power flow solution. The input to the machine learning tool was individual real power output of all generators. During testing, the output was transient stability margin prediction by computing estimated fault clearing time as a function of dispatch. Similar to frequency stability assessment, 200 power flow cases were randomly selected for training and 88 for testing. Figure 2.16 compares the simulated critical clearing time and estimated critical clearing time from test results of the machine learning tool. As seen in Figure 2.17, estimation error of critical clearing time is below 25 ms.

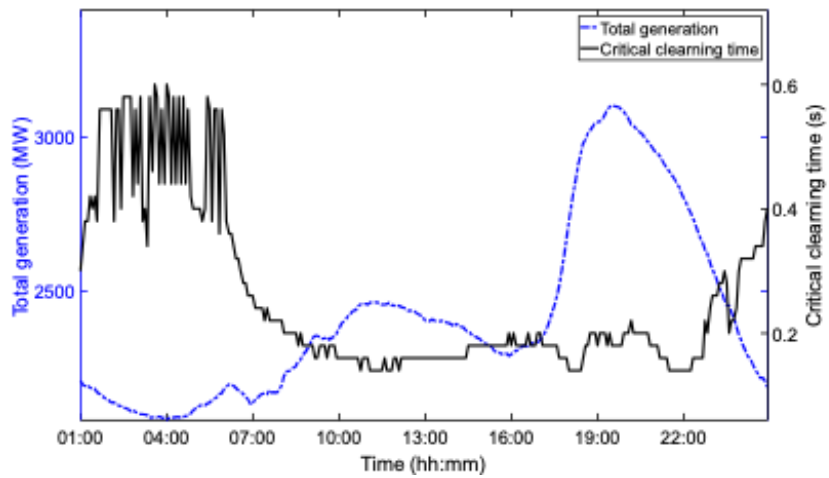


Figure 2.15. Correlation between critical clearing time and total power generation over 24 hours

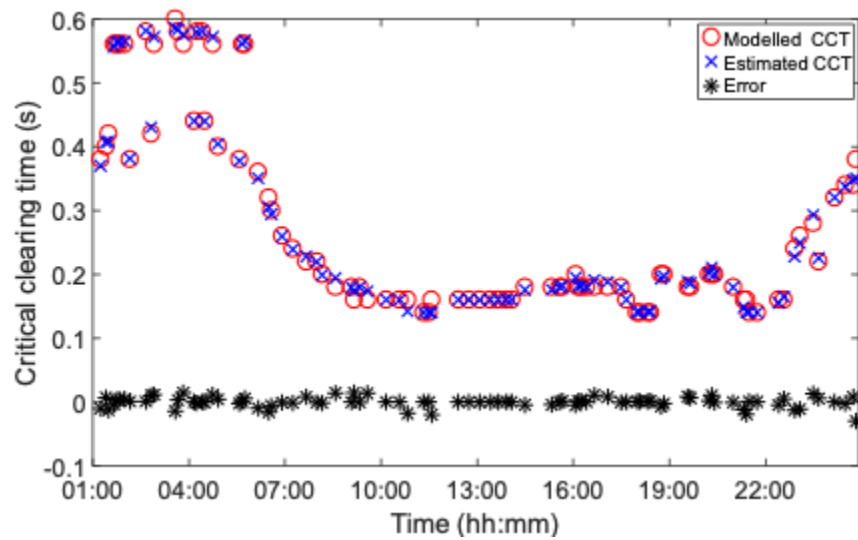


Figure 2.16. Modelled and estimated critical clearing time in testing dataset

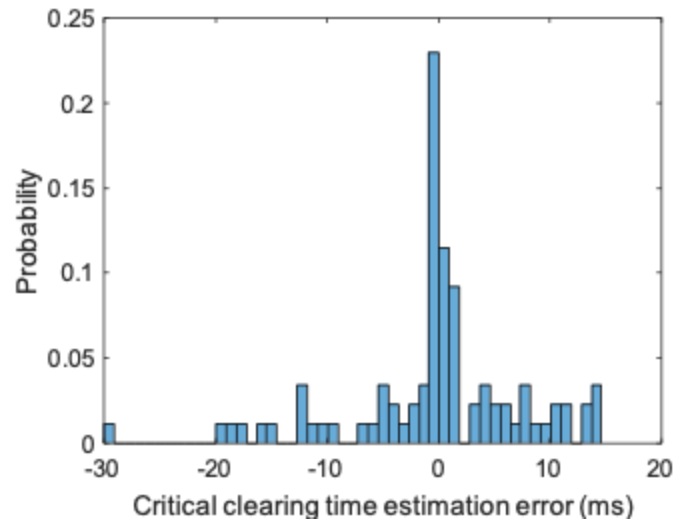


Figure 2.17. Critical clearing time estimation error distribution

2.1.5 Data-Driven Small-Signal Stability Margin Prediction

Cases for training and testing the tool for small-signal stability margin prediction were created using a software called Small-Signal Analysis Tool (SSAT). SSAT is a part of the DSATools software package, which also includes software for power flow and short circuit, transient, and voltage security. SSAT has several small-signal computation methods including eigenvalue analysis, computation of modes, small-signal stability index, small-signal stability limit search, time and frequency response calculations, and others.

SSAT can accept system power flow and dynamic information in PTI PSS@E format, GE PSLF format, and BPA format. Because power flow files had already been generated in PSS@E, these files were input into SSAT to create a case for each dispatch level. Each SSAT case accepts a single PSS@E power flow file in RAW format, along with a single dynamic (.dyr) file. Because 288 power flow files were generated, every five minutes over a 24-hour period, 288 SSAT cases were also created. The same dynamic file was used as input for all 288 SSAT cases. Because SSAT does not have an application programming interface (API) to easily create a batch of dynamic cases, a MATLAB script was used to change the filename of the PSS@E RAW file to be input, since SSAT cases can also be read with a text editor.

After SSAT cases were created for each dispatch level, a small-signal stability computation was run on each case. The selected computation was full eigenvalue analysis. Eigenvalues were derived from the state matrix, which determines the time domain response of the system to small perturbations [37]. Damping ratio was used to decide which of the eigenvalues had the greatest influence on small-signal stability [37]. The damping ratio is defined by (2).

$$\zeta_i = \frac{-\alpha_i}{\sqrt{\alpha_i^2 + \omega_i^2}} \quad (2)[37]$$

where a particular eigenvalue is given as $\zeta_i = \alpha_i + j\omega_i$

All modes, with corresponding frequencies and damping ratios, were outputted for each SSAT case. SSAT has a tool called Case Scheduler to run batch simulations. A list of SSAT cases were loaded into the Case Scheduler and run at once. After full eigenvalue analysis was computed, 47 oscillation modes were found in the 18-bus system at each generation level. Three of the modes had low damping ratio (below 10%), and other modes had high damping ratio (above 18%). Results from the modes with the smallest three damping ratios were incorporated into the machine learning tool. Participation factor is defined as the relative contribution of each state variable to a particular mode [37]. The participation factor of each generator in the system is presented for each of the modes. Factors range from 0.0-1.0, where 1.0 means the generator is fully participating and 0.0 indicates the generator is not participating. Additionally, a

comparison of the modeled vs. estimated results from the machine learning tool is shown, along with the estimation error. To train and test the model, a specific mode was selected at a time. For training, the damping ratio and generator dispatch at each 5-minute interval were provided as input to the model, with 200 of the 288 cases randomly selected to train. The rest of the cases were used to test the accuracy of the model, with only generator dispatch as input and damping ratio as output. Stability criteria was determined as a negative damping ratio being unstable and a positive damping ratio being stable.

Mode 1 had the smallest damping ratio. The frequency was 0.73 Hz, and the damping ratio was 1.11%. According to Table 2.8, West G1 and East G1 are primarily involved in this mode. Mode 2 had a frequency of 1.06 Hz and a damping ratio of 5.83% with all generators involved in the mode, exhibited in Table 2.9. Mode 3 had a frequency of 1.20 Hz and a damping ratio of 6.32%. Generator South G1 was involved most in this mode, as presented in Table 2.10. As seen in Figure 2.18 through Figure 2.23, machine learning estimated results agree well with the generated simulations. Additionally, the change in damping ratio for each of the three selected modes over the 24-hour period is presented in Table 2.11. Each individual generator's real power output and the system total real power output are also provided in Table 2.11. In general, the higher the participation factor of an individual machine for a particular mode, the more the change in damping ratio follows the change in the machine's real power output. For example, West G1 and East G1 were most involved in Mode 1. It can be seen in Table 2.11 that the change in damping ratio for this mode most closely follows the generation dispatch of West G1 and East G1.

Summary

As stated in UTK's task for the MIDAS project, the goal was to determine the data-driven-based security assessment criteria using model integration. This task was completed by developing cases, based on the NREL-provided 18-bus system, for training and testing a machine-learning algorithm. Security assessment criteria was determined for frequency, transient, and small-signal stability. Stability conditions were set based upon typical definitions for each of the stability approaches and the output parameters selected for each simulation.

Table 2.8. Participation factor of generators in Mode 1

Generator	Participation Factor
West G1	1.00
East G1	0.60
South G1	0.09
North G1 H1	0.01
North G2 H2	0.01

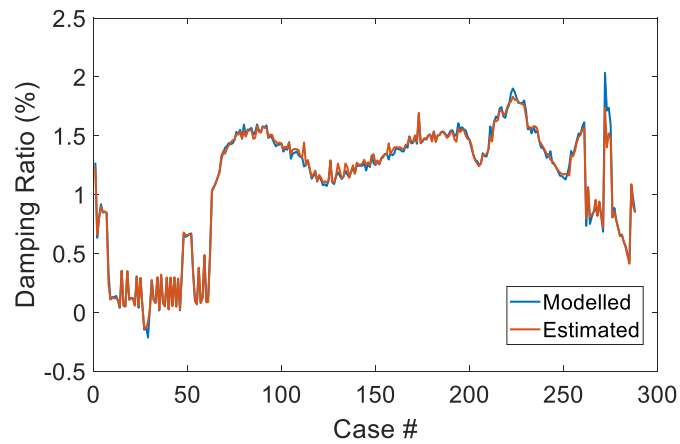


Figure 2.18. Mode 1 modeled vs. estimated damping ratio over 24-hour period

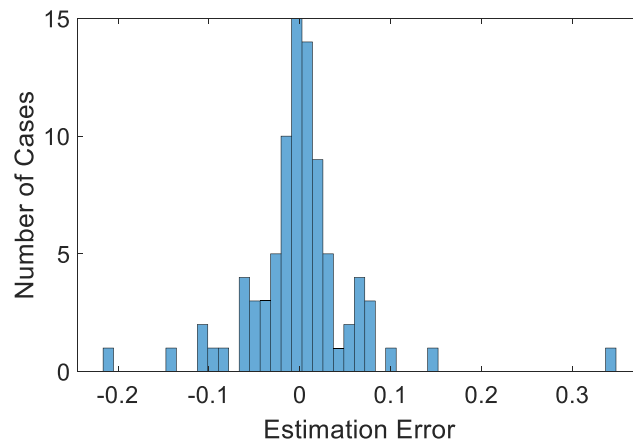


Figure 2.19. Mode 1 damping ratio estimation error distribution

Table 2.9. Participation factor of generators in Mode 2

Generator	Participation Factor
North G1 H1	1.00
North G2 H2	0.88
East G1	0.63
West G1	0.41
South G1	0.26

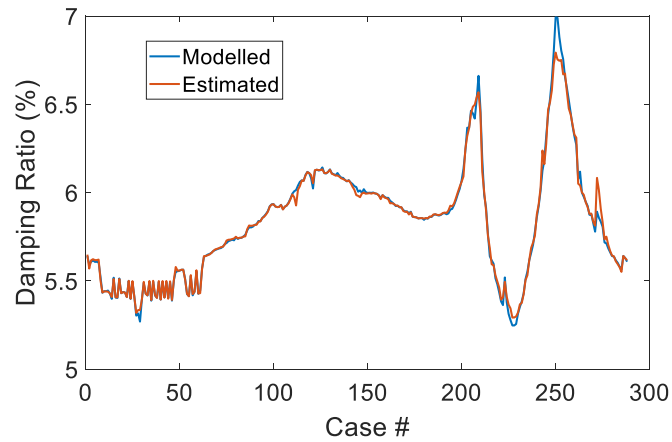


Figure 2.20. Mode 2 modeled vs. estimated damping ratio over 24-hour period

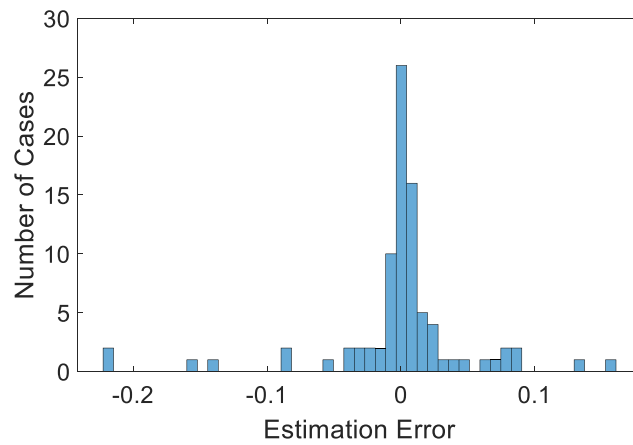


Figure 2.21. Mode 2 damping ratio estimation error distribution

Table 2.10. Participation factor of generators in Mode 3

Generator	Participation Factor
South G1	1.00
North G1 H1	0.16
North G2 H2	0.14
East G1	0.13
West G1	0.01

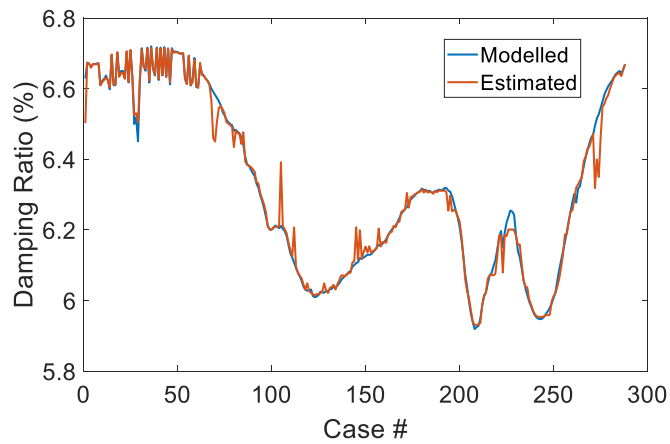


Figure 2.22. Mode 3 modeled vs. estimated damping ratio over 24-hour period

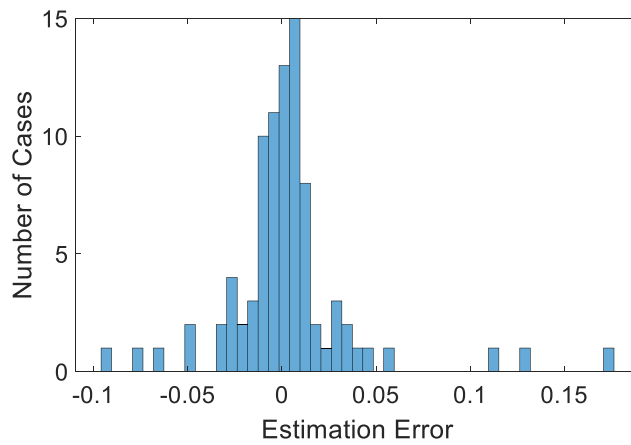
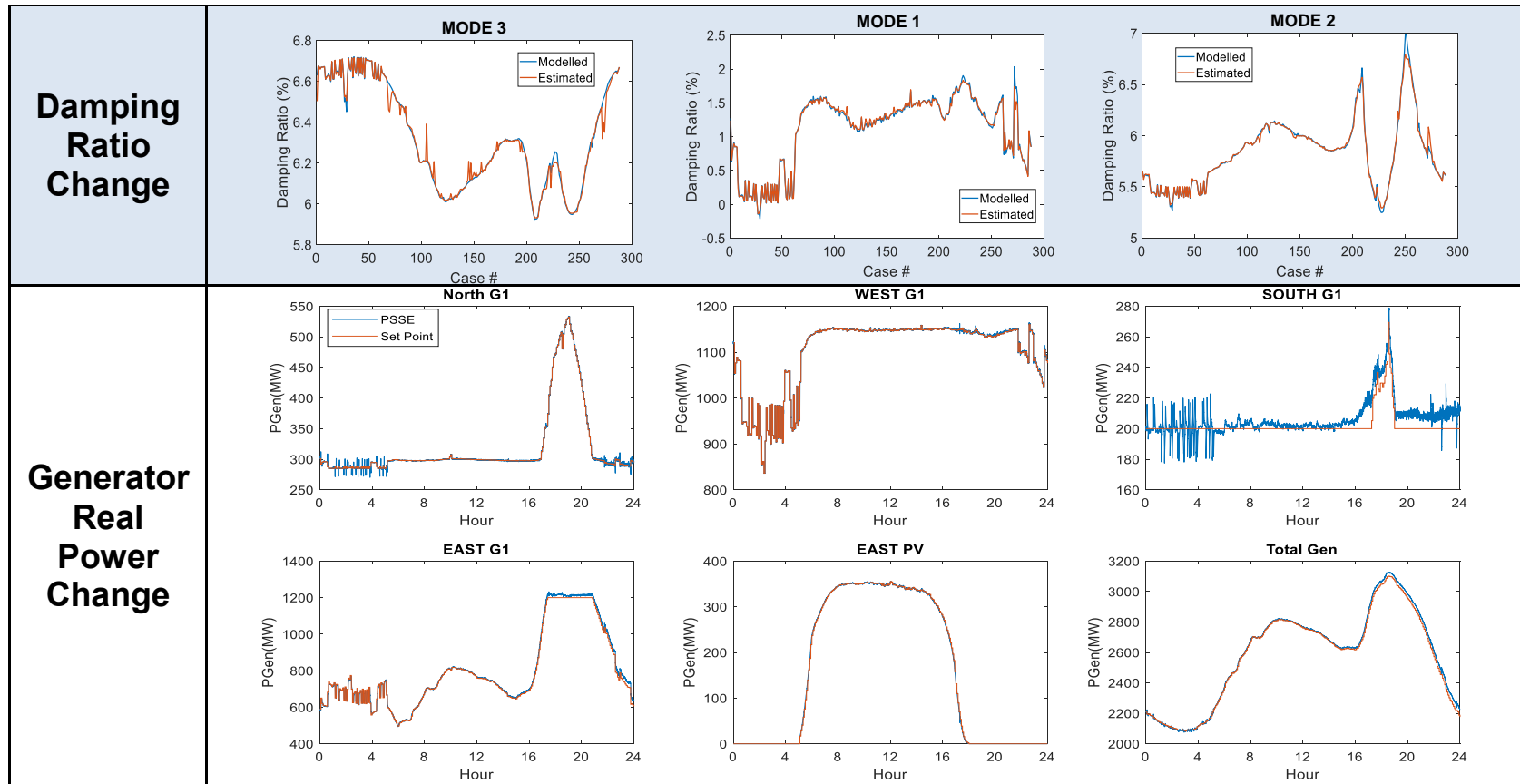


Figure 2.23. Mode 3 damping ratio estimation error distribution

Table 2.11. Damping ratio change of three selected modes compared to individual and total generator output



3 ASSESSING SECURITY DURING NATURAL DISASTERS AND INCREASED RENEWABLE PENETRATION IN PUERTO RICO

This section covers the development of the 2018 model of the PREPA transmission system for the purpose of analyzing the current system's vulnerabilities. Once the 2018 system was developed, several dynamic simulations were performed on the model. After the 2018 system model was created and analyzed, additional models were provided by DOE, including likely modifications to be made to the system. The model selected for study was a day-peak case for the year 2022. Since actual machine parameters were provided in the 2022 model, more system detail was available for study. The effects of increased solar penetration were studied on the 2022 model.

Development of the 2018 Puerto Rico Power Transmission System Study Model

This system is based off of PREPA's transmission system on the main island in 2018, shown in Figure 3.1. Buses were named according to their geographic locations, with each bus representing a substation and voltage level. The two voltage levels in the PSS®E model are 230kV and 115kV. A summary of the system is shown in Table 3.1.

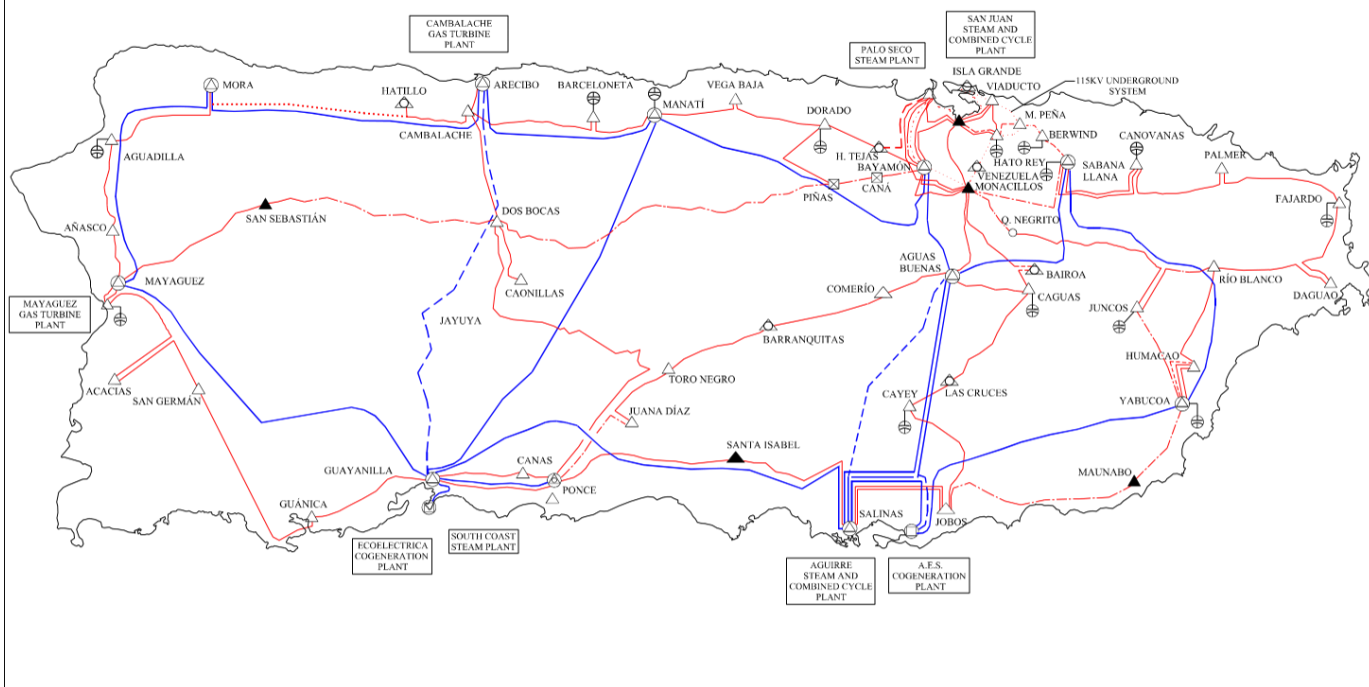
3.1.1 The Power Flow Model of the Puerto Rico Power Transmission System

3.1.1.1 Generation

The generation plants in Table 3.2 were modeled based upon information provided by PREPA [38]. Each plant was modeled as a separate machine with the maximum real power output (PMax) set as each plant's nameplate capacity ¹. For power dispatch for the base case scenario, the real power output (Pout) for each generator was set as 75% of the PMax. In addition, reactive power limits: QMax and QMin, were adjusted individually for each generator according to the PMax and base MVA.

¹ A more detailed explanation on capacity modeling is provided in the Appendix in Section A.2.

PREPA'S TRANSMISSION SYSTEM 2018



LEGEND:	
<ul style="list-style-type: none"> — 230 KV LINE - - - NEW 230 KV LINE - · - · - RECONSTRUCTED 230 KV LINE — 115 KV LINE - - - NEW 115 KV LINE - · - · - RECONSTRUCTED 115 KV LINE - · - · - 115 KV UNDERGROUND LINE - · - · - 115 KV CAPACITOR BANK 	<ul style="list-style-type: none"> ⊗ 230/115 KV TRANSFORMER ⊗ NEW 230/115 KV TRANSFORMER ⊗ 230/115 KV TRANSFORMER INCREASE CAPACITY ⊗ 115/38 KV TRANSFORMER ⊗ NEW 115/38 KV TRANSFORMER ⊗ 115/38 KV TRANSFORMER INCREASE CAPACITY ⊗ 230 KV SWITCHYARD ⊗ NEW 230 KV SWITCHYARD ⊗ NEW 115 KV SWITCHYARD

PLANNED TRANSMISSION SYSTEM IMPROVEMENTS THRU FY 2018

After PREPA

Figure 3.1. PREPA's 2018 transmission system [38]

Table 3.1. PREPA transmission system study model overview

Total 115kV Buses	Total 230kV Buses	Total 115kV Branches	Total 230kV Branches	Total Generation Capacity (MW)	Total Load (MW)
72	13	104	18	6026.4	3265

Table 3.2. Generator types and capacities

Generator Bus Number	Generator Bus Name	Type	Capacity (MW)
4	MAYAGUEZ PLA115.00	Gas	220
9	PONCE 115.00	Solar	2.1
10	DOS BOCAS 115.00	Hydro	10
11	CAONILLAS 115.00	Hydro	21.5
15	VEGA BAJA 115.00	Gas	42
30	PUNTA LIMA 115.00	Wind	26
31	RIO BLANCO 115.00	Hydro	5
39	JOBOS 115.00	Gas	42
40	SANTA ISABEL115.00	Wind	75
43	TORO NEGRO 115.00	Hydro	10.56
47	PALO SECO 115.00	Steam	602
47	PALO SECO 115.00	Gas	126
48	SAN JUAN 115.00	Combined Cycle	440
48	SAN JUAN 115.00	Steam	400
49	AES IIUMINA 115.00	Solar	20
58	COSTA SUR P 115.00	Steam	990
58	COSTA SUR P 115.00	Gas	42
59	ECOELCTRICA 115.00	Gas	507
61	CAMB PLANT 115.00	Gas	248
68	AES PLANT 115.00	Gas	454
69	AGUIRRE P 115.00	Steam	900
69	AGUIRRE P 115.00	Gas	42
69	AGUIRRE P 115.00	Combined Cycle	592
81	YABUCOA PLAN115.00	Gas	42
83	SALINA SOLAR115.00	Solar	16
85	ORIANA SOLAR115.00	Solar	45
86	SAN FERMIN S115.00	Solar	27
87	YAUCO 115.00	Hydro	25
88	GARZAS 115.00	Hydro	12.24
89	DAGUAO 115.00	Gas	42

3.1.1.2 Transmission

A map of the Puerto Rico 2018 transmission system is shown in Figure 3.1. Transmission line impedances and susceptances were calculated using the geographic distance of each branch in miles², with the conversion factors provided in Table 3.3. To do this, each bus was assigned a global positioning system (GPS) coordinate in latitude and longitude degrees. The Haversine formula can be used to calculate the great-circle distance between two points, with each point being a latitude and longitude coordinate. This formula is defined by (3).

$$a = \sin^2\left(\frac{\Delta\varphi}{2}\right) + \cos\varphi_1 * \cos\varphi_2 + \sin^2\left(\frac{\Delta\lambda}{2}\right) \quad (3)[41]$$

$$c = 2 * \text{atan2}(\sqrt{a}, \sqrt{(1-a)})$$

$$d = R * c$$

where φ = latitude, λ = longitude, R = earth's radius in km,
 d = great – circle distance between two points,
 a and c are intermediate parameters

The line impedance and susceptance parameters in p.u. per mile were assumed as values shown in Table 3.3 for each voltage level.

3.1.1.3 Load

Load data was approximated using population data. First, population data was collected for each area in which a substation was located. Each area's population was then divided by the total population to estimate the percentage of total system load that each bus's load accounted for. The peak demand of the Puerto Rico power system was given as 3,265 MW [38]. This peak demand value was multiplied by the population percentage of each bus to derive each bus's individual real power load (Pload) value. It was assumed that the power factor for each bus is 0.98. The load value for each bus is given in Table 3.4.

3.1.2 The Power Flow Solution

After the power flow model and parameters were prepared, the steady-state power flow was solved to obtain a converged power flow solution. Using the Full Newton-Raphson method with a flat start, the convergence information during each iteration is given in Figure 3.2.

² Although some branches in the real system are not perfectly linear, the geographic distances and voltage ratings were used to obtain transmission line parameters as the best estimation based on available information.

Table 3.3. Transmission line resistance, reactance, and susceptance in p.u. per mile

Voltage level	R	X	B
115kV	0.00054	0.0030	0.00048
230kV	0.00017	0.0016	0.0035

Table 3.4. Load value for each bus derived from population distribution in Puerto Rico

Bus Number	Bus Name	Total Population [42]	% Population of Total	Bus Load Real Power (MW)
1	Aguadilla	60,316	2.382%	77.77
2	Añasco	29,281	1.157%	37.78
3	San Sebastian	42,092	1.663%	54.30
5	Acacias	54,507	2.153%	70.30
6	San German	35,254	1.393%	45.48
7	Guanica	19,115	0.755%	24.65
8	Canas	34,065	1.346%	43.95
9	Ponce	149,028	5.887%	192.21
10	Dos Bocas	8,331	0.329%	10.74
12	Hatillo	42,224	1.668%	54.46
13	Cambalache	131	0.005%	0.16
14	Barceloneta	25,013	0.988%	32.26
15	Vega Baja	59,172	2.337%	76.30
16	Dorado	38,524	1.522%	49.69
19	Il Tejas	46,528	1.838%	60.01
20	Venezuela	74,490	2.942%	96.06
21	Hato Rey	20,867	0.824%	26.90
23	Berwind	3,006	0.119%	3.89
24	M Pena	415	0.016%	0.52
25	Viaducto	6,170	0.244%	7.97
26	Isla Grande	753	0.030%	0.98
28	Palmer	1,032	0.041%	1.34
29	Fajardo	36,499	1.442%	47.08
30	Daguao	1,838	0.073%	2.38
32	Humacao	58,189	2.298%	75.03
33	Juncos	40,609	1.604%	52.37
35	Bairoa	2,365	0.093%	3.04
36	Caguas	134,481	5.312%	173.44

Table 3.4. Continued

Bus Number	Bus Name	Total Population [42]	% Population of Total	Bus Load Real Power (MW)
38	Cayey	48,065	1.899%	62.00
40	Santa Isabel	23,389	0.924%	30.17
41	Comerio	20,779	0.821%	26.81
42	Barranquitas	30,402	1.201%	39.21
43	Toro Negro	1,399	0.055%	1.80
44	Juana Diaz	50,676	2.002%	65.37
48	San Juan	355,074	14.025%	457.92
50	Mora	161,884	6.394%	208.76
52	Arecibo	94,658	3.739%	122.08
54	Mayaguez	87,712	3.465%	113.13
56	Guayanilla	21,368	0.844%	27.56
62	Pfizer	108,862	4.300%	140.40
63	Manatí	43,772	1.729%	56.45
65	Salinas	30,981	1.224%	39.96
67	Guyama	45,345	1.791%	58.48
72	Aguas Buenas	28,599	1.130%	36.89
74	Bayamón	189,159	7.472%	243.96
76	Yabucoa	37,655	1.487%	48.55
80	Manuabo	12,225	0.483%	15.77
84	Monacillos	96,226	3.801%	124.10

ITER	DELTAP	BUS	DELTAQ	BUS	DELTA/V/	BUS	DELTAANG	BUS
0	9.3886(69)	1.8286(56)				
					0.02000(43)	0.23903(1)
1	0.1943(69)	0.6170(65)				
					0.01487(45)	0.02633(68)
2	0.0026(56)	0.0066(45)				
					0.00022(45)	0.00038(59)
3	0.0000(56)	0.4328(31)				
					0.01077(30)	0.00194(30)
4	0.0008(89)	0.0047(30)				
					0.00051(30)	0.00007(48)
5	0.0000(89)	0.0054(31)				
					0.00013(31)	0.00002(31)
6	0.0000(31)	0.0000(31)				

Reached tolerance in 6 iterations

Largest mismatch: -0.00 MW 0.00 Mvar 0.00 MVA at bus 31 [RIO BLANCO 115.00]
System total absolute mismatch: 0.00 MVA

SWING BUS SUMMARY:

BUS#	X--	NAME	--X	BASKV	PGEN	PMAX	PMIN	QGEN	QMAX	QMIN
58		COSTA	SUR	P 115.00	715.7	1032.0	0.0	40.5	358.4	-356.4

Figure 3.2. Power flow solution of the Puerto Rico system using Newton-Raphson method

According to the transmission power flow of the Puerto Rico system, contour maps were generated to visually show the real and reactive power at each bus, along with the real and reactive power flow in the lines, as seen in Figure 3.3 to Figure 3.6. From the contour maps, it is confirmed that real power consumption is highest in the northern part of the island. Real power flow is also highest on the transmission lines coming from the south of the island where most of the power is generated.

3.1.3 Overview of the Dynamics of the Puerto Rico Power Transmission System

The dynamics of the Puerto Rico system were generated using typical generator, exciter, and turbine governor dynamic models based on the plant type: thermal³, hydroelectric, or renewables. The models used for each generation type are summarized in Table 3.5. Since the capacities of hydro power plants in the Puerto Rico power grid are small, no turbine governors are considered and modeled for hydro power plants. Solar power plants use the generic PV dynamic model developed by General Electric. Wind power plants apply the Type 3 (doubly-fed induction generator) wind turbine generator model, also from General Electric. For all thermal plants, frequency deadbands have been modeled into the turbine governors. Specific model parameters for each model can be found in the dynamic file.

3.1.4 Dynamic Simulations Performed on the Developed 2018 PREPA Transmission Model

To test the dynamic model and better understand the impact of various contingencies on the system, a few dynamic simulations were run. First, a base case with no contingencies was simulated. As seen in Figure 3.7, the system frequency stays at 60 Hz at the steady state.

Next, a few dynamic simulations were tested to examine system response after contingencies.

Generation Trip: The first contingency was tripping the Costa Sur steam plant located in Guayanilla, a municipality located in southern coast of the island (as displayed in Figure 3.8). This plant is loaded at about 681 MW in steady state conditions. A drop in frequency can be seen in Figure 3.9 due to the loss of generation. The frequency nadir is close to 59.3 Hz, which is a value of typical under-frequency-load-shedding thresholds in contiguous U.S. power grids.

³ In this first-stage study, all thermal plant machines (gas, steam, and combined cycled) were given the same type of dynamic models.

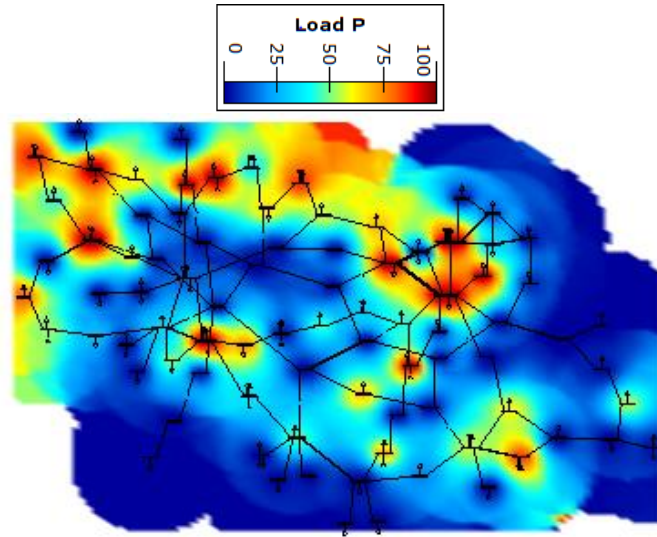


Figure 3.3. Contour map of real power at each bus in the PREPA system

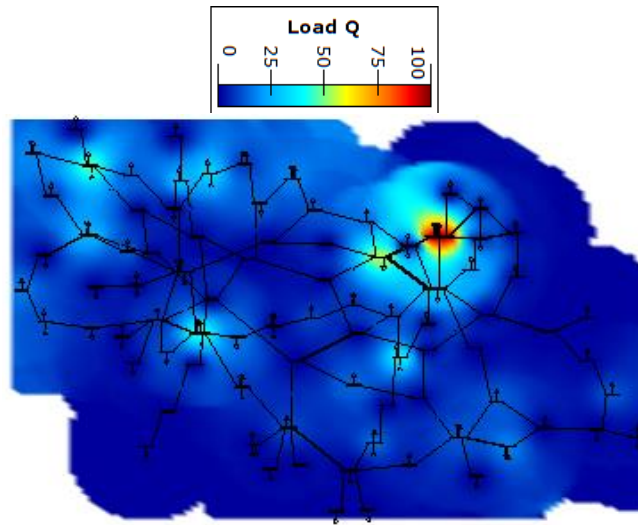


Figure 3.4. Contour map of reactive power at each bus in the PREPA system

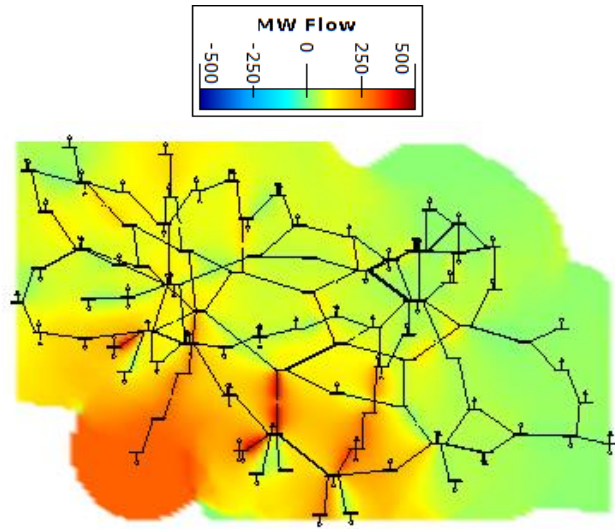


Figure 3.5. Contour map of line MW flow in the PREPA system

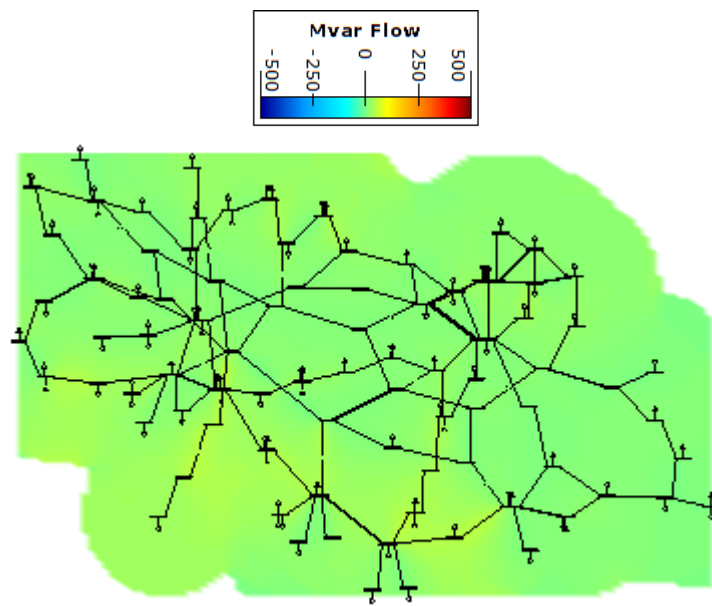


Figure 3.6. Contour map of line MVar flow in the PREPA system

Table 3.5. Generator dynamic models in the Puerto Rico power system model

Generator Type	Generator	Exciter or Electrical Controller	Turbine Governor
Gas, Steam, and Combined Cycle	GENROU	EXPIC1	URGS3T
Hydro	GENSAL	SCRX	None
Solar	GEPVG	GEPVE	None
Wind	GEWTG2	GEWTE2	GEWTT1

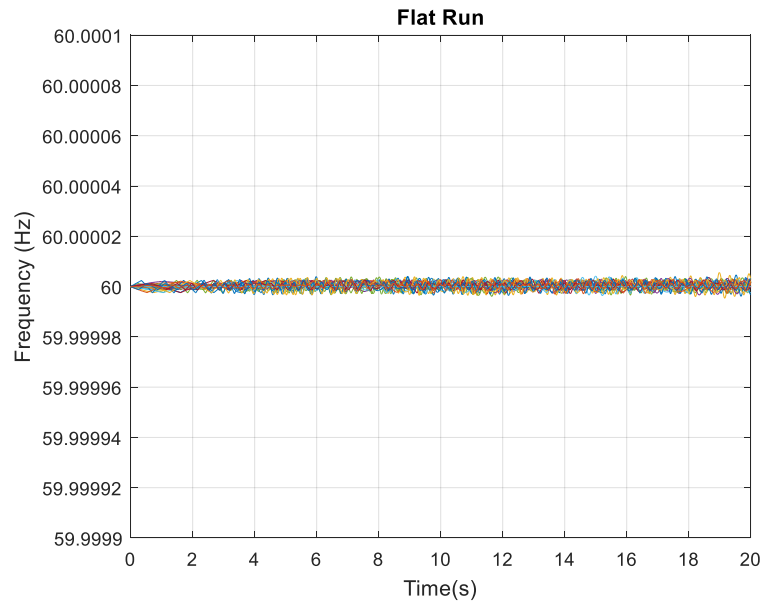


Figure 3.7. Frequency response in no-contingency simulation



Figure 3.8. Map of Puerto Rico indicating Guayanilla [43]

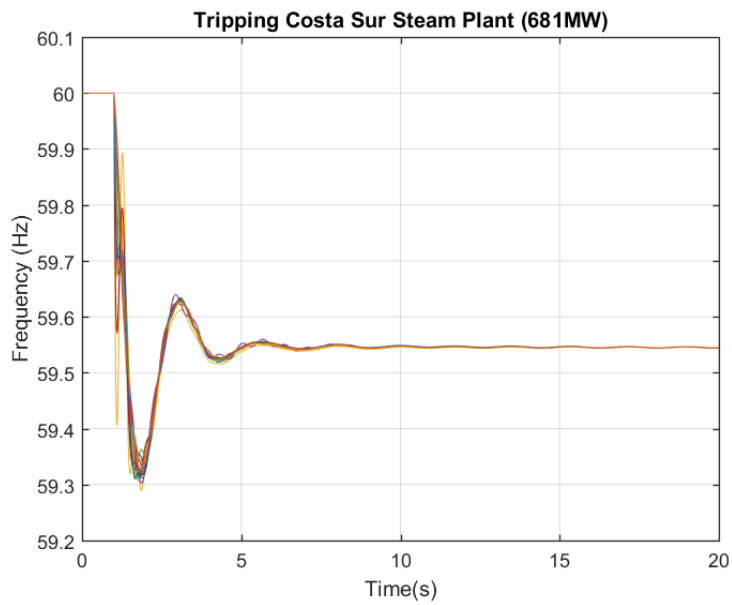


Figure 3.9. Frequency response after tripping the Costa Sur Steam Plant (681 MW)

Load Shedding: In the second contingency, load at a substation was tripped in Caguas, a city and municipality of Puerto Rico located south of San Juan (as shown in Figure 3.10). The tripped load amount is 198 MW. An increase in frequency can be seen in Figure 3.11 after the load shedding. As this load shedding amount is relatively small, this frequency deviation is within the safe range of the typical over-frequency protection relay setting for generators.

Bus/Branch Fault: Bus fault and branch fault contingency simulations were also performed. A zero-impedance fault was applied for both the bus and branch at 1 second and then cleared at 1.05 seconds. The bus fault occurred at the 115kV bus at the Hato Rey substation (Figure 3.14), a densely populated barrio in the municipality of San Juan. The branch fault occurred on the 230kV transmission line connecting Guayanilla and Manatí (Figure 3.15), a municipality on the northern coast. Results for the bus fault are shown in Figure 3.13 and Figure 3.14, and results for the branch fault are presented in Figure 3.16 and Figure 3.17. For both fault contingencies, the system frequency had an increase due to the acceleration of the generator rotors, followed by a ring-down process after clearing the fault. Additionally, for the transmission fault contingency, a local oscillation can be observed during frequency restoration, seen in Figure 3.16.

Substation Failure: The Santa Isabel substation was tripped. Santa Isabel is a municipality located near the southern coast of the island (as shown in Figure 3.18). This plant is loaded at about 34 MW and has 49.5 MW of generation in the steady state condition. This generation is from a wind farm in Santa Isabel with a capacity of 75 MW. A drop in frequency can be seen Figure 3.19 due to the loss of generation and the fact that the total generation loss from this bus is greater than the total load loss.

Corridor Trip: A few major corridors, or clusters, of transmission lines were tripped. The transmission lines selected for each group act as key pathways to transmit power from major generation buses in the south to large load buses in the north. After individual clusters were tripped, groups of two adjacent clusters were tripped at the same time. The purpose of these simulations is to show what would happen if a natural disaster, such as a hurricane, would trip a group of main transmission lines.

After each simulation was run, a branch loading report was generated to see if any branches in the system were over 100% of their rating and if any bus voltages were outside of 0.95 p.u. and 1.05 p.u. Results are summarized in Table 3.6.



Figure 3.10. Map of Puerto Rico indicating Caguas [43]

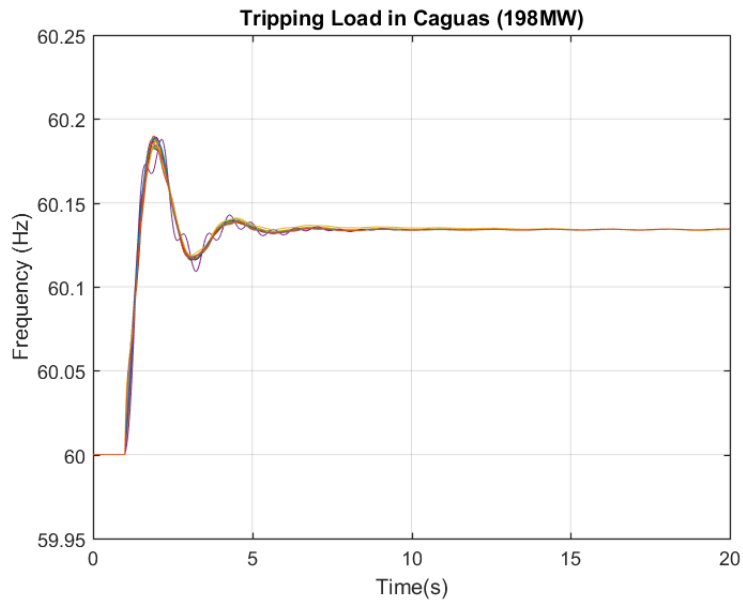


Figure 3.11. Frequency response after 198MW load shedding in Caguas



Figure 3.12. Map of Puerto Rico indicating the Hato Rey substation [43]

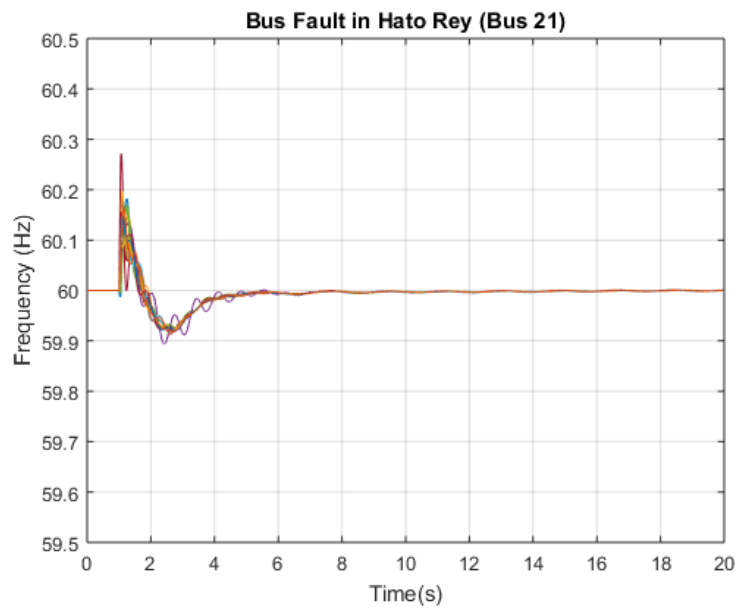


Figure 3.13. Frequency response after a fault on the 115kV bus at the Hato Rey substation (Bus 21)

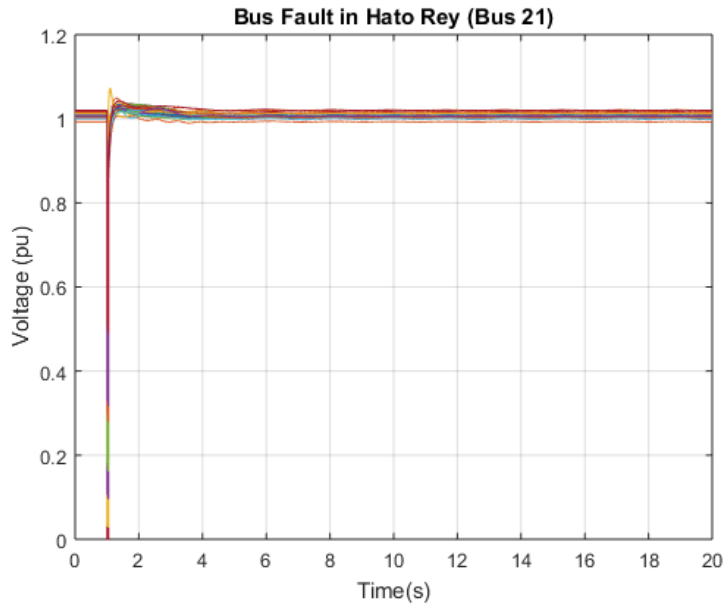


Figure 3.14. System voltage after a fault on the 115kV bus at the Hato Rey substation (Bus 21)



Figure 3.15. Map of Puerto Rico indicating approximate 230kV transmission path from Guayanilla to Manatí [43]

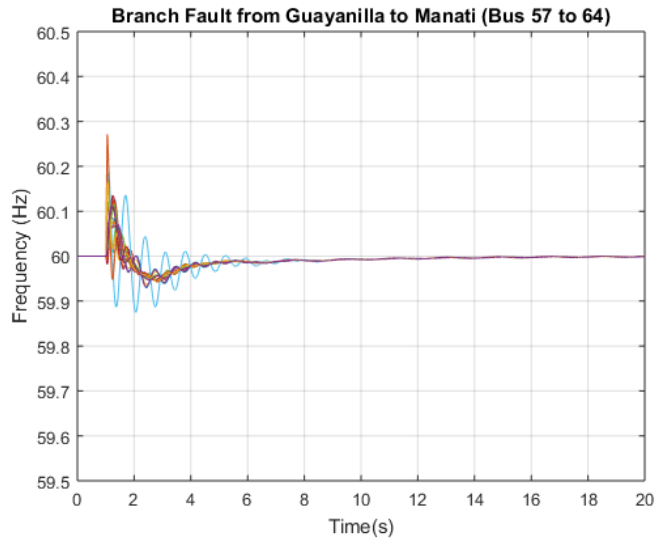


Figure 3.16. Frequency response after a three-phase short-circuit fault on the Guayanilla- Manatí 230kV transmission line

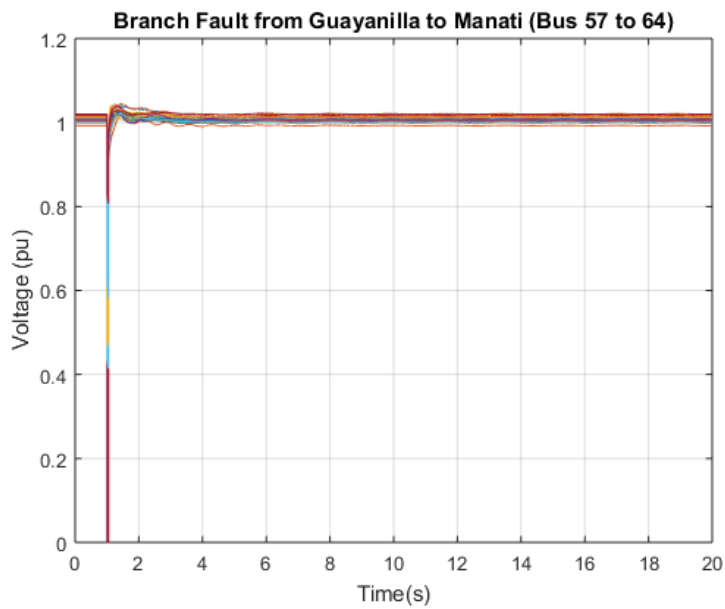


Figure 3.17. System voltage after a three-phase short-circuit fault on the Guayanilla-Manati 230kV transmission line



Figure 3.18. Map of Puerto Rico indicating the Santa Isabel substation [43]

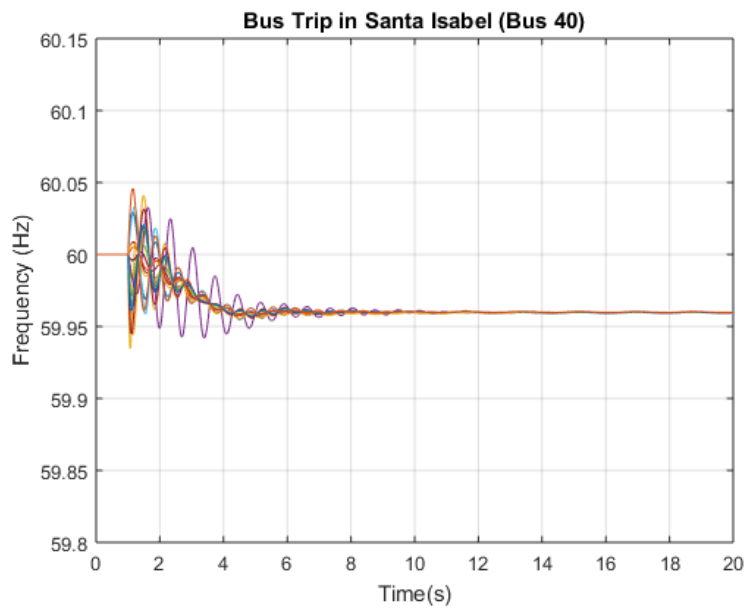
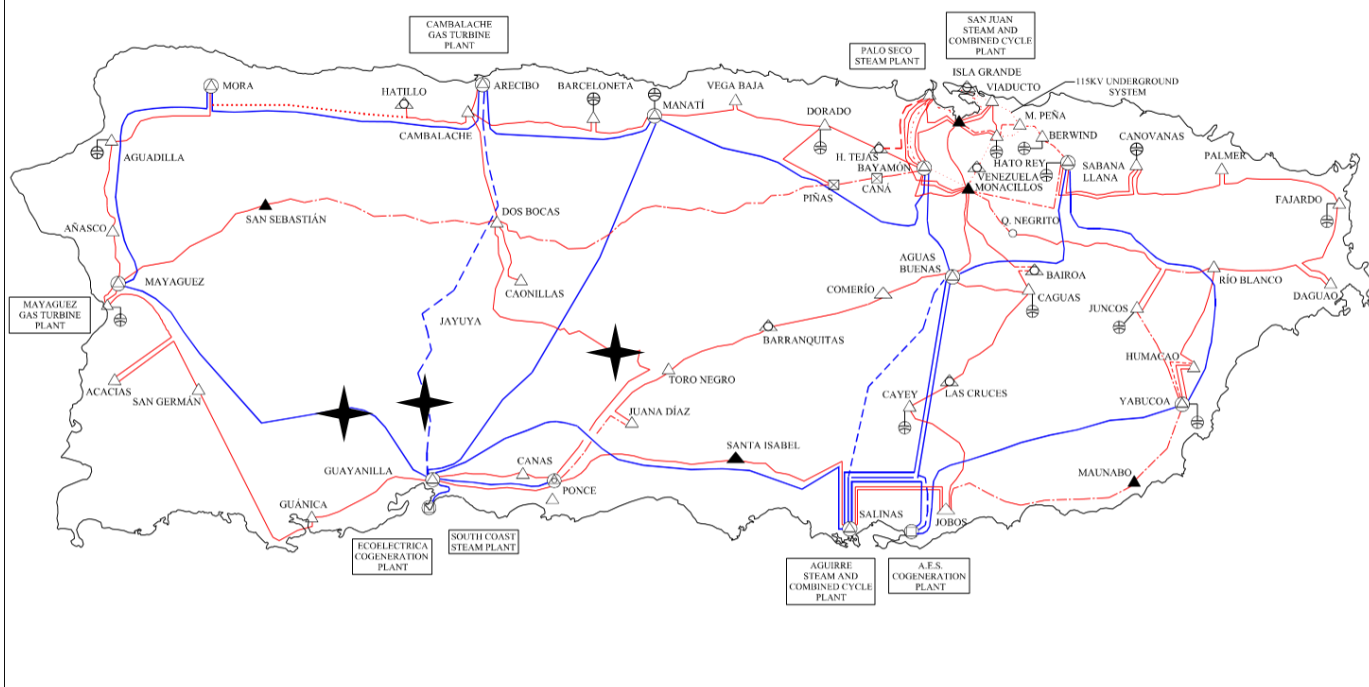


Figure 3.19. Frequency response after tripping Santa Isabel substation

PREPA'S TRANSMISSION SYSTEM 2018



LEGEND:	
<ul style="list-style-type: none"> ——— 230 KV LINE - - - - - NEW 230 KV LINE - · - · - RECONSTRUCTED 230 KV LINE ——— 115 KV LINE - - - - - NEW 115 KV LINE - · - · - RECONSTRUCTED 115 KV LINE - · - · - 115 KV UNDERGROUND LINE - · - · - 115 KV CAPACITOR BANK 	<ul style="list-style-type: none"> ⊗ 230/115 KV TRANSFORMER ⊕ NEW 230/115 KV TRANSFORMER ⊗ 230/115 KV TRANSFORMER INCREASE CAPACITY ⊕ 115/38 KV TRANSFORMER ⊗ NEW 115/38 KV TRANSFORMER ⊕ 115/38 KV TRANSFORMER INCREASE CAPACITY ⊗ 230 KV SWITCHYARD ⊕ NEW 230 KV SWITCHYARD ⊗ NEW 115 KV SWITCHYARD

PLANNED TRANSMISSION SYSTEM IMPROVEMENTS THRU FY 2018

After PREPA

Figure 3.20. Transmission map indicating Cluster 1 with annotations added to map from [38]

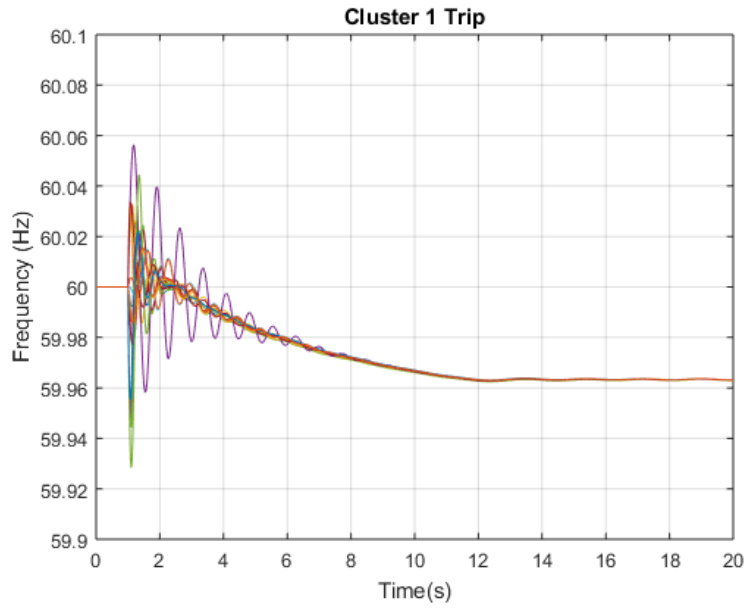


Figure 3.21. Frequency response after tripping Cluster 1

PREPA'S TRANSMISSION SYSTEM 2018

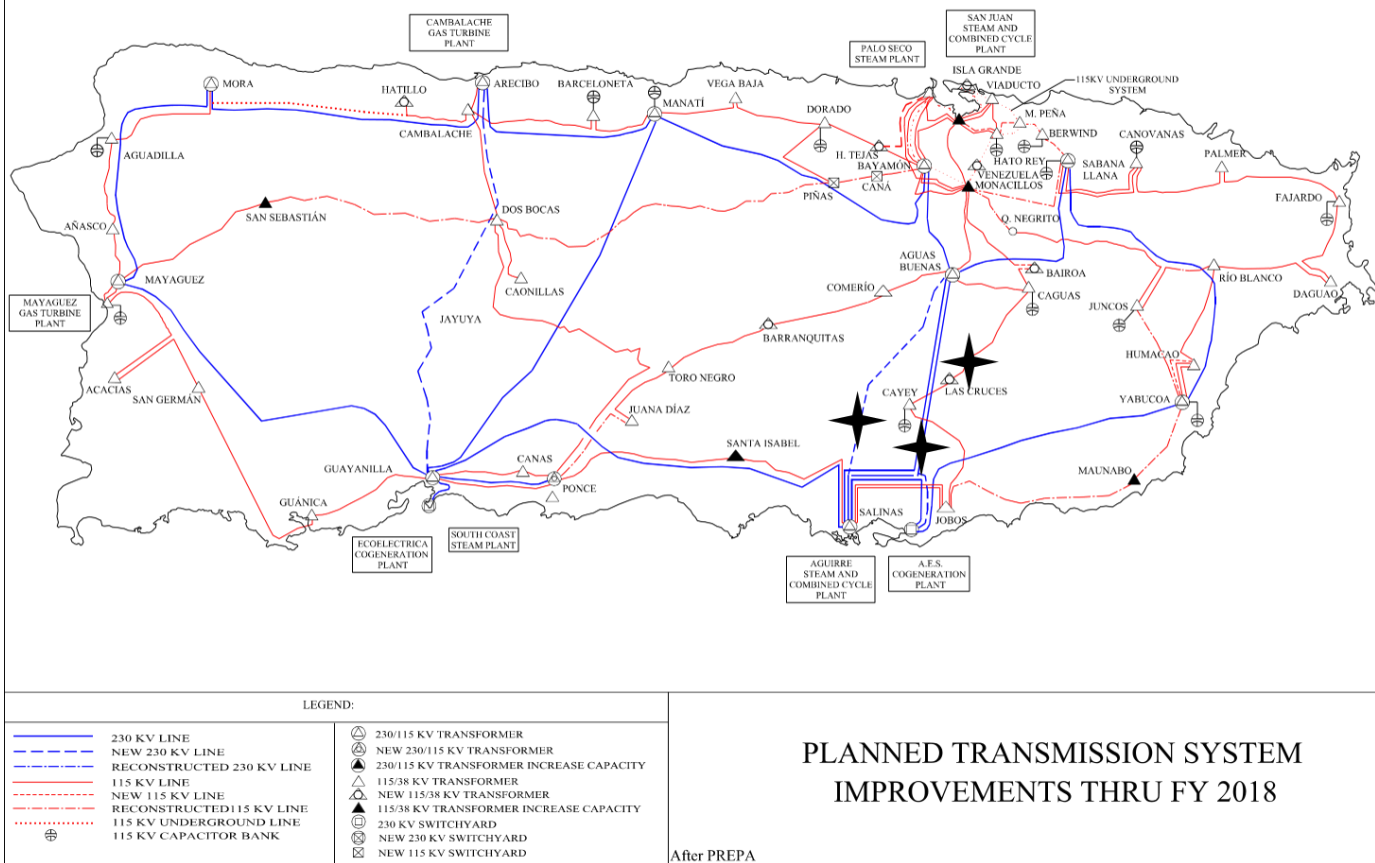


Figure 3.22. Transmission map indicating Cluster 2 with annotations added to map from [38]

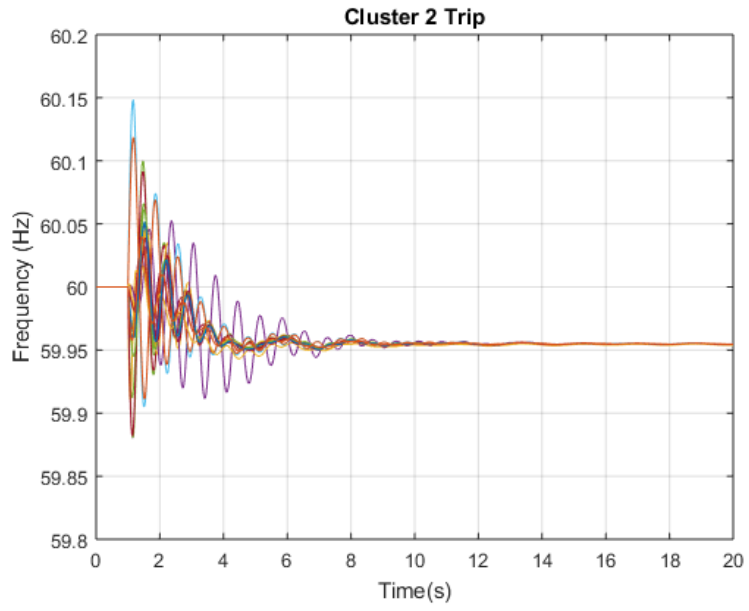
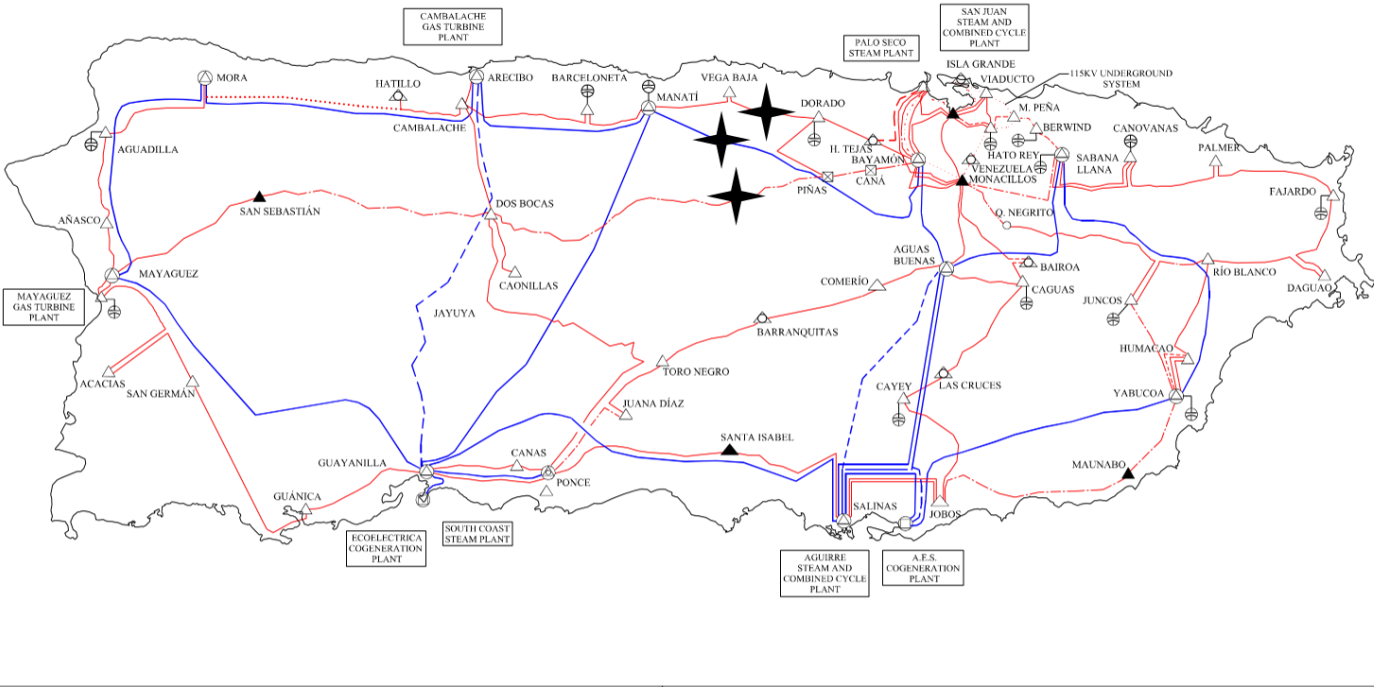


Figure 3.23. Frequency response after tripping Cluster 2

PREPA'S TRANSMISSION SYSTEM 2018



LEGEND:	
<ul style="list-style-type: none"> — 230 KV LINE - - - NEW 230 KV LINE - · - · - RECONSTRUCTED 230 KV LINE — 115 KV LINE - - - NEW 115 KV LINE - · - · - RECONSTRUCTED 115 KV LINE - · - · - 115 KV UNDERGROUND LINE - · - · - 115 KV CAPACITOR BANK 	<ul style="list-style-type: none"> ⊗ 230/115 KV TRANSFORMER ⊕ NEW 230/115 KV TRANSFORMER ⊗ 230/115 KV TRANSFORMER INCREASE CAPACITY ⊕ 115/38 KV TRANSFORMER ⊗ NEW 115/38 KV TRANSFORMER ⊕ 115/38 KV TRANSFORMER INCREASE CAPACITY ⊗ 230 KV SWITCHYARD ⊕ NEW 230 KV SWITCHYARD ⊗ NEW 115 KV SWITCHYARD

PLANNED TRANSMISSION SYSTEM IMPROVEMENTS THRU FY 2018

After PREPA

Figure 3.24. Transmission map indicating Cluster 3 with annotations added to map from [38]

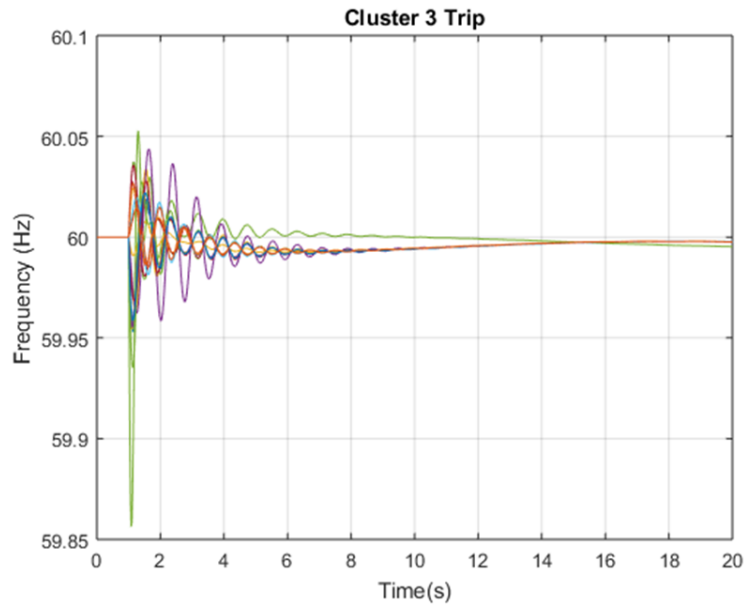


Figure 3.25. Frequency response after tripping Cluster 3

PREPA'S TRANSMISSION SYSTEM 2018

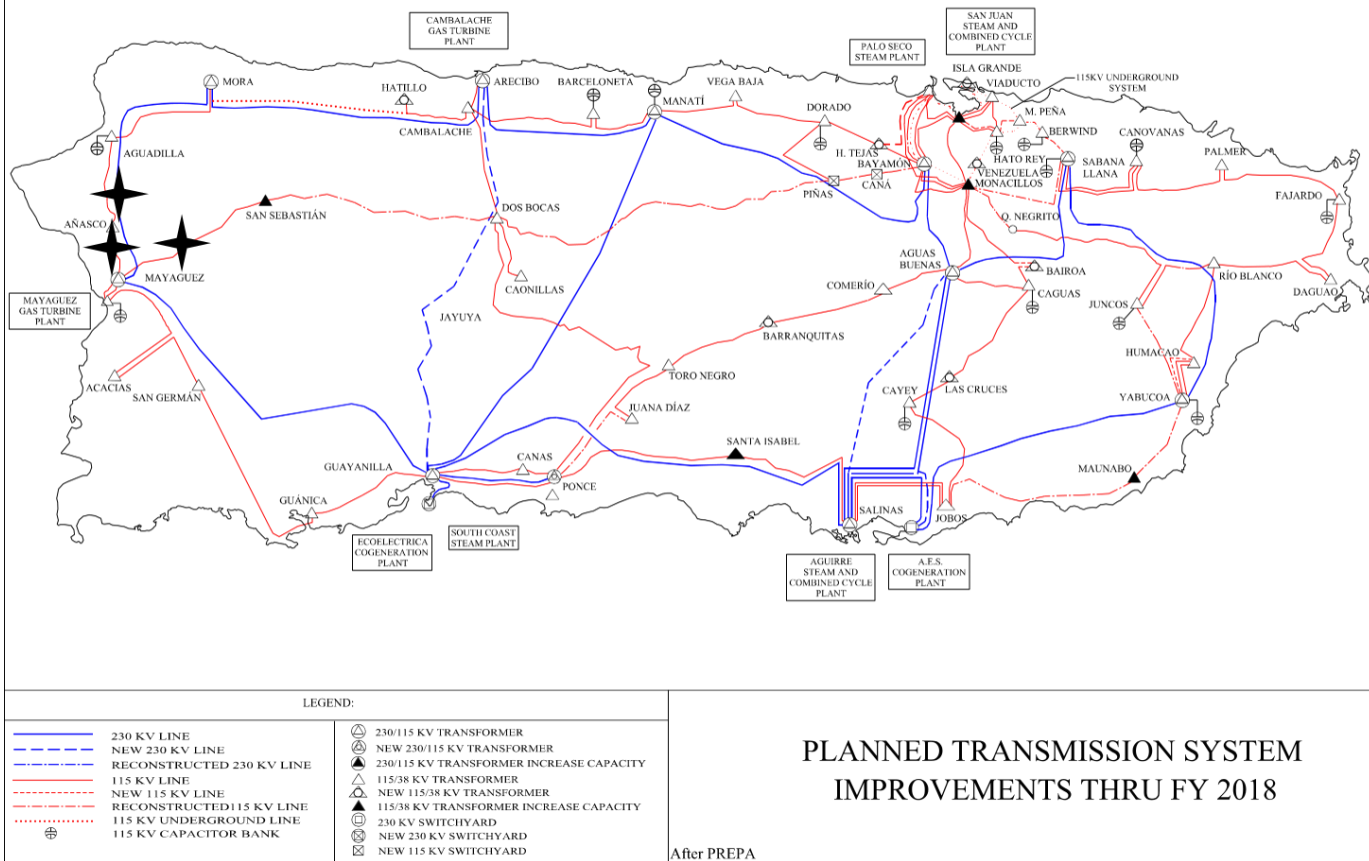


Figure 3.26. Transmission map indicating Cluster 4 with annotations added to map from [38]

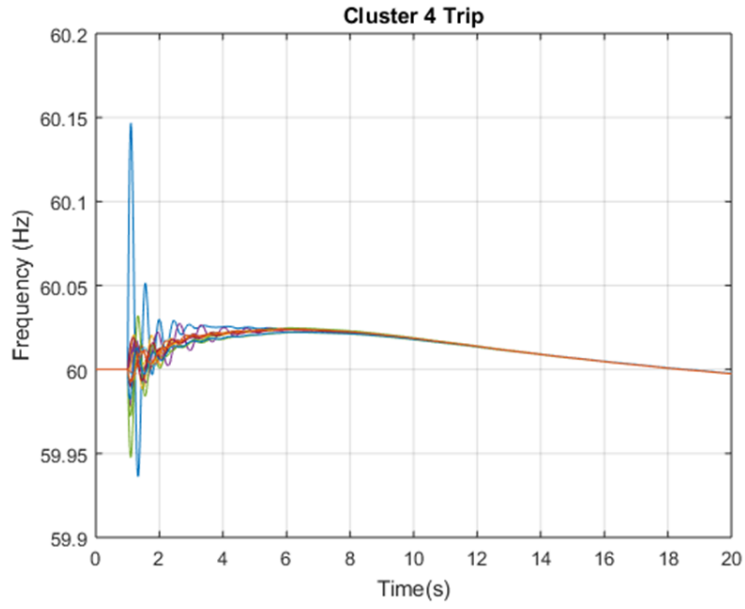


Figure 3.27. Frequency response after tripping Cluster 4

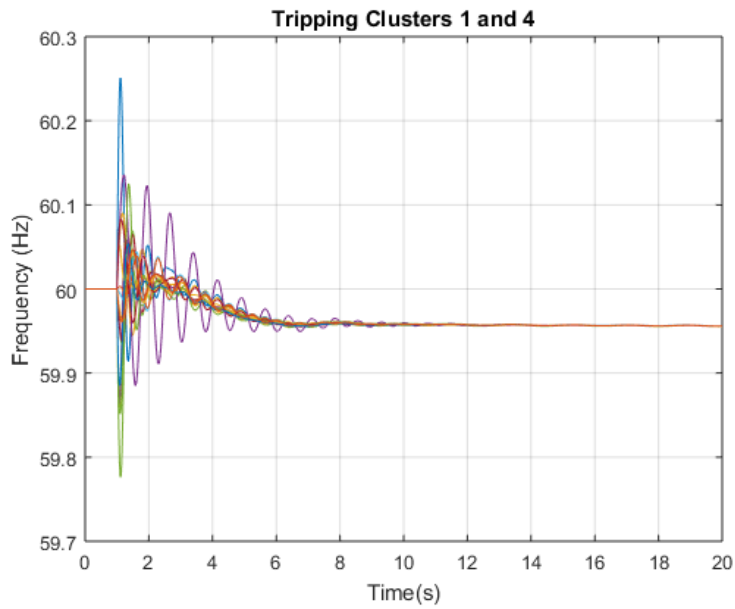


Figure 3.28. Frequency response after tripping Cluster 1 and Cluster 4

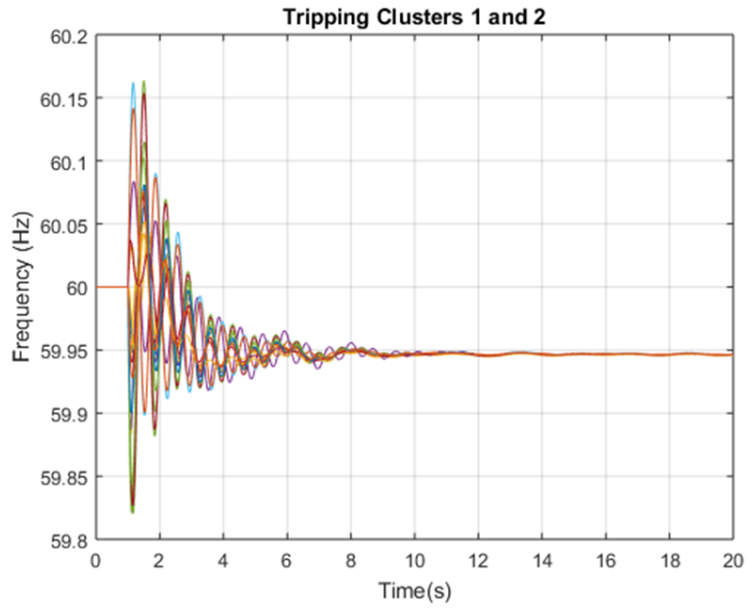


Figure 3.29. Frequency response after tripping Cluster 1 and Cluster 2

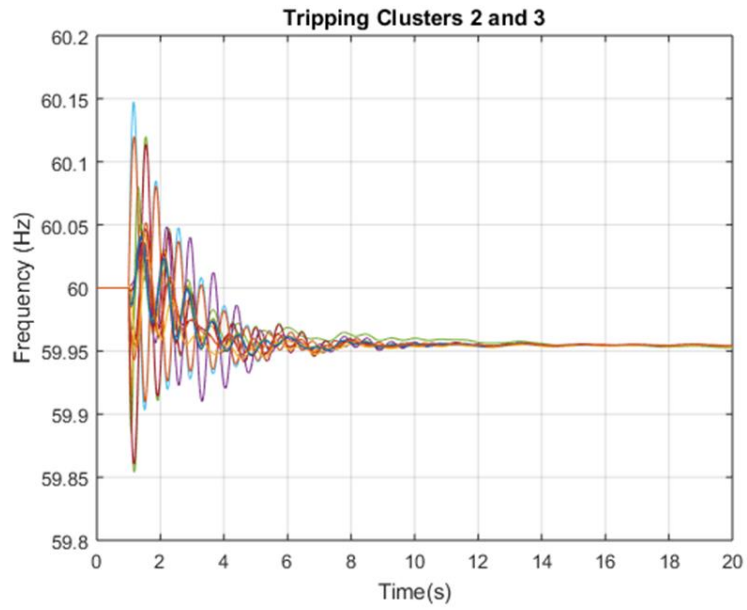


Figure 3.30. Frequency response after tripping Cluster 2 and Cluster 3

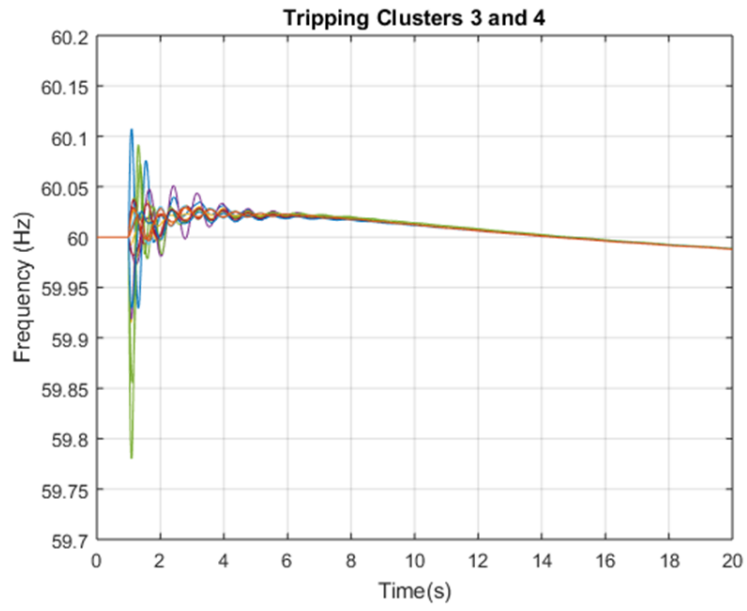


Figure 3.31. Frequency response after tripping Cluster 3 and Cluster 4

Table 3.6. Branch overload and out-of-limit voltage report from corridor trip simulations

Cluster(s) Tripped	Branch Overload Results	Out-of-Limit Voltage Results
Cluster 1	No branches above 100% of rated loading	No buses outside of 0.95 p.u. and 1.05 p.u.
Cluster 2	1 transformer branch overloaded: Salinas A and Salinas B – 103.0% of Rate1 loading	No buses outside of 0.95 p.u. and 1.05 p.u.
Cluster 3	No branches above 100% of rated loading	No buses outside of 0.95 p.u. and 1.05 p.u.
Cluster 4	No branches above 100% of rated loading	No buses outside of 0.95 p.u. and 1.05 p.u.
Clusters 1 and 4	No branches above 100% of rated loading	No buses outside of 0.95 p.u. and 1.05 p.u.
Clusters 1 and 2	1 transformer branch overloaded: Salinas A and Salinas B – 100.1% of Rate1 loading	No buses outside of 0.95 p.u. and 1.05 p.u.
Clusters 2 and 3	1 transformer branch overloaded: Salinas A and Salinas B – 102.3% of Rate1 loading	No buses outside of 0.95 p.u. and 1.05 p.u.
Clusters 3 and 4	No branches above 100% of rated loading	No buses outside of 0.95 p.u. and 1.05 p.u.

Though the system appears to be relatively robust during corridor trips, these results will need to be validated by real-time frequency and voltage measurements from deployed UGA units. Further detail regarding the placement of UGA sensors is provided in Section 3.2. Additionally, equipment parameters may need to be adjusted to more truly reflect the PREPA system.

3.1.5 PPREPA Transmission System Mapping

To better visualize the PREPA 2018 transmission model, and more easily compare connections to the transmission map in Figure 3.1, a map of the system was generated in ArcMap software. Each substation was assigned an approximate GPS coordinate based on its geographic location. Buses and branches were mapped in ArcMap, as displayed in Figure 3.32. To do this, bus and branch coordinates were imported as layers into ArcMap. Branches were assumed to be linear between each bus. The two voltage levels are indicated by distinct colors, where 115kV is red, and 230kV is blue.

Placement of Universal Grid Analyzer (UGA) Measurements for Dynamic Model Validation

The UGA is low-cost, GPS-synchronized device that measures highly accurate frequency, voltage, phase angle, and power quality measurements. UGAs are a part of the FNET/GridEye system, which is a wide-area power system frequency network of grid measurement devices. UGAs are installed by connecting the device to a standard 120V electrical outlet and connecting a GPS antenna for data synchronization. Although UGAs are directly connected at the distribution level, a network of UGAs can provide both wide-area and local event location and detection.

A more accurate power grid model will facilitate many advanced operation and planning functions in the control center of the PREPA system. Since the UGA has the capability to capture power grid behaviors accurately, this work will deploy UGA units in the PREPA system and use measurement data to validate the PREPA system model. Additionally, it is predicted that the Puerto Rico power grid will likely see a large increase in solar and other renewables in the next 2-10 years. It is necessary to have models with high renewable penetration to forecast any system stability problems. Deployment of these sensors can provide situational awareness to understand impacts on changes within the infrastructure.

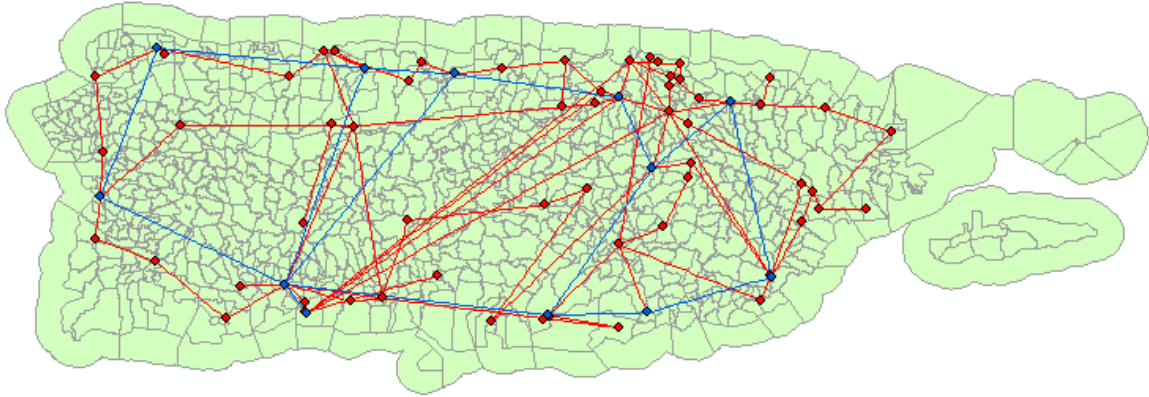


Figure 3.32. PREPA transmission system generated in ArcMap (red - 115kV; blue - 230kV)

UGAs in the Puerto Rico system can collect data system-wide and share data with Puerto Rico power engineers to assist them in their system performance assessment and system enhancement effort. Currently there are four UGA units deployed. Eighteen locations were proposed as sites for installation of additional units. Possible locations include a few large generation plants, large load areas, and hydro plants, along with a solar farm and wind farm.

Several criteria were involved in sensor placement, including the following: monitoring locations with high generation, monitoring locations with high load, geographically placing sensors to cover the island, and placing sensors near a variety of generation sources and renewable machines. Additionally, sensors were requested to be placed near transmission substations with telecommunications capabilities. Table 3.7 lists existing locations, Table 3.8 lists proposed locations, and Figure 3.33 geographically shows both existing and proposed UGA locations.

To provide examples of how this monitoring system can assist PREPA and other stakeholders in grid-wide and local situational awareness, a few system events are shown in following figures. An outage was reported in the Mayaguez region on 08/02/2018 around 4:51 UTC, as shown in Figure 3.34. Looking at the results from the measured data, there was a drop in frequency due to the loss of generation at the Mayaguez power plant, and frequency swings are evident as the system tries to stabilize to a settling frequency. Fast frequency ramp-up and local oscillations are also very common in the system, as shown in Figure 3.35 and Figure 3.36. In Figure 3.35, the increase in frequency suggests either a load drop or fast frequency ramp up occurred. Local oscillations in the system are common. An example of a local oscillation is shown in Figure 3.36, indicated by fluctuations in measured frequency.

A more systematic analysis of PREPA measurement will be carried out in Phase II. Additionally, data from UGAs deployed in Puerto Rico will be used to validate and refine the UTK-developed 2018 model and PREPA-developed models of the system. To validate the models, events captured by UGAs can be simulated. Simulated results will reveal differences between model parameters and the actual system. Model parameters can then be modified to more closely match the behavior of the actual system.

Table 3.7. Existing Puerto Rico UGA Locations

Existing UGA Locations	
UGA Number	Location
1	Mayaguez
2	Yauco
3	San Juan
4	Viaducto

Table 3.8. Proposed Puerto Rico UGA Locations

Proposed UGA Locations	
UGA Number	Location
1	Manatí
2	Caguas
3	Humacao
4	Canóvanas
5	Fajardo
6	Victoria
7	Acacias
8	Martín Peña
9	Barrio Piñas
10	Bayamón
11	Arecibo
12	Ponce
13	Jobos
14	Covadonga
15	Barranquitas
16	Juan Martín
17	Juncos
18	Santa Isabel

Existing and Proposed UGA Locations in Puerto Rico

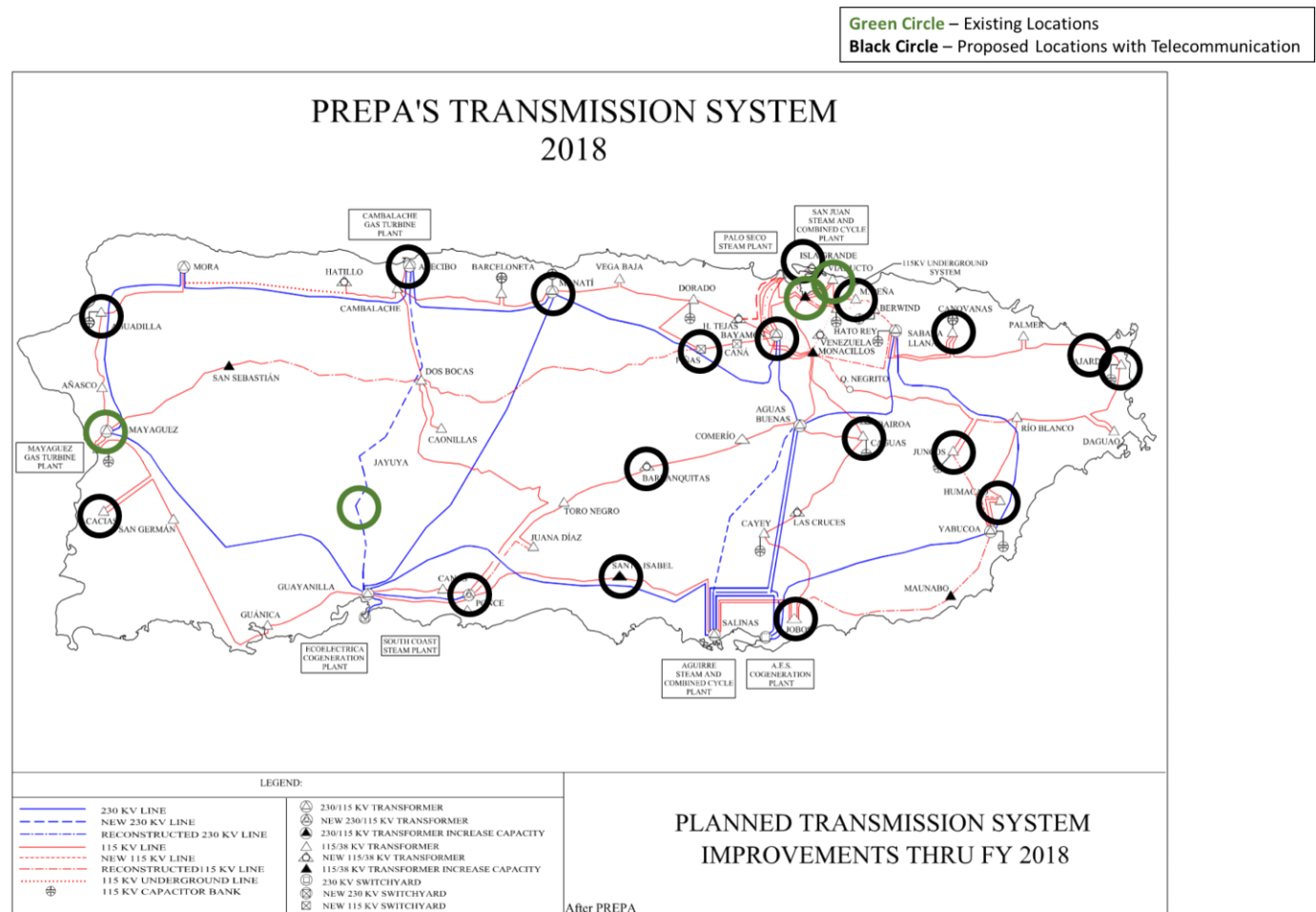


Figure 3.33. Map of existing and proposed UGA locations in Puerto Rico with annotations added to map from [38]

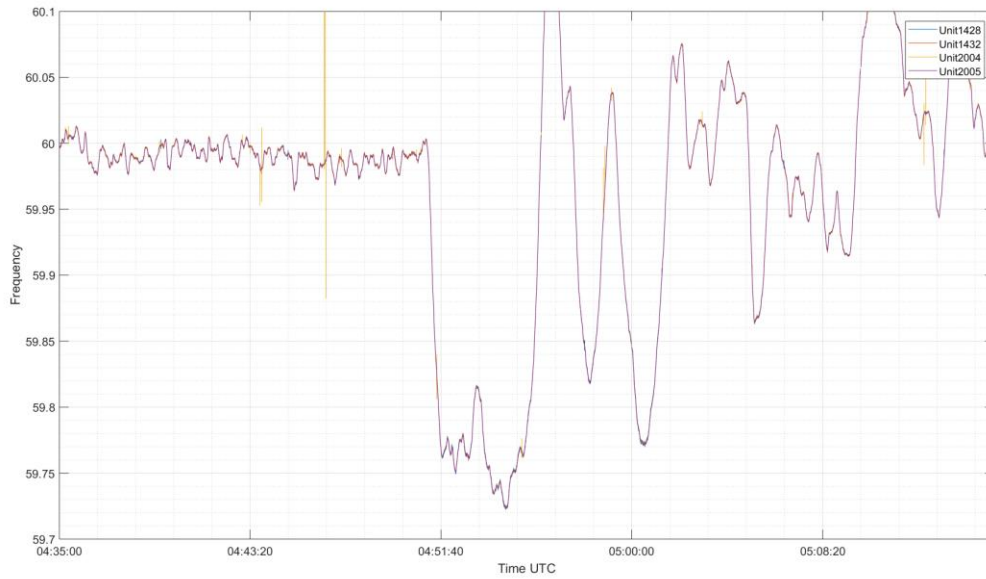


Figure 3.34. Frequency measured by UGAs during generation trip event followed by power swings detected on 08/02/2018 at 04:51:02 UTC



Figure 3.35. Frequency measured by UGAs during fast frequency ramp up or possible load drop detected on 09/03/2018 at 12:17:20 UTC

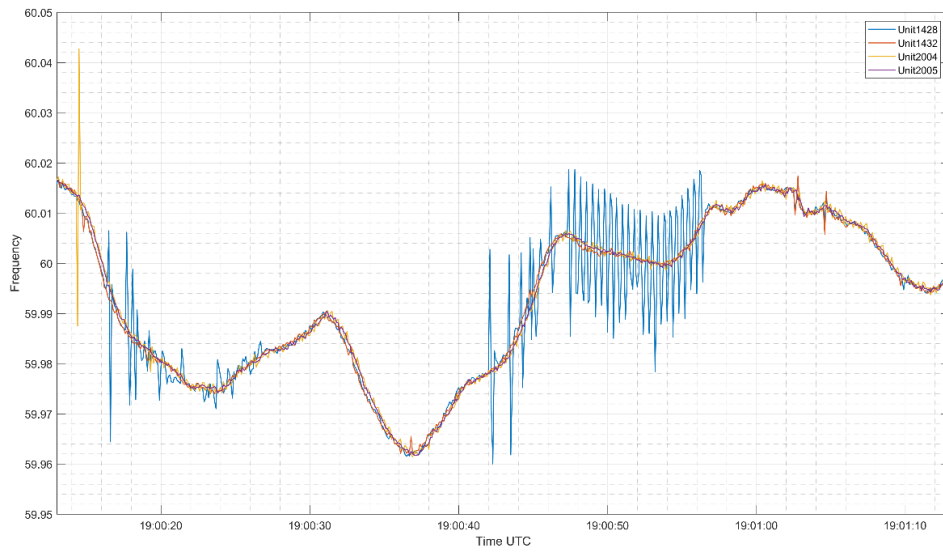


Figure 3.36. Frequency measured by UGAs during local oscillation detected on 08/02/2018 at 19:00:42 UTC

Dynamic Simulations Performed on the 2022 PREPA-Developed Model

After developing the transmission model for PREPA's 2018 model, additional models, developed by PREPA and Pacific Northwest National Laboratory (PNNL), were provided. These models were based on PREPA's system expected for years 2019, 2021, and 2022 but were developed before the hurricane occurred. Therefore, an additional model needed to be developed to represent the system as it was before the hurricane, along with other models that could represent the system during and after the rebuilding process. Before other post-hurricane models were created, one of the PREPA-developed models was used for study. The 2022 day-peak model was selected because it reflects the system's behavior under peak demand. A benefit of using the PREPA-developed model is increased detail of the model and equipment parameters. The 2022 PREPA-developed model contains 1,394 buses at the transmission, subtransmission, and distribution levels, with 91 in-service machines.

Branch corridor trips, similar to what were performed on the 2018 model, were simulated on the 2022 model. Since the 2022 model has a greater number of buses, more voltage levels, and different topology than the 2018 model, results are not directly comparable between the two models. Out of all branch corridor trip combinations, the worst case was tripping the clusters indicated in Figure 3.37, with overloading occurring at 27 buses in the system mostly at the 38kV level. The frequency response after tripping these branches is provided in Figure 3.38. These results show the criticality of the main branches that transfer power from the key generation facilities to the main load areas.

As Puerto Rico continues to rebuild their grid after recent hurricanes, increased solar penetration is expected to be integrated in the system. In the PREPA-developed 2022 peak demand case, the generation mix is approximately 29% renewable, when considering the real power output of in-service machines. Penetration was increased by approximately 20% each time by replacing non-renewable machines with real power output equal to approximately 20% of total generation. To substitute non-renewable machine models in the dynamic file, the generator model for the replaced machine was set to GEPVG, and the exciter model was set to GEPVE. These models are generic PV dynamic models developed by General Electric. Typical parameters for the GEPVG and GEPVE models are provided in Table 3.9 and Table 3.10.

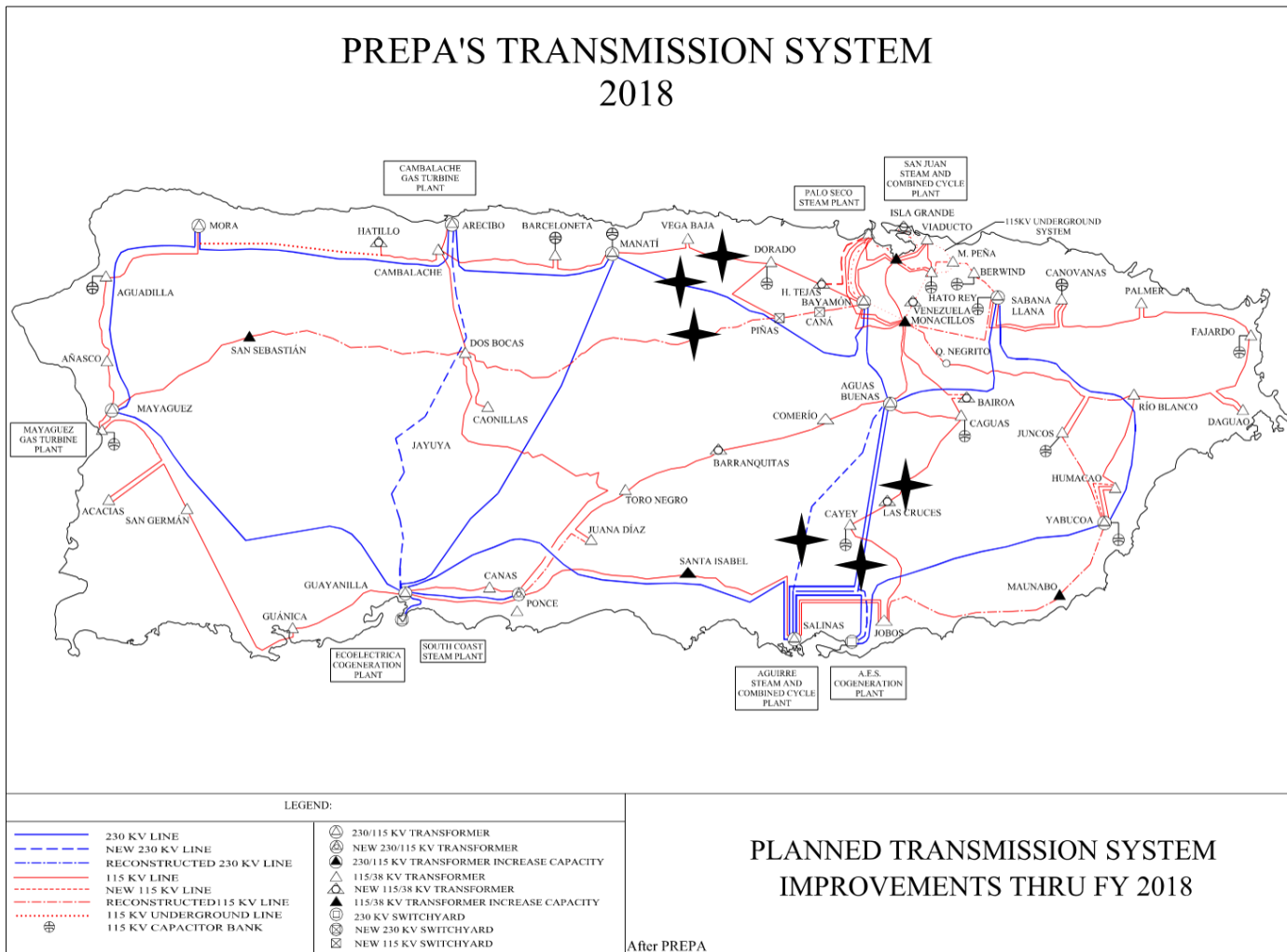


Figure 3.37. Worst-case corridor trip combination for 2022 PREPA-developed model with annotations added to map from [38]

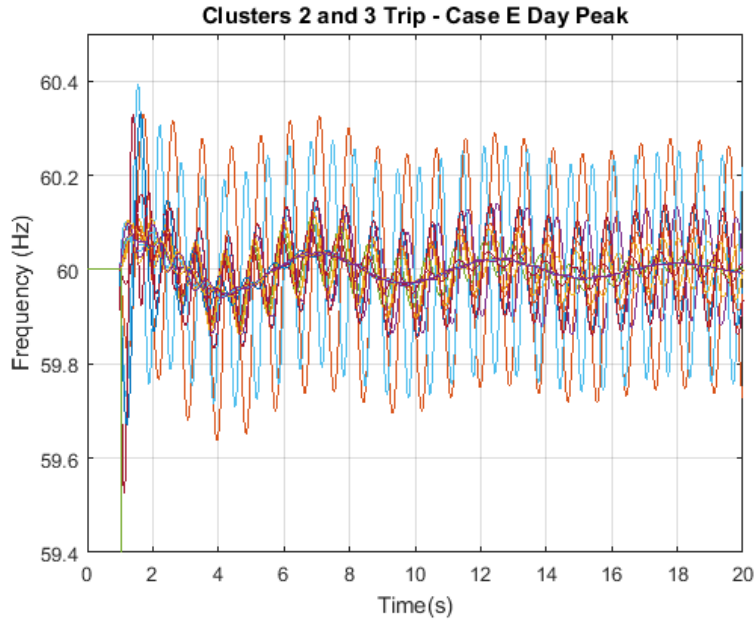


Figure 3.38. Frequency response of tripping worst-case corridor trip combination for 2022 PREPA-developed model

Table 3.9. Typical parameters for GEPVG model

Parameter	Value
Xeq-equivalent reactance for current injection	99999
VHVR2- HVR2 voltage 2	1.2
CURHVR2- Max reactive current at VHVR2	2.0
Rip_LVPL-Rate of active current change	5.0
T_LVPL-Voltage sensor for LVPL	0.02
LVPL voltage 1	0.0
LVPL power 1	0.0
LVPL voltage 2	0.5
LVPL power 2	0.167
LVPL voltage 3	0.9
LVPL power 3	0.9
XLVPL	0.0

Table 3.10. Typical parameters for GEPVE model

Parameter	Value
Tfv - V-regulator filter	0.15
Kpv - V-regulator proportional gain	18.0
Kiv - V-regulator integrator gain	5.0
Rc - line drop compensation resistance	0.0
Xc - line drop compensation reactance	0.0
QMX - V –regulator max limit	1.0
QMN - V –regulator min limit	-1.0
IPMAX – Max active current limit	1.12
TRV - V-sensor	0.02
KQi – MVAR/Volt gain	0.1
VMINCL	0.88
VMAXCL	1.15
KVi – VoltMVAR gain	120
XIQmin - min. limit for Eq'cmd	0.55
XIQmax – max. limit for Eq'cmd	1.55
TV - Lag time constant in WindVar Controller	0.05
Tp - Pelec filter in fast PF controller	0.05
Fn - A portion of the on-line PV controllers	1.0
ImaxTD – Converter current limit	1.12
Iphl - Hard active current limit	1.12
Iqhl - Hard reactive current limit	1.12
Tlpqd - Reactive droop time constant	5.0
Kqd - Reactive droop gain	0.0
Xqd - Reactive droop synthesizing Impedance	0.0
Vermx - Reactive power control maximum error signal	0.01
Vermn - Reactive power control minimum error signal	-0.01
Vfrz - Reactive power control freeze voltage	0.7
PFAFLG: (=1 if PF fast control enabled)	0.0
VARFLG: (=1 if Qord is provided by SolarVar)	1.0
PQFLG: (=1 for P priority, =0 for Q priority)	1.0

The solar penetration of the system was increased by replacing more non-renewable machines with solar. The graphs in Figure 3.39, Figure 3.40, and Figure 3.41 show the dynamic effects of tripping a machine at the Ecosteam Power Plant, 98.5 MW of generation, at various penetration levels without relays incorporated into the model. Frequency of each machine was monitored. From the results, it can be seen that the frequency nadir, or minimum post-contingency frequency, decreases as solar penetration increases.

Additionally, frequency does not appear to settle for a long duration, even after 30 seconds, in cases with higher solar levels. These results infer the system becomes less stable with increased penetration. Because large rotating machines are being replaced with solar, some inertia in the system is lost. Frequency nadir and setting frequency are directly affected by system inertia level.

These simulations were repeated with the inclusion of load and line relays in the system. Under-frequency load and line relays were included in the original 2022 PREPA-developed model. The load relay protection model was DLSHBL. This protection model was only added to some of the load buses at the 38kV level. The parameters for each DLSHBL protection model, listed in Table 3.11, varied for each individual load so that different loads were shed at specified frequencies and times. UFLT relays were set so that if the frequency, measured at a certain bus, dropped below a threshold for the duration of the under-frequency timer, a specified branch would trip. The main parameters for this model include the under-frequency threshold, under-frequency timer, and the bus for the frequency measurement. Machine voltage and frequency relays were not included in this model. System frequency response of tripping 98.5 MW, with relays included in the model, is presented in Figure 3.42, Figure 3.43, and Figure 3.44. Load and line under-frequency relays reduced the magnitude of swings in frequency seen in the system and increased the frequency nadir. Despite this, frequency nadir still drops with increased solar penetration. Sustained oscillations are also seen for cases with more solar.

Summary

Through this project, UTK was able to provide DOE with a 2018 transmission study model based on data provided in PREPA's Fourteenth Annual Report and operational profile provided on their website. Additionally, system security was assessed through corridor trip simulations and increased solar penetration. These studies provided DOE with more insight into with what areas of the system are most vulnerable and how dynamic response is affected by increased solar integration.

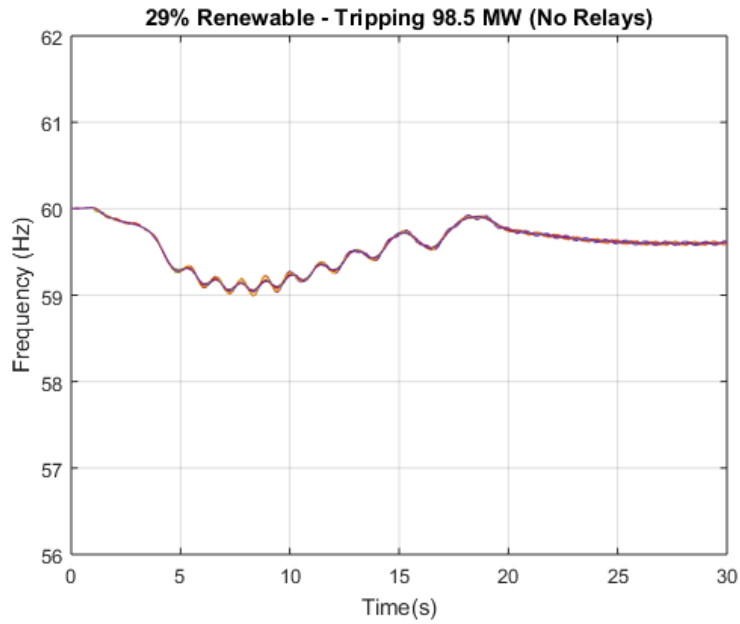


Figure 3.39. Frequency response of tripping 98.5 MW in 2022 PREPA-developed system with 29% renewable penetration

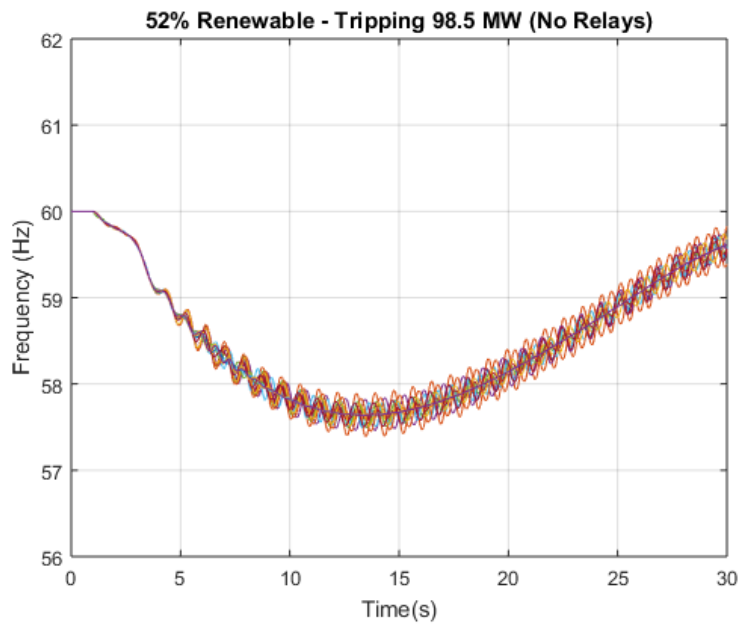


Figure 3.40. Frequency response of tripping 98.5 MW in 2022 PREPA-developed system with 52% renewable penetration

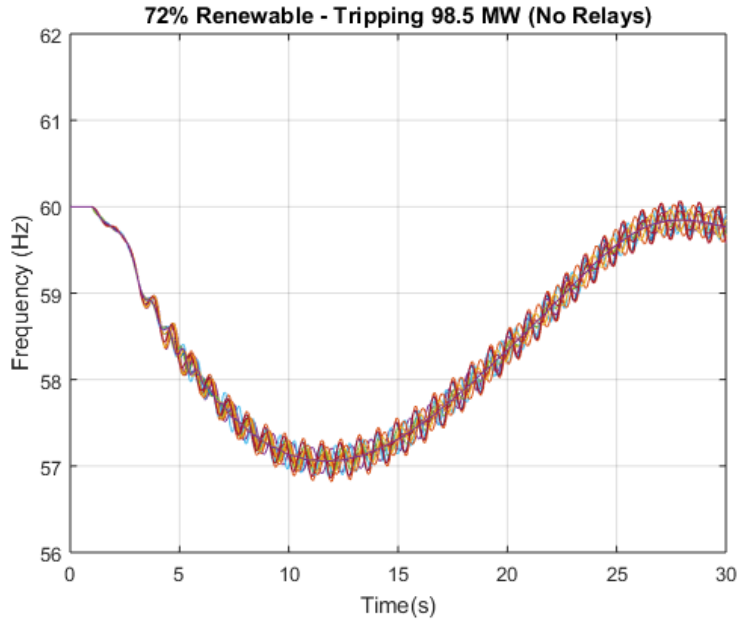


Figure 3.41. Frequency response of tripping 98.5 MW in 2022 PREPA-developed system with 72% renewable penetration

Table 3.11. Parameters for DLSHBL load under-frequency protection model

Con Number	Con Description
1	f1, first load shed point (Hz)
2	t1, first point pickup time (Sec.)
3	frac1, first fraction of load shed
4	f2, second load shed point (Hz)
5	t2, second point pickup time (Sec.)
6	frac2, second fraction of load shed
7	f3, third load shed point (Hz)
8	t3, third point pickup time (Sec.)
9	frac3, third fraction of load shed
10	TB, breaker time (Sec.)
11	df1, first rate of freq. shed pt. (Hz/sec.) (≥ 0)
12	df2, second rate of freq. shed pt. (Hz/sec.) (≥ 0)
13	df3, third rate of freq. shed pt. (Hz/sec.) (≥ 0)

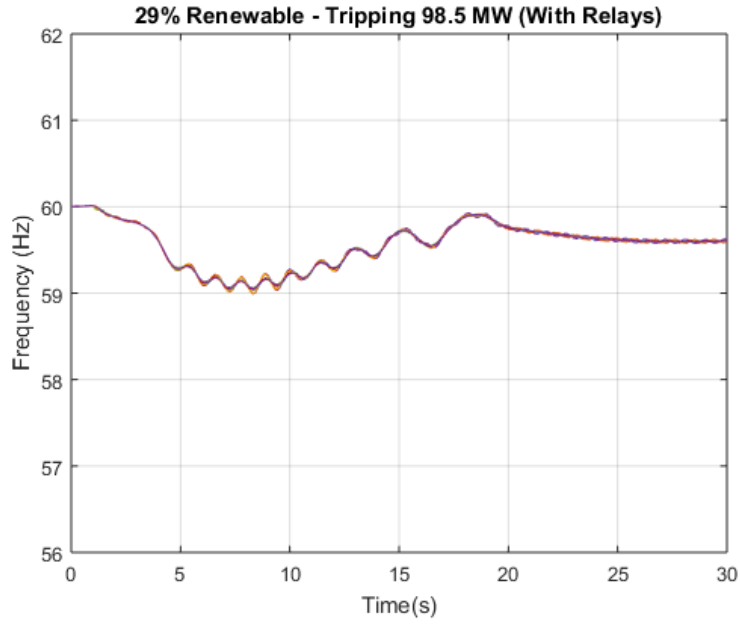


Figure 3.42. Frequency response of tripping 98.5 MW in 2022 PREPA-developed system with 29% renewable penetration and load and line relays

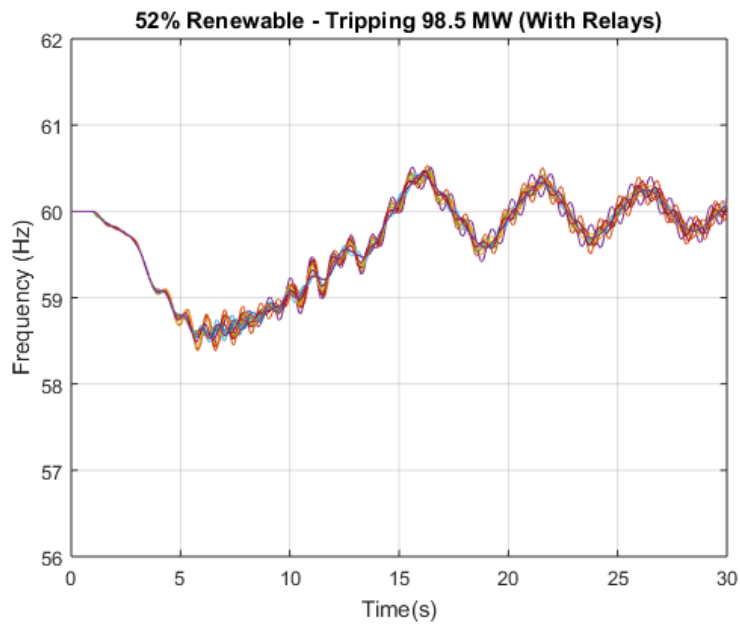


Figure 3.43. Frequency response of tripping 98.5 MW in 2022 PREPA-developed system with 52% renewable penetration and load and line relays

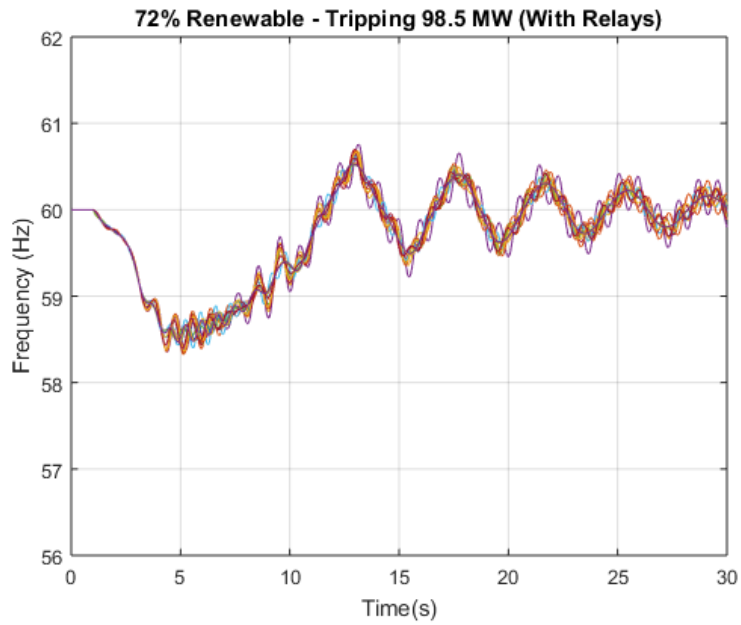


Figure 3.44. Frequency response of tripping 98.5 MW in 2022 PREPA-developed system with 72% renewable penetration and load and line relays

ASSESSING SECURITY DURING CYBER-ATTACKS AND WIDE-AREA PHYSICAL ATTACKS ON BULK ELECTRIC SYSTEM ASSETS

The focus of the study was to analyze the effects of targeted attacks on substations, or a specific group of substations. It was assumed that the intended attack was successful and that contingencies have occurred. This security assessment primarily focuses on dynamic frequency stability immediately following a major contingency. The study involves two main parts: 1) creating a geographic map representing the system model used in the study and 2) performing possible cyber-attack scenarios and analyzing the system's response.

Literature Review

On December 23rd, 2015, the first successful cyber-induced power outage that disrupted an electric power grid occurred in Ukraine. Up to 225,000 customers were affected over the 6-hour period of the attack, with more than 50 substations impacted [44]. The primary equipment remotely operated within the substations were circuit breakers [45]. Most of these stations were at the transmission and sub-transmission level. For 3 hours following attack, 7 110kV and 23 35kV substations were disconnected [45].

The success of an attack on the bulk electric system reiterates the enforcement of North American Electric Reliability Corporation (NERC) Critical Infrastructure Protection (CIP) standards, which involve identifying, categorizing, and protecting critical assets. The attack also revealed how vulnerable the power grid can be and what catastrophic consequences a cyber-attack could have. Some of the largest electric utilities in the U.S. cover a huge territory and serve millions of customers, which makes them potential targets of hackers. For example, Dominion Energy's generating facilities produce approximately 31 GW electric power and its network consists of 93,600 miles of transmission and distribution lines [46]. If a hacker manages to hack into a large electric utility's control center into the supervisory control and data acquisition (SCADA) system, catastrophic consequences could occur. Although the SCADA Internet Protocol (IP) communication network should be separated from other corporate networks, hackers can gain access to SCADA at either the supervisory control level or the direct control level. The supervisory control level is comprised of a user interface that allows operators to monitor and control system equipment; the direct control level contains devices, such as programmable logic controllers (PLCs) and remote terminal units (RTUs) that actuate system equipment under specified conditions [47]. If firmware of direct control level devices is not updated,

encryption data protocols are not used for data transmission, or devices are not properly password protected, these controllers could be vulnerable to an attack [47].

Threats of an attack of from an electromagnetic pulse (EMP) are also a major concern. An EMP is a nuclear weapon detonated in the upper atmosphere so that a pulse causes interference with electronic devices across a large geographic area [48]. The effects of an EMP depend on the size of the weapon, along with the altitude at which the EMP is detonated. In some cases, an EMP may be able to take out an area as big as an entire large city, or country in some cases. A geomagnetic disturbance (GMD) is caused by solar flares and associated coronal mass injections, or solar storms [49]. A GMD induces transmission lines with additional, unregulated current, causing mechanical failures and power outages [49].

According to previous research in cyber-attacks on bulk electric systems, more research is needed to predict stability of several combinations of hypothesized attacks, such as tripping multiple substations, considering both their steady-state and dynamic effects [50]. This would reduce the number of permutations of possible attacks and identify critical points in the system. Previous studies have developed algorithms, such as the reverse pyramid model, to identify combinations of critical substations, that when disconnected could cause cascading outages [51]. Though these methods are useful for classifying substations as critical or non-critical based on power flow, they do not always recognize dynamic behaviors that may cause instability. Dynamic security assessment is necessary because even though a system may converge in power flow, the system may not be dynamically stable after certain contingencies have occurred. In past research that looks at both power flow and dynamic study of cyber-attacks, substations are classified as being critical or non-critical. In one study, dynamic effects are created by the sequence of switching actions. Further research is needed to determine critical switching actions that would cause the system to become unstable, even if a system could still be defined as stable in steady state [50]. Therefore, in this study, dynamic stability of the system is assessed while multiple substations are switched offline at once in various configurations to create more vulnerable scenarios.

Development of the Atlantis 9000 Model Mapping for the Purpose of Cyber-Security System Study

4.1.1 Introduction of Atlantis 9000 Model

The purpose of the Atlantis 9000 model was to assign GPS coordinates to a system in PSS®E where GPS coordinates are not provided, and then display the system on a map. For the cybersecurity study, the mapping tool provides a way

to geographically display the size of a critical contingency. The model is named Atlantis because the system is mapped to represent an imaginary island, and 9000 is the approximate number of buses in the system. Two different methods were used to generate a map of the system: 1) programmatic conversion of PSS®E Cartesian coordinates to GPS coordinates and 2) Power Systems Graphic Toolbox (PSGT) developed by Dr. Zhuohong Pan.

4.1.2 Programmatic Conversion of PSS®E Cartesian Coordinates to GPS Coordinates

4.1.2.1 Step 1: Mapping in PSS®E

The Auto-Draw function in PSS®E allows a user to create a diagram centered on a bus and then grow the diagram up to 15 levels from the center bus. In the following example, a system containing 9,241 buses is shown. To include all 9,241 buses in the diagram, the diagram was expanded several times. This was achieved by selecting a border bus as the center bus and growing the diagram 15 levels from this bus. A full diagram containing all buses and branches in the system is presented in Figure 4.1.

4.1.2.2 Step 2: Conversion of Bus Cartesian Coordinates to GPS Coordinates

Cartesian coordinates of a diagram in PSS®E can be extracted by exporting bus locations as Cartesian coordinates. These coordinates were saved into a PSS®E location file and then copied into a Python script. The Python script converted the Cartesian coordinates to GPS coordinates by assigning a scale of the X and Y coordinates to latitude and longitude, respectively. A GPS origin was provided so that the user could assign where to center the map on the globe. In the example provided, the origin was specified as a point in the middle of the Atlantic Ocean since the diagram did not geographically correspond to any geographic continent. A rotation function was also included so the system could be rotated 90 degrees clockwise. The modified coordinates were then written to a CSV file.

4.1.2.3 Step 3: Displaying System in Google Earth

In Google Earth, a list of GPS coordinates, in latitude/longitude pairs, can be imported from a CSV file, as long as “Latitude” and “Longitude” are given as the first two column headings and each corresponding points are underneath these headings. A map of the system in Google Earth is shown in Figure 4.2

4.1.3 Mapping the System Using PSGT

PSGT is a tool developed by Dr. Zhuohong Pan. The purpose of the tool is to locate substations and transmission lines on a map with computer-aided design to display data and results. PSGT displays power grids based on GPS coordinates of the system; draws lines according to the topology; and color-codes areas of the system by the area, zone, voltage level, or other attributes.



Figure 4.1. Atlantis 9000 system diagram showing buses and branches

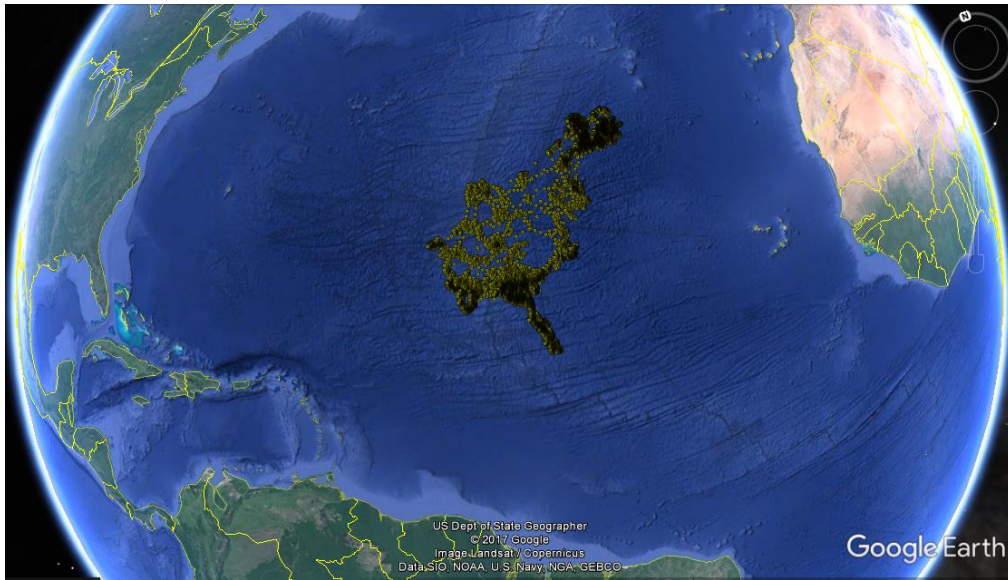


Figure 4.2. Google Earth view of Atlantis 9000 system

A more detailed description of how to use the tool is in the Appendix in Section A.4. The 9,241-bus system mapped previously in Google Earth was also mapped in the PSGT tool. The system is color-coded by zone and by voltage levels in Figure 4.3 and Figure 4.4, respectively. The 9,241-bus system contains 24 zones and 9 voltage levels ranging from 110kV-750kV. Zone 1 acts as an interconnection between the other 23 zones.

Modeling Dynamic Effects of Possible Cyber-Attack Scenarios

The Atlantis 9000 model was used for all simulations in studying the effects of cyber-attack scenarios. The simulations performed could imitate someone hacking into a large electric utility, attacking a Regional Transmission Organization (RTO) or Independent Service Organization (ISO), or even creating a cascading cyber-attack. An example of a cascading cyber-attack would be if a group of cyber-attackers hack into more than one electric utilities/RTO/ISO in an organized way. In this case, the entire interconnection may be in danger because of the system synchronization. Though many types and combinations of contingencies could be introduced during a cyber-attack, worst case scenarios were considered, starting from tripping the largest generators, loads, or major substations within areas of the system. During the initial phases of this project, frequency and voltage stability issues were the focus of this impact evaluation study, although small-signal, and transient stability issues could also be considered. The base frequency of the Atlantis 9000 model is 50 Hz. The system contains 353,178.8 MW of total generation and 340,610.8 MW of total load.

4.1.4 Scenario #1: Tripping Largest Generation Facilities within a Given Zone

This scenario simulates the effects of a hacker obtaining access to a large electric utility's control center. In this part, dynamic simulations were conducted to investigate the impacts of shutting down multiple generation facilities within an electric utility.

For example, in Zone 6, all generation facilities over a specified real power output were tripped in each simulation. Zone 6 had 133 machines with a combined real power output of approximately 38,779 MW. The threshold was adjusted until a boundary between convergence and divergence of the system was obtained.

From the results, the system diverged when tripping generator buses with output greater than 565 MW and converged when changing this threshold to 570 MW. The results, summarized in Table 4.1 and Table 4.2, show the boundary of percentage of total generation in the system tripped is around 4%.

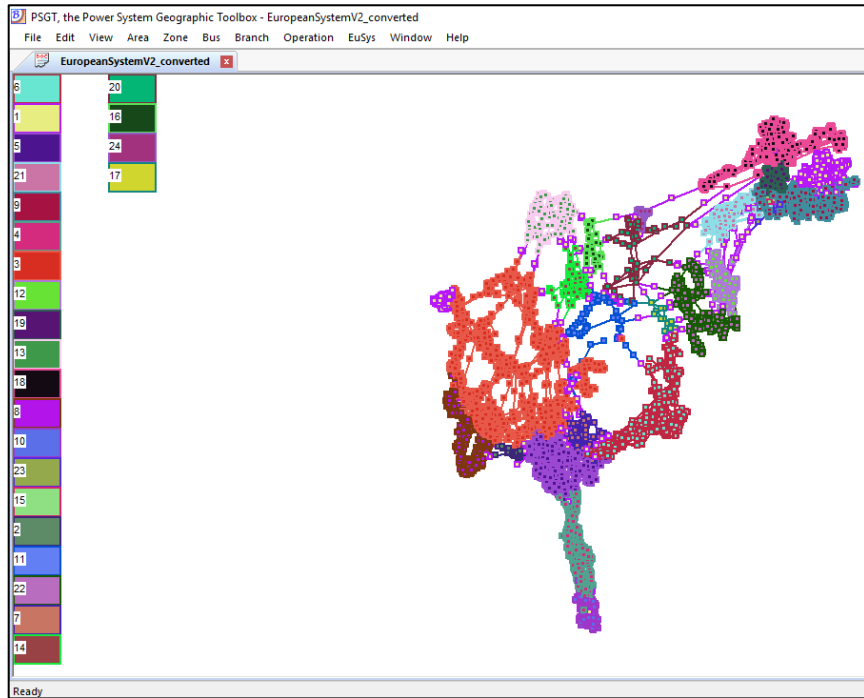


Figure 4.3. Zone view in PSGT

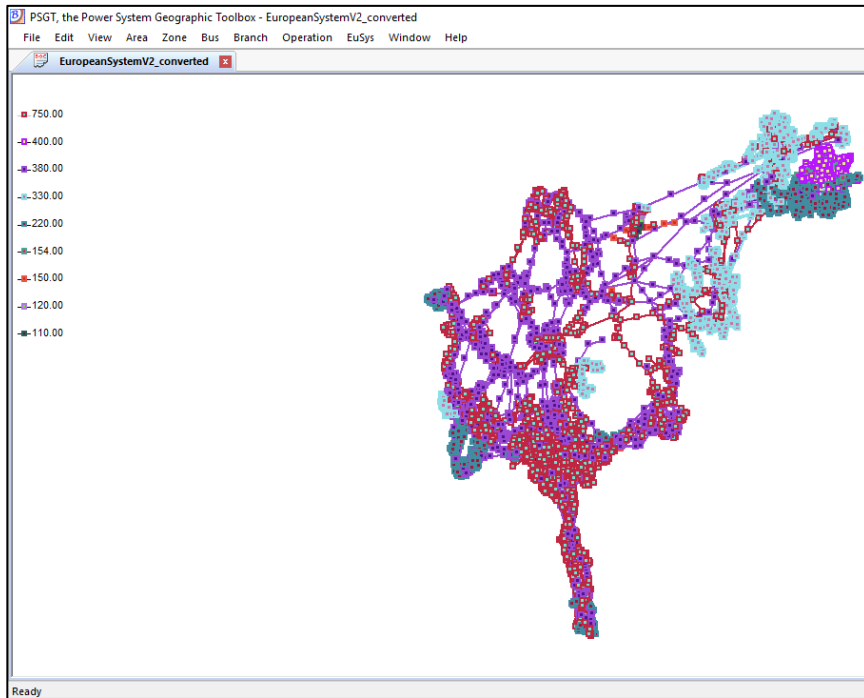


Figure 4.4. Voltage level view in PSGT

Table 4.1. Summary of simulations results from tripping generator buses with output greater than 570 MW in Zone 6

Threshold (MW)	570
Total Tripped (MW)	14131.02
Total Generation in Zone (MW)	39778.96
Percentage of Generation in Zone Tripped	35.52%
Percentage of Generation in System Tripped	4.00%
Convergence	Yes

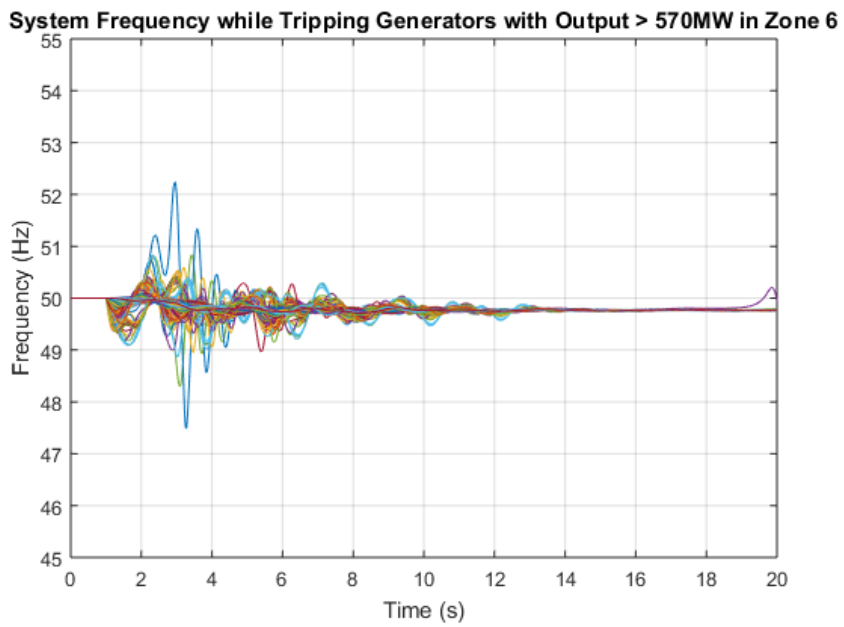


Figure 4.5. Frequency response of tripping generators with output greater than 570 MW in Zone 6

System Voltage while Tripping Generators with Output > 570MW in Zone 6

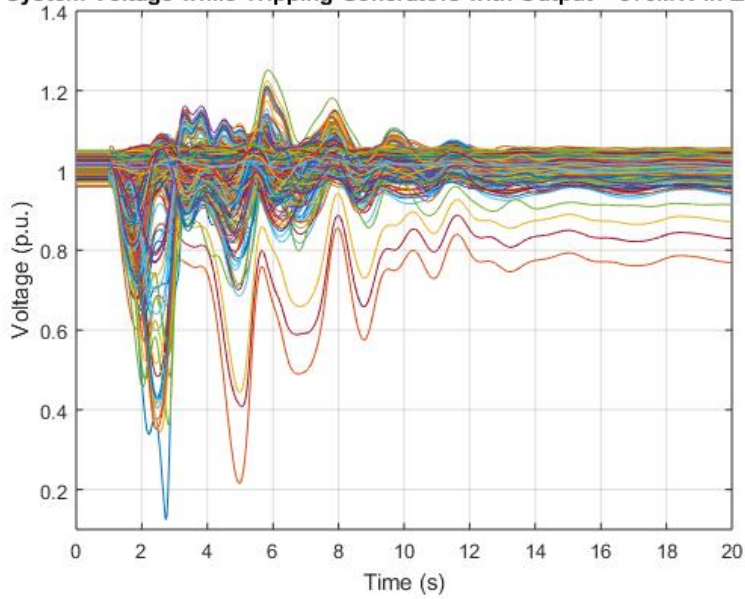


Figure 4.6. System voltage while tripping generators with output greater than 570 MW in Zone 6

Table 4.2. Summary of simulations results from tripping generator buses with output greater than 565 MW in Zone 6

Threshold (MW)	565
Total Tripped (MW)	14698.02
Total Generation in Zone (MW)	39778.96
Percentage of Generation in Zone Tripped	36.95%
Percentage of Generation in System Tripped	4.16%
Convergence	No

System Frequency while Tripping Generators with Output > 565MW in Zone 6

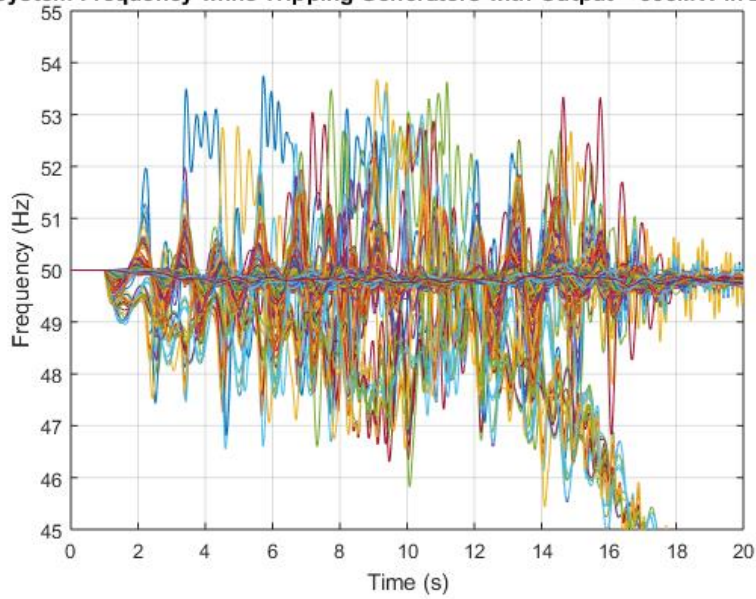


Figure 4.7. Frequency response of tripping generators with output greater than 565 MW in Zone 6

System Voltage while Tripping Generators with Output > 565MW in Zone 6

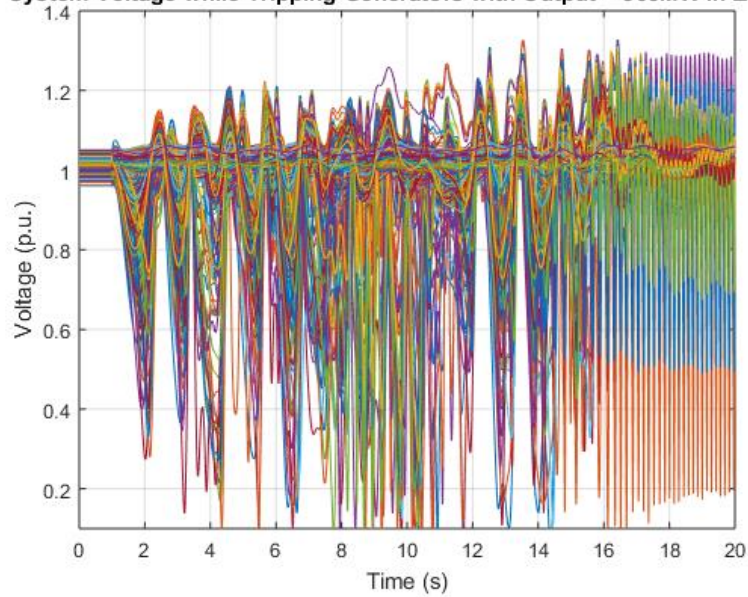


Figure 4.8. System voltage while tripping generators with output greater than 565 MW in Zone 6

Although frequency appears to be stable when tripping generators with output greater than 570 MW, some buses deviate outside of stable voltage limits (0.95 p.u.-1.05 p.u.) when approaching the border. When the threshold is changed so that all generators greater than 565 MW are tripped, frequency splits into two separate systems, and the voltage is clearly out of stable limits at several buses.

Scenario #1 was repeated for several zones. The ratio of generation tripped to total system generation was below 10% for all cases tested, but the threshold and percentage of generation tripped in the zone greatly varied depending on the size of the zone.

4.1.5 Scenario #2: Tripping Multiple High-Voltage Substations in a Given Zone

An RTO/ISO coordinates, controls and monitors the operation of the electric transmission system encompassing a large area. If a hacker seizes an RTO/ISO SCADA under control using malware, he or she can remotely switch substations off and potentially disrupt electricity supply to several customers. In this scenario, a successful hacking of an RTO/ISO is simulated by tripping a number of high-voltage substations within a large zone.

As mentioned in Section 4.2, the system contains nine voltage levels ranging from 110kV-750kV. Because the Atlantis 9000 model is a transmission model without showing distribution details, load buses were typically included at the lower end of the transmission voltage range. Step-up transformers were also included in the model to increase the voltage at substations connecting generation facilities to the grid. Though all system voltage levels were considered high-voltage, substations at only the highest voltages were selected to trip. Since only three buses in the system were at 750kV, buses at 400kV tripped. The 400kV buses were all located in Zone 1, which acts as the main interconnection between the other 23 zones.

In Zone 1, there are 126 buses at 400kV. If all 126 buses are tripped, the system diverges. Therefore, a set number of the 400kV buses were selected to trip at one time. The exact 400kV buses to trip in Zone 1 were selected at random. In a specific example using this method, the maximum number of 400kV buses that could be tripped without the system diverging was 20 buses. The frequency response and bus voltages, monitored at the machine buses, while disconnecting 20 400kV buses are displayed in Figure 4.9 and Figure 4.10.

From the plots, it can be seen that frequency and voltage are stable after disconnecting a random set of 20 400kV buses in Zone 1. If one additional 400kV bus is tripped in Zone 1, system frequency and voltage are no longer stable, as seen by the plots in Figure 4.11, Figure 4.12, and Figure 4.13.

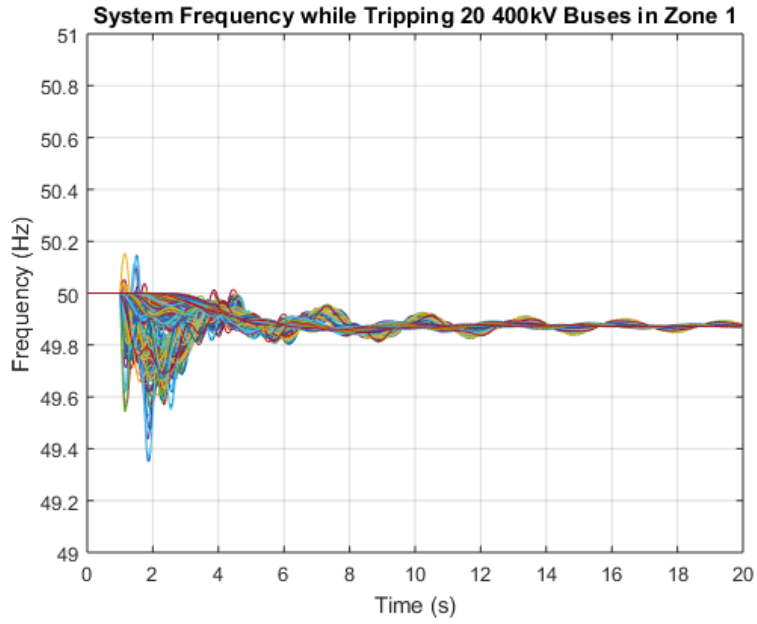


Figure 4.9. Frequency response of tripping 20 400kV buses in Zone 1

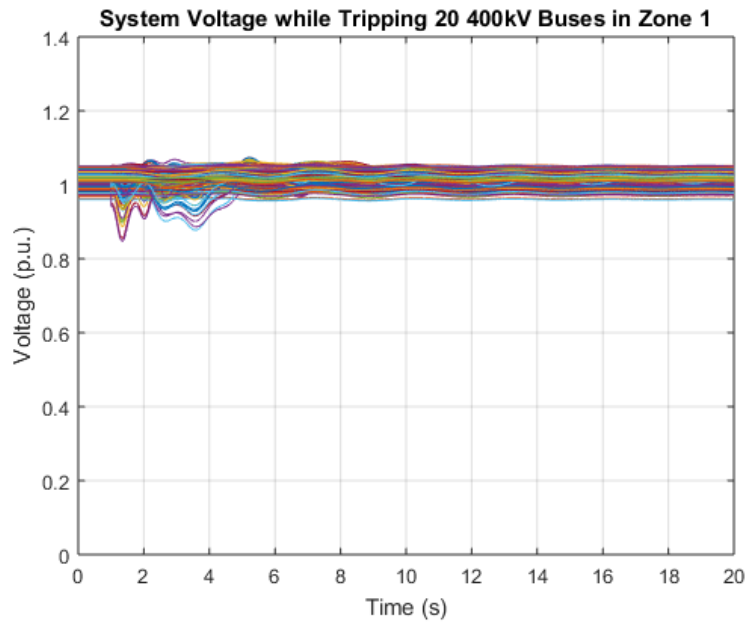


Figure 4.10. System voltage while tripping 20 400kV buses in Zone 1

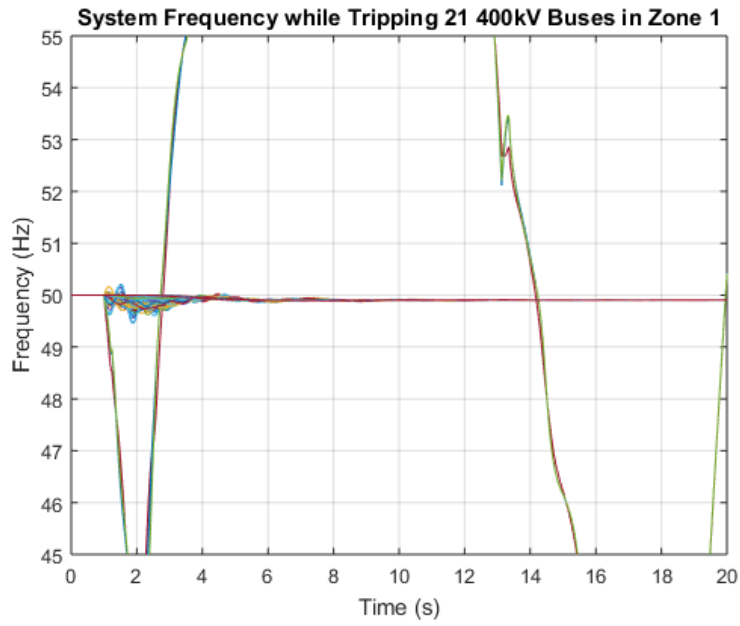


Figure 4.11. Frequency response of tripping 21 400kV buses in Zone 1

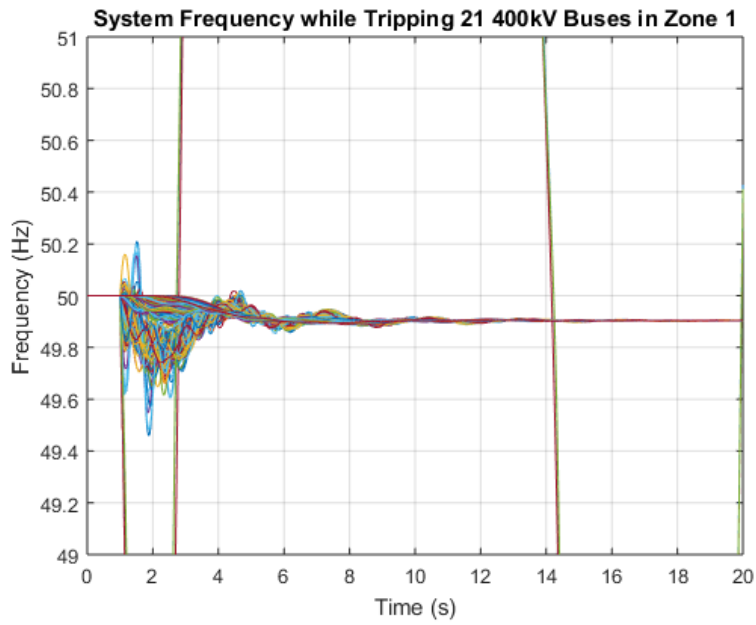


Figure 4.12. Frequency response of tripping 21 400kV buses in Zone 1 zoomed in view

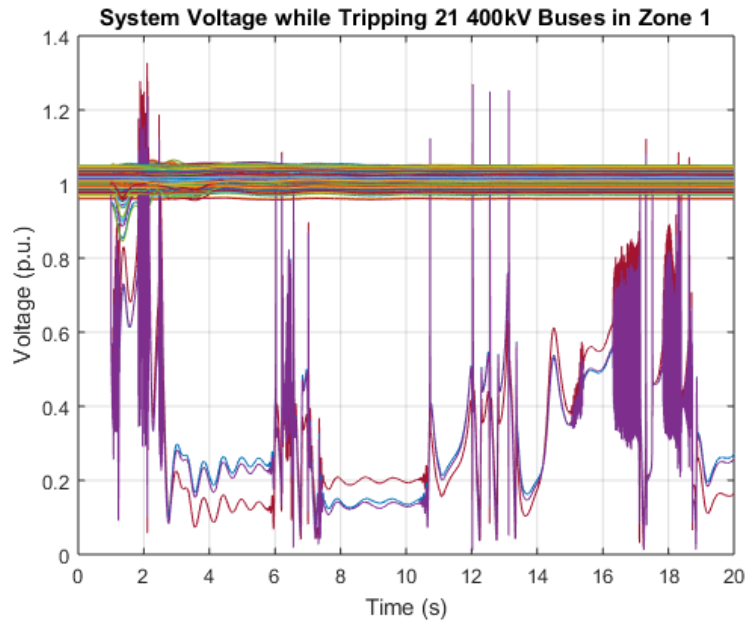


Figure 4.13. System voltage while tripping 21 400kV buses in Zone 1

The system appears to split into two parts, with some machines stabilizing around nominal voltage and frequency, while others continue to wildly oscillate. The number of 400kV buses in Zone 1 tripped that cause instability vary depending on what set of buses are selected to trip. In some cases, even tripping less than 10 400kV buses could cause instability due to the criticality of the buses.

4.1.6 Scenario #3: Radial Area Attack Created by Tripping N-Levels from the Largest Generator in a Given Zone

This scenario models the effects of an EMP or strategic cyber-attack targeting a specific radial area of the system. The largest generator in a specified zone was selected as the origin point for the attack. The geographic area affected by the attack was expanded, in stages, to determine the point where the system would no longer be stable. The contingency expansion was performed by disconnecting buses at each level from the origin, along with the transmission lines between them. Although any generator in a zone could be chosen at the origin point, the largest generator was selected because it represents the largest N-1 contingency. First, a simulation was run in PSS®E where the largest generator bus was tripped in Zone 20. Under this contingency, the frequencies of all machine buses in the system were monitored and plotted over a period of 20 seconds, as seen in Figure 4.14 and Figure 4.15.

This scenario targets a group of directly connected substations. The goal was to determine the maximum amount of load and generation that could be tripped before the system diverged, essentially by seeing how many substations directly connected to the selected bus could be tripped. To do this, a series of contingencies were applied in stages. First, the bus containing the largest generator within a particular zone was tripped. The example shown in is bus 7979 in Zone 20. Next, every bus directly connected to the bus containing the largest generator was also tripped. In this example, the buses directly connected to bus 7979 are buses 8580, 8715, 4817, 5062, and 6790. This step was called Stage 1 and is represented in Figure 4.17. In Stage 2, every bus connected to the additional buses tripped in Stage 1 were also tripped. The buses included in Stage 2 are shown in Figure 4.18. Five buses are connected to buses 8580, 8715, 4817, 5062, and 6790.

Simulations were run for each additional contingency stage. The size of the contingency was grown by one level at a time until the system diverged. The system frequency responses of tripping a number of bus levels from the largest generator in Zone 20 are included in Table 4.3 through Table 4.7. The frequency of every machine bus in the entire system was monitored for a period of 20 seconds, with the contingency being introduced at 1 second.

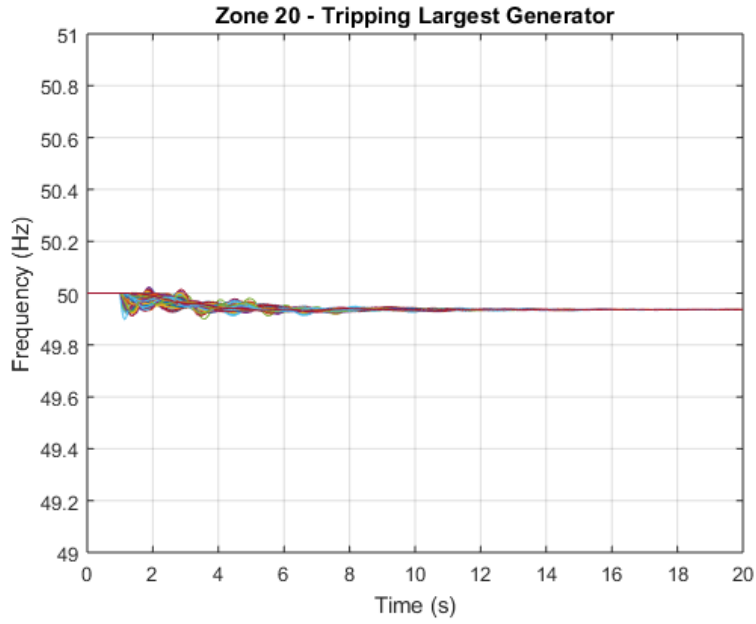


Figure 4.14. Frequency response while tripping the largest generator in Zone 20

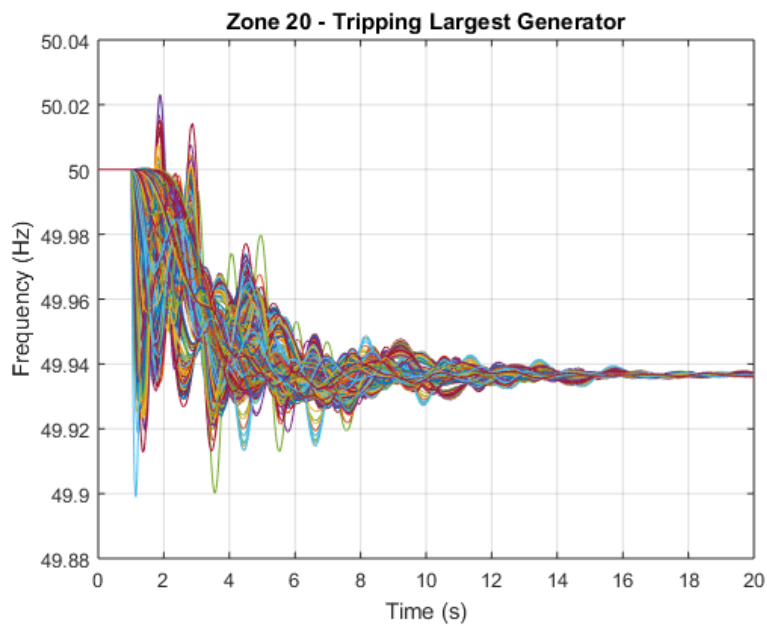


Figure 4.15. Frequency response while tripping the largest generator in Zone 20 zoomed in view

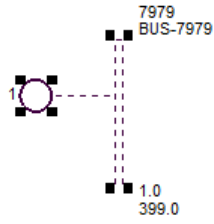


Figure 4.16. Atlantis 9000 model generator bus 7979

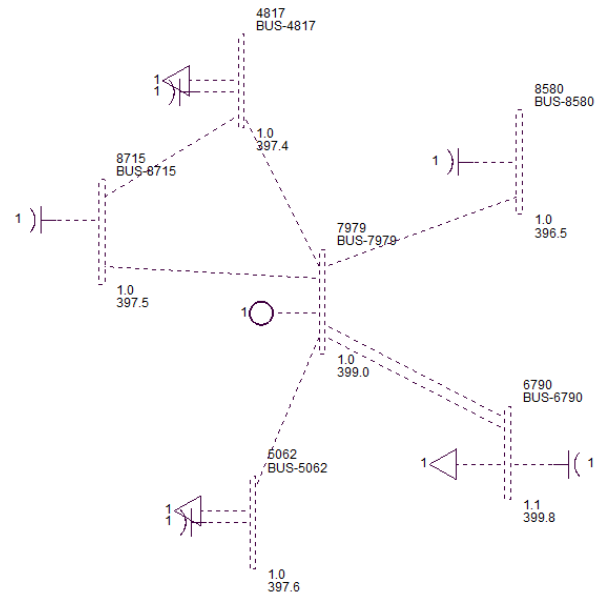


Figure 4.17. Atlantis 9000 Stage 1 connections to bus 7979

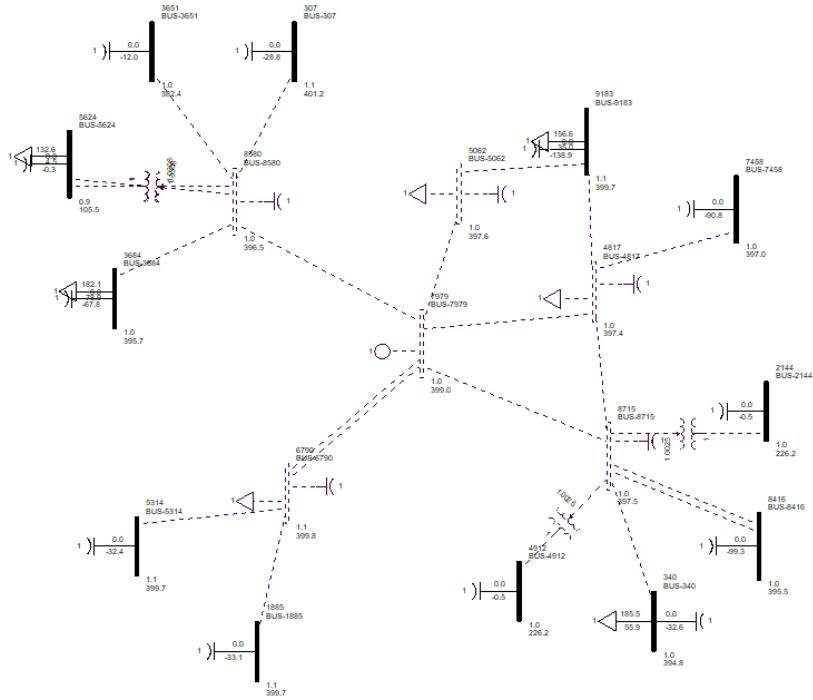


Figure 4.18. Atlantis 9000 Stage 2 connections to bus 7979

Table 4.3. Frequency response of tripping 1 level from largest generator in Zone 20

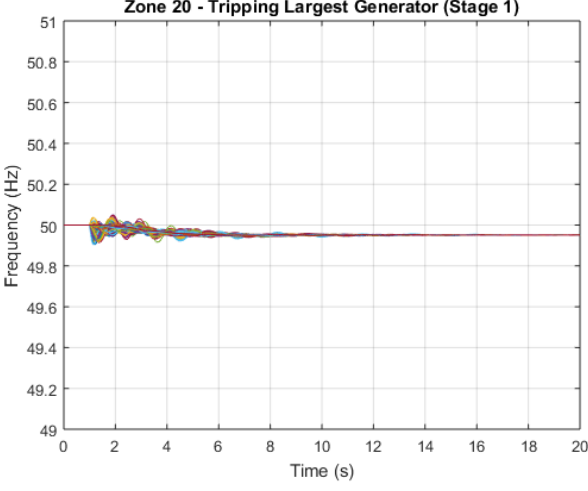
Contingency Frequency Response	Total Load Tripped	Total Generation Tripped
	586 MW	1637 MW

Table 4.4. Frequency response of tripping 2 levels from largest generator in Zone 20

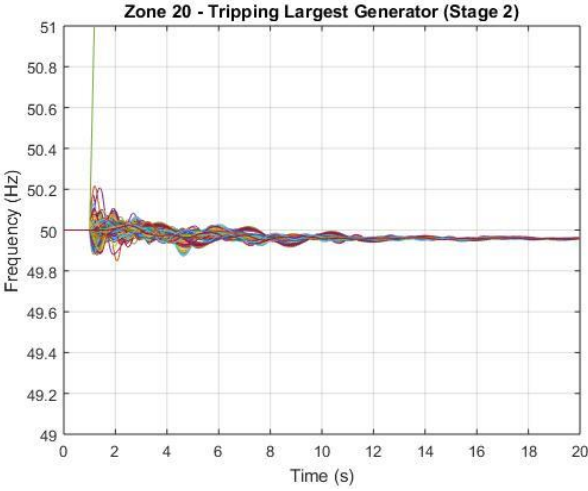
Contingency Frequency Response	Total Load Tripped	Total Generation Tripped
	1264 MW	1637 MW

Table 4.5. Frequency response of tripping 3 levels from largest generator in Zone 20

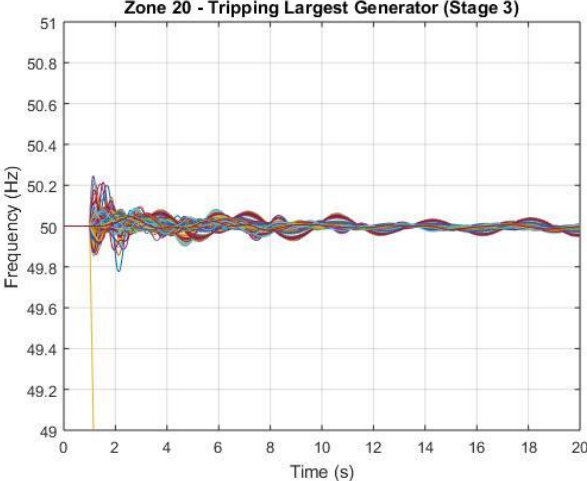
Contingency Frequency Response	Total Load Tripped	Total Generation Tripped
	1929 MW	2804 MW

Table 4.6. Frequency response of tripping 4 levels from largest generator in Zone 20

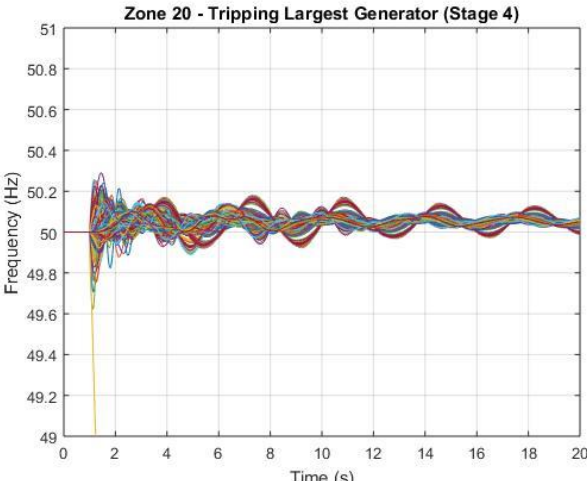
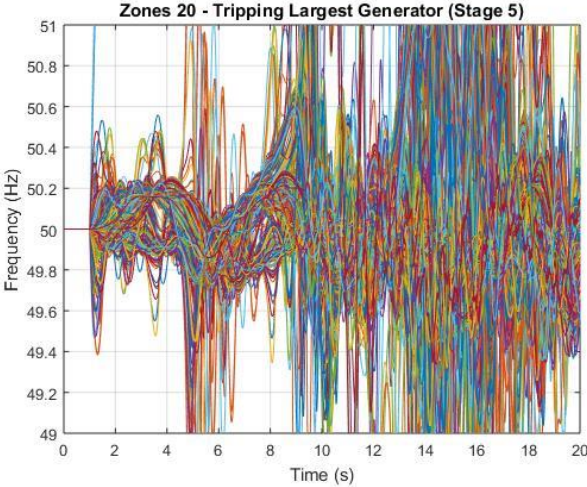
Contingency Frequency Response	Total Load Tripped	Total Generation Tripped
	4008 MW	2988 MW

Table 4.7. Frequency response of tripping 5 levels from largest generator in Zone 20

Contingency Frequency Response	Total Load Tripped	Total Generation Tripped
	6369 MW	5292 MW

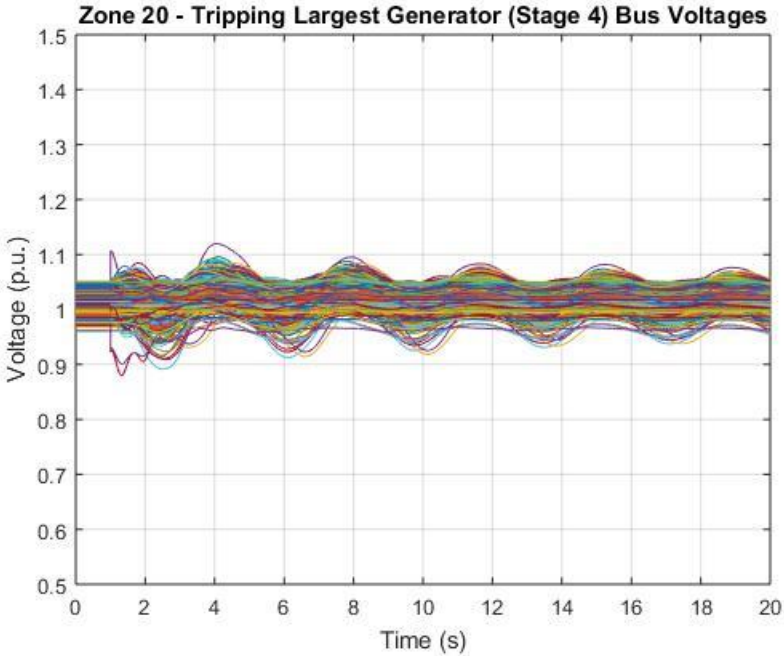


Figure 4.19. System voltage while tripping 4 levels from largest generator in Zone 20

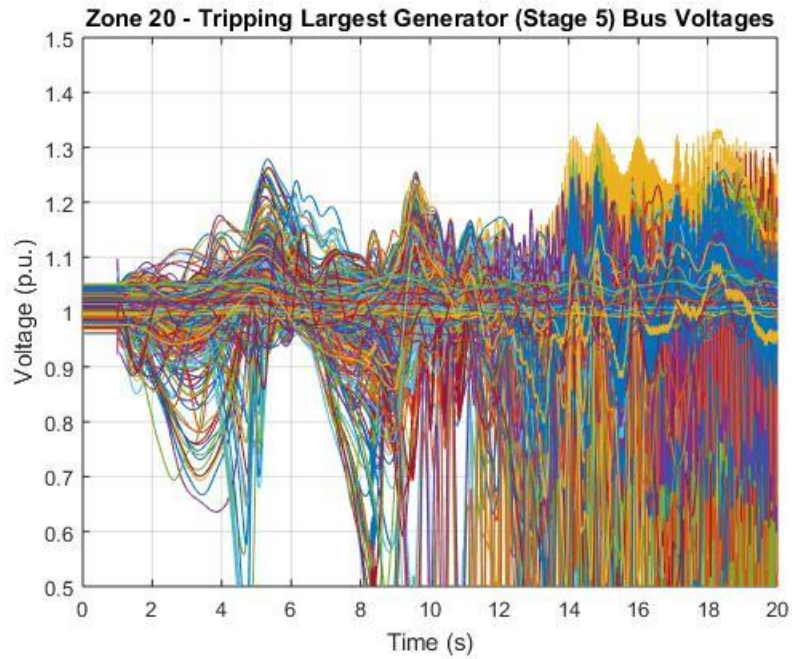


Figure 4.20. System voltage while tripping 5 levels from largest generator in Zone 20

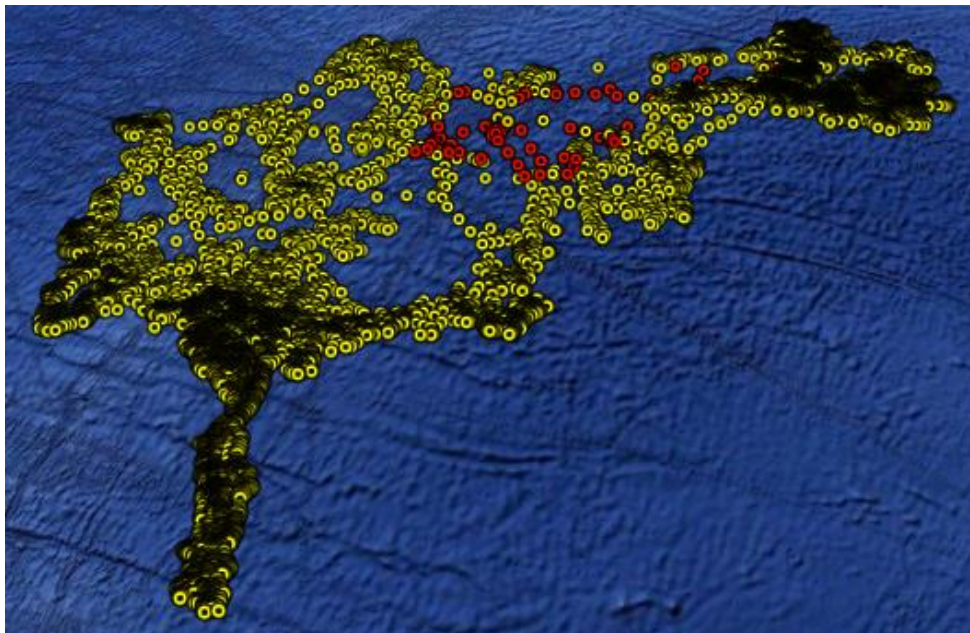


Figure 4.21. Google Earth image of entire Atlantis 9000 system buses (yellow) and buses tripped in Stage 5 (red) from tripping largest generator in Zone 20

In Stages 2 and 3, the frequency of one machine begins to go out of sync with the rest of the system. This is recognized by seeing how the frequency of the machine diverges. Although stability seems to be maintained through Stages 1-4, since nearly all machine frequencies converge close to the nominal frequency of 50 Hz, the system is clearly not stable in Stage 5. It can be concluded that the system becomes unstable between Stages 4 and 5, or tripping 4,008-6,369 MW of load and 2,988-5,292 MW of generation. Because both generation and load are tripped as the contingency grows beyond the origin, it is difficult to find an exact boundary, as far as the maximum generation and load that can be tripped in this scenario.

Bus voltages can also be compared between Stage 4 and Stage 5. In Stage 4, some voltages begin to oscillate to magnitudes outside of the range 0.95-1.05 p.u. In Stage 5, most machine bus voltages diverge well beyond this range.

To show the buses tripped in Stage 5 within the entire system, an additional layer is added to the map developed in Google Earth. The buses tripped in Stage 5 are indicated by red dots.

4.1.7 Scenario #4: Radial Area Attack Tripping N-Levels from the Largest Load in a Given Zone

This scenario is similar to the previous one in that a radial area is tripped with a load bus selected as the origin point. This time, the largest load bus within a zone is chosen as the center of the attack. Although any load in a zone could be tripped, the largest load was selected because it represents a critical N-1 contingency. A simulation was run in PSS®E where the largest load, 542 MW, was tripped in Zone 14. Under this contingency, the frequency of all machine buses in the system were monitored and plotted over a period of 20 seconds, as shown in Figure 4.22 and Figure 4.23.

Results from tripping stages beyond the largest load in Zone 14 are shown until the system is unstable. System frequency response at each stage is presented in Table 4.8, and Table 4.9. The system frequency converged in Stage 1 but did not converge in Stage 2. Additionally, machine bus voltages remained stable through Stage 1 (Figure 4.24), staying within the range of 0.95-1.05 p.u., but were quite unstable in Stage 2 (Figure 4.25). The amount of total load tripped at Stage 1 was 806 MW, and the load tripped at Stage 2 is 2,937 MW. The boundary point can be found by tripping only some of the additional buses tripped in Stage 2 until the system converges again. In this specific scenario, this is more easily done since only load, no generation, has been tripped though Stage 2. By using this method, a boundary of approximately 1,500-1,600 MW of load was found, which accounts for less than 1% of the system total load.

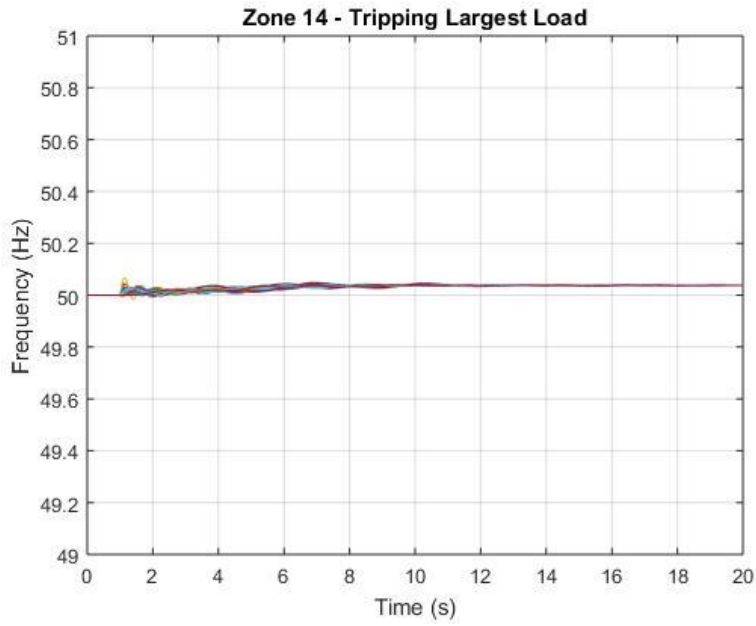


Figure 4.22. Frequency response while tripping the largest load in Zone 14

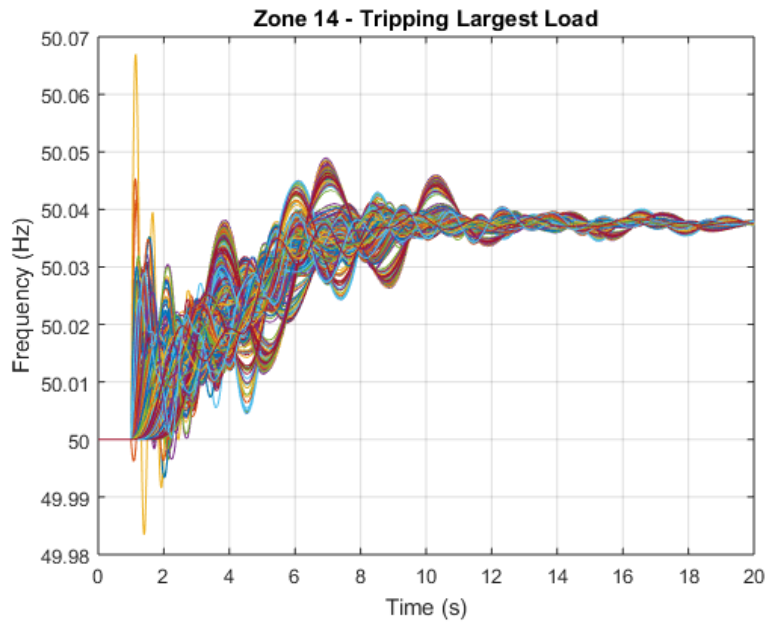


Figure 4.23. Frequency response while tripping the largest load in Zone 14 zoomed in view

Table 4.8. Frequency response of tripping 1 level from largest load in Zone 14

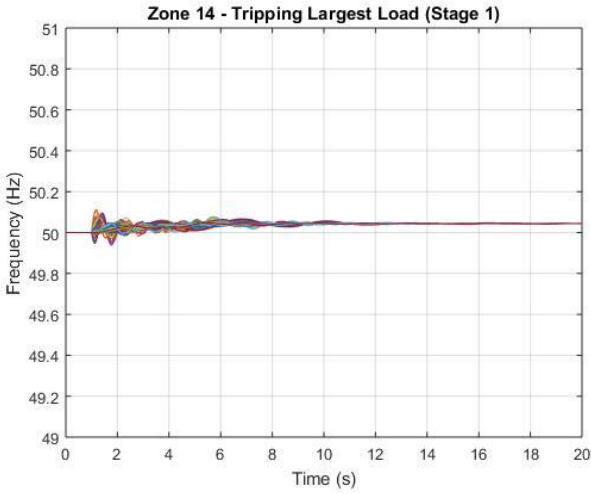
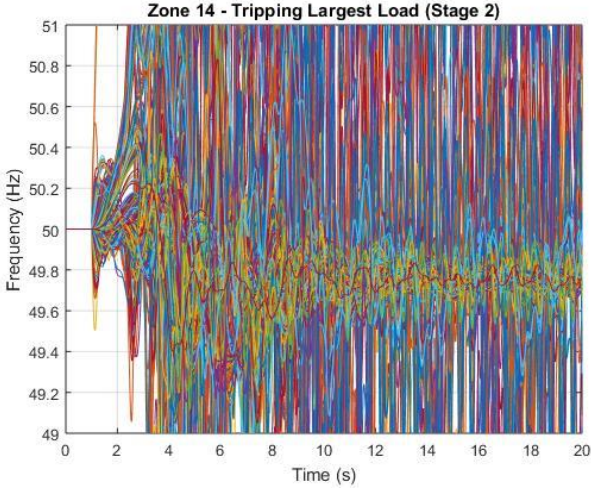
Contingency Frequency Response	Total Load Tripped	Total Generation Tripped
	806 MW	0 MW

Table 4.9. Frequency response of tripping 2 levels from largest load in Zone 14

Contingency Frequency Response	Total Load Tripped	Total Generation Tripped
	2937 MW	0 MW

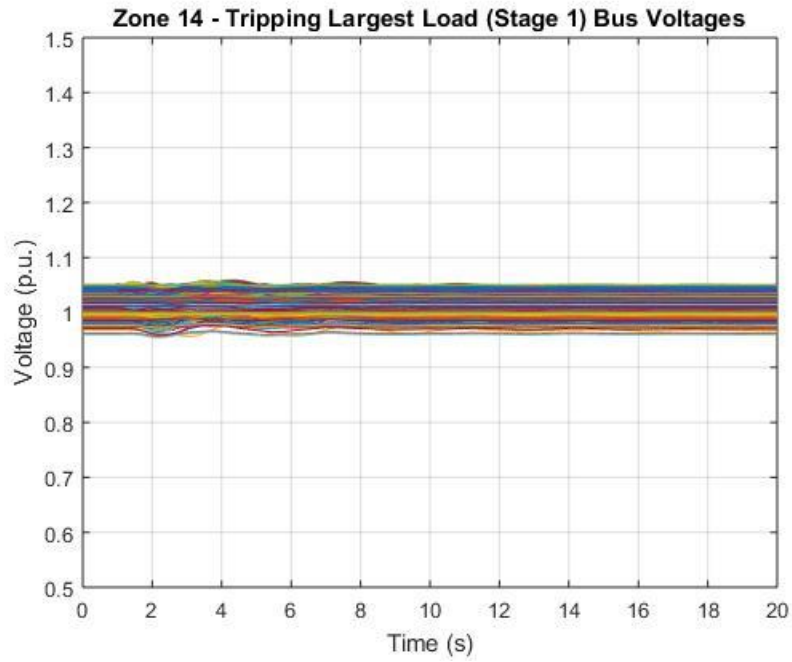


Figure 4.24. System voltage while tripping 1 stage from largest load in Zone 14

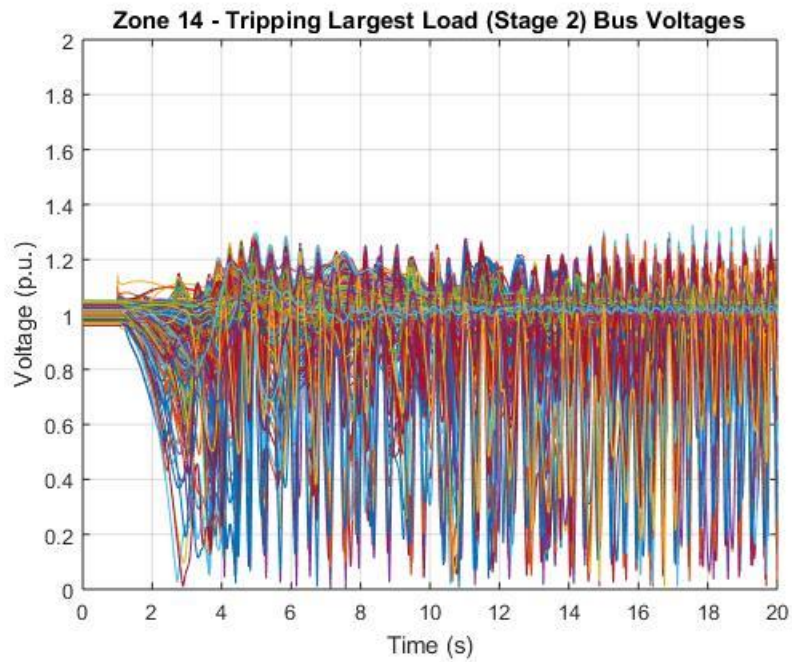


Figure 4.25. System voltage while tripping 2 stages from largest load in Zone 14

As indicated by the red dots in Figure 4.26, a smaller geographic region of tripped buses were necessary to cause the system to become unstable. Because frequency is dependent upon system balance between generation and load, it is concluded that this may be due to the significant load drop, without any additional generation trip.

4.1.8 Adding Generator and Load Relays into the Model During Radial Area Simulations

In an actual system, relays will be connected to loads and generators. To model this in PSS®E and see its effect on previous simulation results, relays were added to all loads and machines. The LDSHAL relay model was associated with all loads in the system dynamic file with the parameters in Table 4.10. The FRGDCAT relay model was added to all machines in the system dynamic file with the parameters in Table 4.11.

The inclusion of load and generator relays in the model did not allow many contingencies to expand beyond the stage where instability occurred without relay protection. Again, expanding the contingency from the largest generator in Zone 20, the results from the final stage when instability occurs are shown. In the previous example without relay protection, the stage where non-convergence occurred was Stage 5. The frequency of all machine buses is plotted, this time with relays added to the model. Comparing through to the results without relays, it can be seen that the relays do not have a significant effect in stabilizing the system at this contingency stage.

Similarly, expanding the contingency from the largest load in Zone 14 was also performed with relays in the system. Though overall frequency deviation is smaller, relays do not prevent the system from diverging. According to results in Figure 4.29, the system machine bus frequencies appear to split into two separate parts. Voltage stability appeared to improve with the inclusion of relays for this case, as seen in Figure 4.30.

When testing other zones in the system, similar results were observed, where frequency response somewhat improved but did not prevent the system from becoming unstable. This is hypothesized to be a result of both load and generation tripping due to under-frequency and over-frequency settings. Though the relays are technically implemented to bring the system back to nominal frequency by balancing load and generation, the tripping of these units, based upon relay settings, may not necessarily be able to bring the system back to a stable state.



Figure 4.26. Google Earth image of entire Atlantis 9000 system buses (yellow) and buses tripped in Stage 2 (red) from tripping largest load in Zone 14

Table 4.10. LDSHAL relay model parameter settings

Parameter	Value
First load shed point (Hz)	59.5
First point pickup time (sec.)	0.2
Frac1, first fraction of load shed	0.07
Second load shed point (Hz)	59.3
Second point pickup time (sec.)	0.2
Frac2, second fraction of load shed	0.07
Third load shed point (Hz)	59.1
Third point pickup time (sec.)	0.2
Third fraction of load shed	0.07
TB, breaker time (sec.)	0.1

Table 4.11. FRGDCAT relay model parameter settings

Parameter	Value
FL, lower frequency threshold (Hz)	57.8
FU, upper frequency threshold (Hz)	61.8
TP, relay pickup time (sec.)	0.0
TB, breaker time (sec.)	0.1

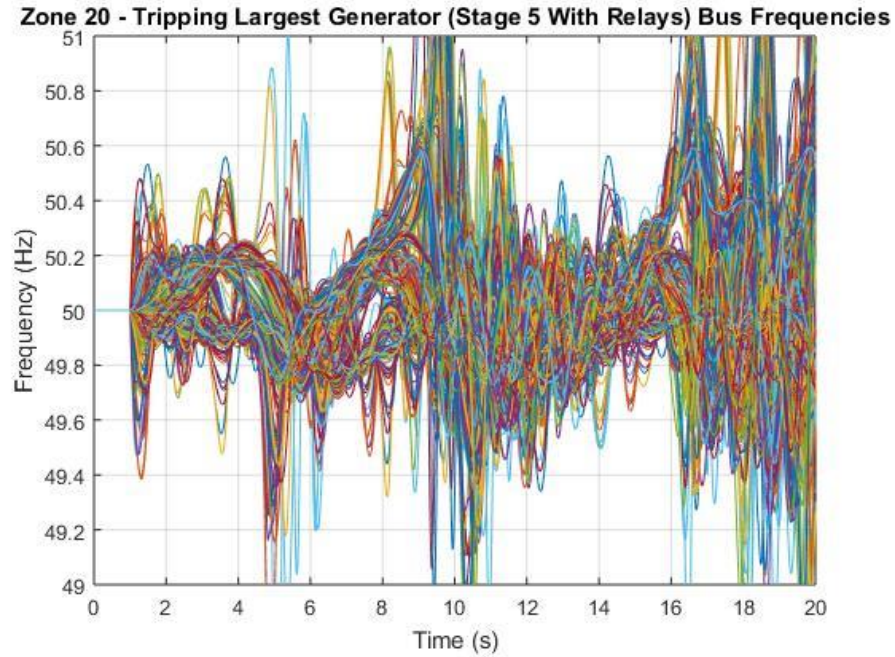


Figure 4.27. Frequency response of tripping 5 stages from largest generator in Zone 20 with relays

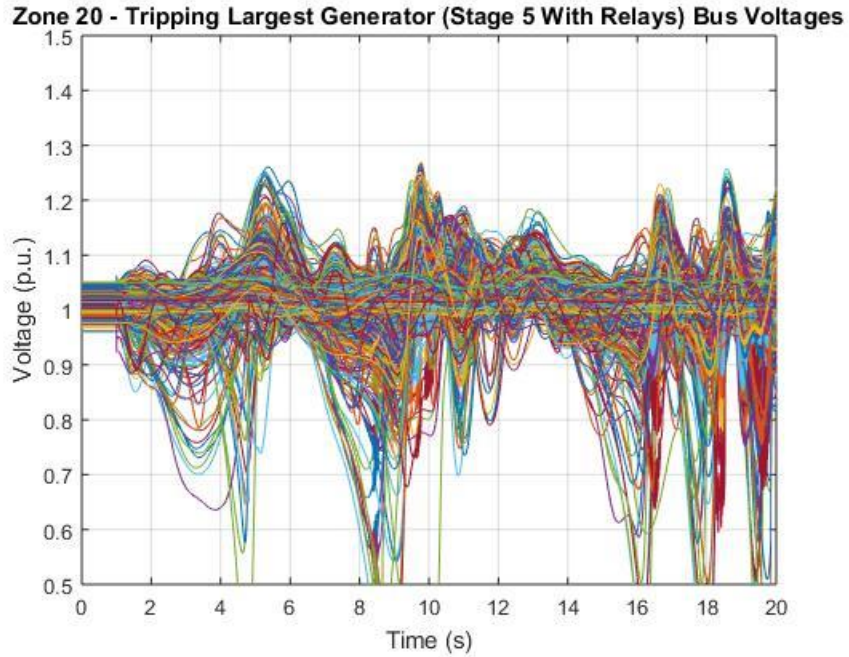


Figure 4.28. System voltage while tripping 5 stages from largest generator in Zone 20 with relays

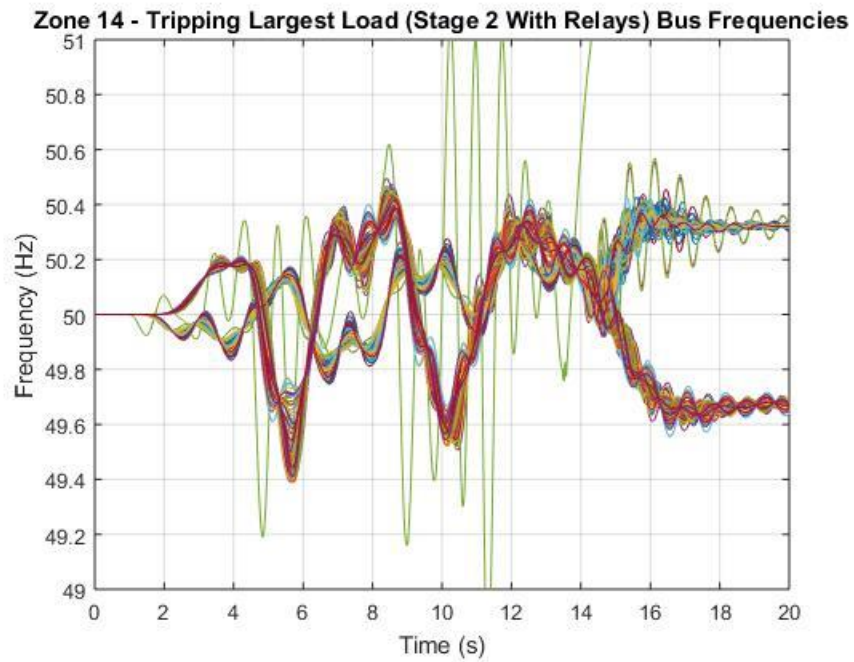


Figure 4.29. Frequency response of tripping 2 stages from largest load in Zone 14 with relays

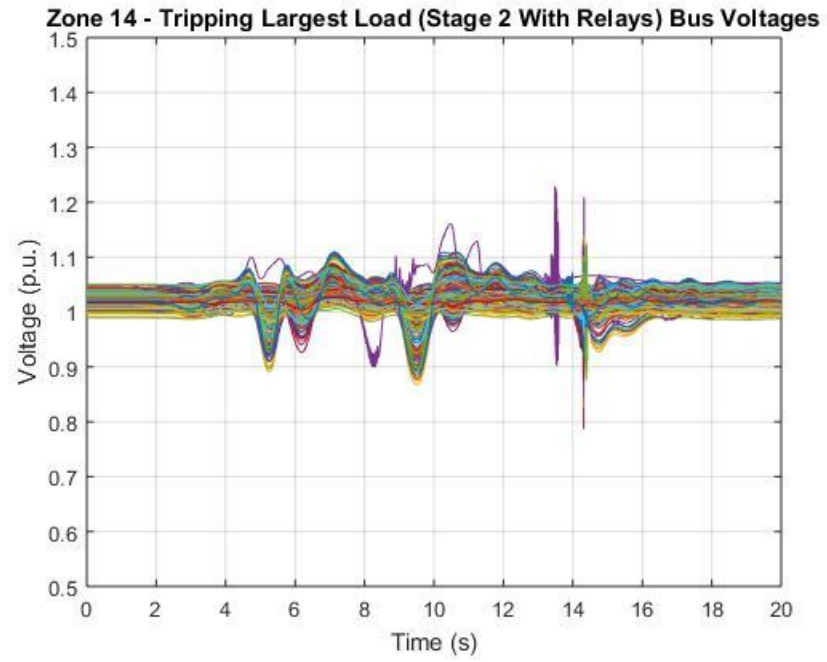


Figure 4.30. System voltage while tripping 2 stages from largest load in Zone 14 with relays

4.1.9 Scenario #5: Tripping Buses in Multiple Areas Simultaneously

Another type of attack could be groups of substations in two different zones being tripped simultaneously. For example, the largest generator in Zone 5 and the largest generator in Zone 22 could be disconnected at the same time. Similar to the previous examples, a hacker could also trip n-levels beyond a single bus in one area and n-levels beyond a single bus in another area. The general concept of this is shown in Figure 4.31. Results are presented for tripping buses in multiple areas simultaneously.

In this example, the points of origin of the contingency are buses with the largest generation in Zone 5 and Zone 21. A plot was generated showing the system frequency response when tripping just the largest generator buses in Zone 5 and Zone 21.

The frequency response at each stage is shown in Table 4.12 and Table 4.13. Though some oscillations occurred in Stage 1, the system clearly did not converge in Stage 2. When tripping n-levels from the largest generator in Zone 5 and Zone 21 individually, the system became unstable in Stage 2 for Zone 5 and in Stage 3 for Zone 21. Due to the instability caused by the buses tripped in Zone 5, the entire system was already unstable at Stage 2. A map generated in Google Earth, in Figure 4.32, shows the buses tripped the two areas in Stage 2.

In other scenarios tested while tripping buses in multiple zones simultaneously, divergence was also reached at the stage when at least one of the areas caused non-convergence. Though it was previously hypothesized that tripping buses in multiple areas simultaneously would cause the system to more quickly reach instability, results inferred that instability of the entire system is dependent upon which area becomes unstable first for these particular scenarios.

Summary

While studying dynamic effects of possible cyber-attack scenarios, security was assessed by analyzing consequences of instability under the loss of several buses or equipment at a time. From the scenarios studied, it can be determined that percentage of total system generation tripped, percentage of total system load tripped, and number and location of substations disconnected at a specified voltage level can all be considered to predict dynamic stability under a cyber-attack or wide-area physical attack. System topology and the criticality of each individual station also greatly affect frequency and voltage stability.

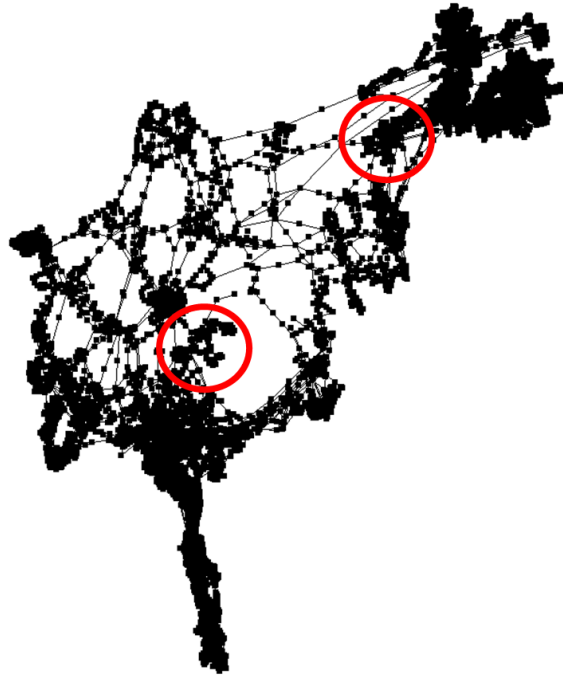


Figure 4.31. Tripping multiple areas

Table 4.12. Frequency response of tripping 1 level from largest generator in Zones 5 and 21

Contingency Frequency Response	Total Load Tripped	Total Generation Tripped
<p>Zones 5 and 21 - Tripping Largest Generator</p> <p>The graph plots Frequency (Hz) on the y-axis (ranging from 49 to 51) against Time (s) on the x-axis (ranging from 0 to 20). Multiple colored lines represent different frequency responses. All lines start at 50 Hz at time 0. Between 1 and 2 seconds, there is a sharp dip in frequency, with some lines reaching approximately 49.7 Hz. Following this initial drop, the lines oscillate and gradually converge back to a steady state of 50 Hz by approximately 10 seconds, remaining stable until 20 seconds.</p>	0 MW	4153 MW

Table 4.13. Frequency response of tripping 2 levels from largest generator in Zones 5 and 21

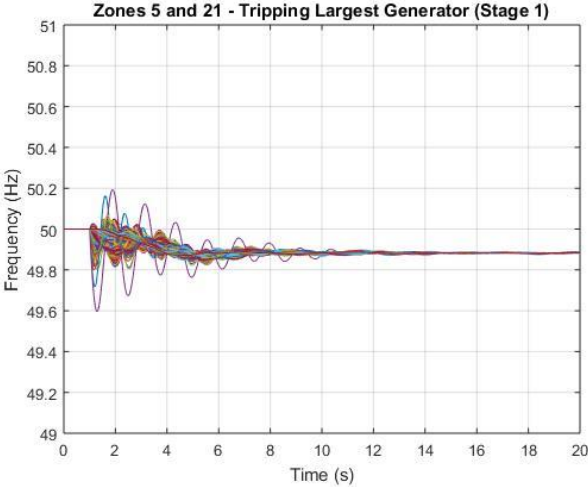
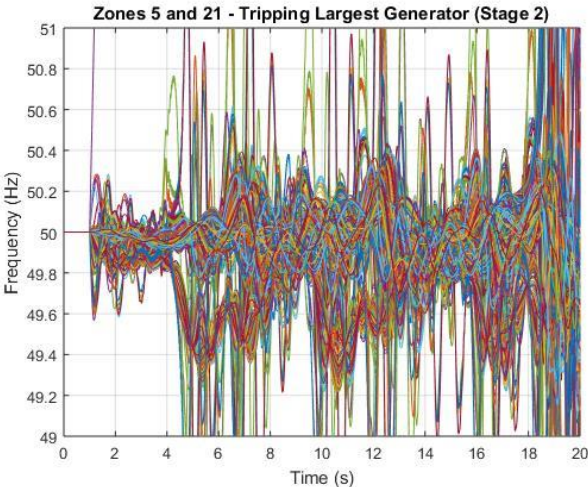
Contingency Frequency Response	Total Load Tripped	Total Generation Tripped
	330 MW	4789 MW

Table 4.14. Frequency response of tripping 3 levels from largest generator in Zones 5 and 21

Contingency Frequency Response	Total Load Tripped	Total Generation Tripped
	591 MW	5821 MW

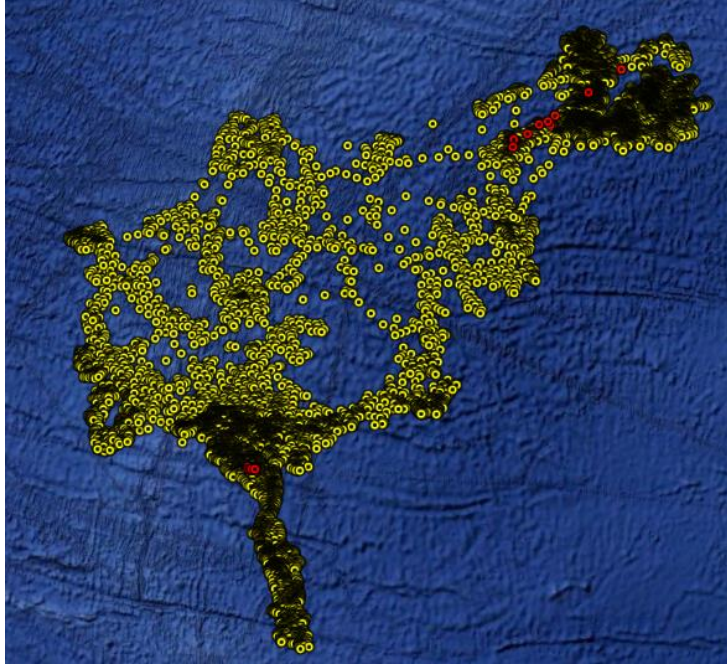


Figure 4.32. Google Earth image of entire Atlantis 9000 system buses (yellow) and buses tripped in Stage 2 (red) from tripping largest generators in Zones 5 and 21

Patterns can be drawn from the analyzed scenarios. For example, in the radial area studies, boundaries can be determined by studying the amount and location of load and generation tripped in the final stage before divergence and the stage when divergence occurs. In general for the radial area attacks, less than 1% of the system's total generation or total load was tripped before divergence occurred.

Though individual zones have differing generation and load amounts that can be tripped before diverging, the ratio of total load to generation lost in the zone, and within the entire system, could be further analyzed to observe more conclusions from the results. When tripping the largest generation facilities in a zone, the percentage of generation disconnected in the zone varied greatly depending on the area selected. Generally, the ratio of generation tripped to total system generation was typically below 10%.

5 CONCLUSIONS AND RECOMMENDATIONS FOR FUTURE WORK

Security assessment through dynamic stability analysis was performed on three power systems using three different methods. In the MIDAS project, dynamic stability criteria was determined by generating power flow, dynamic, and contingency data to serve as input to a machine learning tool. The dynamic effects of tripping main generation facilities, loads, transmission lines, and substations were simulated on the developed Puerto Rico 2018 transmission system. Additionally, models with high PV integration were created to study the dynamic effects under a generation trip. Lastly, dynamic simulations were conducted to investigate impacts of hackers shutting down multiple generators, loads, or other substations within an electrical utility and determining what scenarios would lead to system collapse.

Dynamic Security Assessment (DSA) for Multi-Timescale Integrated Dynamics and Scheduling for Solar (MIDAS) Future Work

In the next phase of the MIDAS project, a larger model, the Western Electricity Coordinating Council (WECC) system, will be used to create cases for the machine learning tool. Test creation for this system should be more straightforward because the approach for case development for each stability method has already been determined, and Python scripts to automate tasks in PSS®E have already been written. Additionally, system power flow information will be provided for a longer period than 24 hours to better analyze stability changes due to seasonal effects, weather, load consumption, or other causes.

As test cases are regenerated for the WECC system, improvements can be made to the test generation scripts to include more complex scenarios. For example, aside from just inertia, governor status combinations could also be incorporated into frequency stability analysis. Because inertia is not usually perfectly linear with generation level, other inputs may need to be provided into the machine learning model, given that a specified generation output could have multiple total system inertia values. Similar to what was done with the 23-bus system, steady-state cases could also incorporate events such as generator maintenance and probability of transmission line outages.

Lastly, the effects of increased solar penetration will be included in the model. The ability of the machine learning algorithm to accurately predict frequency, transient, and small-signal stability margin will be assessed with a higher amount of PV in the system.

Assessing Security During Natural Disasters and Increased Renewable Penetration in Puerto Rico Future Work

Since the UTK 2018 PREPA transmission model was created and initial PREPA-developed models were provided for study, updated 2019 cases have been created by PREPA. Using these updated models, which may more accurately represent the system following the hurricane, corridor trip simulations and high PV studies, along with other contingency simulations, can be done. During the time this thesis was written, an additional solar penetration study was performed on the PREPA 2019 day-peak model, and results are included in the Appendix in Section A.3. In the Phase II effort, the ORNL/PREPA team will continue to deploy UGAs based on the locations outlined in Section 3.2. Additionally, a new project was started in October 2018 to develop and deploy a phasor data concentrator for PREPA to collect the streaming data from all UGA units in PREPA system. The data analytics effort will start as more data becomes available. Using this data, the UTK-developed 2018 model and PREPA-developed models can be validated.

Assessing Security During Cyber-Attacks and Wide-Area Physical Attacks on Bulk Electric System Assets Future Work

The scenarios studied are not exhaustive or comprehensive. Future work could be done to go through more permutations of possible attacks. Additionally, other dynamic characteristics, such as transient stability could be studied. The same scenarios could also be analyzed while varying the time that each bus is disconnected instead of disconnecting multiple buses or machines at once. Systems of various sizes and topologies could also be assessed. For example, in a smaller system, less generation or load could be lost to cause system collapse, as compared to a larger system.

Lastly, a combination of system power flow data, along with dynamic response, could be used to predict the possible effects of tripping combinations of substations and other equipment. For example, [50] describes how hypothesized outage combinations can first go through steady-state simulation screening and then dynamic simulation verification to predict whether the contingency will cause a cascading outage.

LIST OF REFERENCES

- [1] P. Kundur et al., "Definition and classification of power system stability," *IEEE transactions on Power Systems*, vol. 19, no. 2, pp. 1387-1401, 2004.
- [2] National Renewable Energy Laboratory, "Multi-timescale Integrated Dynamics and Scheduling for Solar (MIDAS-Solar)," *FY19-BP1-Q1 Project Update*, 2019.
- [3] P. Marsters and T. Houser, "America's Biggest Blackout," *Rhodium Group*, 25-Feb-2019. [Online]. Available: <https://rhg.com/research/americas-biggest-blackout-2/>. [Accessed 19 Feb. 2019].
- [4] E. Schwartz, "Quick facts: Hurricane Maria's effect on Puerto Rico," *Mercy Corps*, 04-Feb-2019. [Online]. Available: <https://www.mercycorps.org/articles/united-states/quick-facts-hurricane-marias-effect-puerto-rico> [Accessed 19 Feb. 2019].
- [5] A. Kwasinski, F. Andrade, M. Castro-Sitiriche and E. O'Neill-Carrillo, "Hurricane Maria Effects on Puerto Rico Electric Power Infrastructure," in *IEEE Power and Energy Technology Systems Journal*, vol. 6, no. 1, pp. 85-94, March 2019.
- [6] J. Geeganage, U. Annakkage, T. Weekes, and B. A. Archer, "Application of energy-based power system features for dynamic security assessment," *IEEE Transactions on Power Systems*, vol. 30, no. 4, pp. 1957-1965, 2015.
- [7] M. Mohammadi, G. Gharehpetian, and M. Raoufat, "A new BVM based approach to transient security assessment," *European Transactions on Electrical Power*, vol. 20, no. 8, pp. 1163-1176, 2010.
- [8] L. Moulin, A. A. Da Silva, M. El-Sharkawi, and R. J. Marks, "Support vector machines for transient stability analysis of large-scale power systems," *IEEE Transactions on Power Systems*, vol. 19, no. 2, pp. 818-825, 2004.
- [9] Y. Zhou, J. Wu, L. Hao, L. Ji, and Z. Yu, "Transient stability prediction of power systems using post-disturbance rotor angle trajectory cluster features," *Electric Power Components and Systems*, vol. 44, no. 17, pp. 1879-1891, 2016.
- [10] Z. Pannell, B. Ramachandran and D. Snider, "Machine learning approach to solving the transient stability assessment problem," *2018 IEEE Texas Power and Energy Conference (TPEC)*, College Station, TX, 2018, pp. 1-6.
- [11] F. Hang, S. Huang, Y. Chen, and S. Mei, "Power system transient stability assessment based on dimension reduction and cost-sensitive ensemble learning," in *Energy Internet and Energy System Integration (EI2)*, 2017 IEEE Conference on, 2017, pp. 1-6: IEEE.
- [12] B. P. Soni, A. Saxena, and V. Gupta, "Online identification of coherent generators in power system by using SVM," in *Power, Control & Embedded Systems (ICPCES)*, 2017 4th International Conference on, 2017, pp. 1-5: IEEE.

- [13] W. Zhang, W. Hu, Y. Min, L. Chen, L. Zheng, and X. Liu, "A novel stability classifier based on reformed support vector machines for online stability assessment," in *Power and Energy Engineering Conference (APPEEC), 2015 IEEE PES Asia-Pacific, 2015*, pp. 1-5: IEEE.
- [14] A. D. Rajapakse, F. Gomez, K. Nanayakkara, P. A. Crossley, and V. V. Terzija, "Rotor Angle Instability Prediction Using Post-Disturbance Voltage Trajectories," *IEEE Transactions on Power Systems*, vol. 25, no. 2, pp. 947-956, 2010.
- [15] Y. Xu, Z. Y. Dong, J. H. Zhao, P. Zhang, and K. P. Wong, "A reliable intelligent system for real-time dynamic security assessment of power systems," *IEEE Transactions on Power Systems*, vol. 27, no. 3, pp. 1253-1263, 2012.
- [16] Y. Tang, F. Li, Q. Wang, and Y. Xu, "Hybrid method for power system transient stability prediction based on two-stage computing resources," *IET Generation, Transmission & Distribution*, vol. 12, no. 8, pp. 1697-1703, 2017.p
- [17] Y. Zhang, Y. Xu, Z. Y. Dong, Z. Xu, and K. P. Wong, "Intelligent early warning of power system dynamic insecurity risk: Toward optimal accuracy-earliness tradeoff," *IEEE Transactions on Industrial Informatics*, vol. 13, no. 5, pp. 2544-2554, 2017.
- [18] N. Amjady and S. F. Majedi, "Transient stability prediction by a hybrid intelligent system," *IEEE Transactions on Power Systems*, vol. 22, no. 3, pp. 1275-1283, 2007.
- [19] S. Jafarzadeh and V. M. I. Genc, "Probabilistic dynamic security assessment of large power systems using machine learning algorithms," *Turkish Journal of Electrical Engineering and Computer Sciences*, vol. 26, no. 3, pp. 1479-1490, 2018.
- [20] J. James, D. J. Hill, A. Y. Lam, J. Gu, and V. O. Li, "Intelligent time-adaptive transient stability assessment system," *IEEE Transactions on Power Systems*, vol. 33, no. 1, pp. 1049-1058, 2018.
- [21] J. James, A. Y. Lam, D. J. Hill, and V. O. Li, "Delay Aware Intelligent Transient Stability Assessment System," *IEEE Access*, vol. 5, pp. 17230-17239, 2017.
- [22] R. Liu, G. Verbič, and Y. Xu, "A new reliability-driven intelligent system for power system dynamic security assessment," in *Universities Power Engineering Conference (AUPEC), 2017 Australasian, 2017*, pp. 1-6: IEEE.
- [23] L. Zhang, X. Hu, P. Li, F. Shi, and Z. Yu, "ELM model for power system transient stability assessment," in *Chinese Automation Congress (CAC), 2017, 2017*, pp. 5740-5744: IEEE.
- [24] B. Tan, J. Yang, X. Pan, J. Li, P. Xie, and C. Zeng, "Representational learning approach for power system transient stability assessment based on convolutional neural network," *The Journal of Engineering*, vol. 2017, no. 13, pp. 1847-1850, 2017.

- [25] X. Chu and Y. Liu, "Real-time transient stability prediction using incremental learning algorithm," in *Power Engineering Society General Meeting*, 2004. IEEE, 2004, pp. 1565-1569: IEEE.
- [26] R. Diao, V. Vittal, and N. Logic, "Design of a real-time security assessment tool for situational awareness enhancement in modern power systems," *IEEE Transactions on Power Systems*, vol. 25, no. 2, pp. 957-965, 2010.
- [27] C. Zhang, Y. Li, Z. Yu, and F. Tian, "A weighted random forest approach to improve predictive performance for power system transient stability assessment," in *Power and Energy Engineering Conference (APPEEC)*, 2016 IEEE PES Asia-Pacific, 2016, pp. 1259-1263: IEEE.
- [28] C. Zhang, Y. Li, Z. Yu, and F. Tian, "Feature selection of power system transient stability assessment based on random forest and recursive feature elimination," in *Power and Energy Engineering Conference (APPEEC)*, 2016 IEEE PES Asia-Pacific, 2016, pp. 1264-1268: IEEE.
- [29] T. Amraee and S. Ranjbar, "Transient instability prediction using decision tree technique," *IEEE Transactions on Power Systems*, vol. 28, no. 3, pp. 3028-3037, 2013.
- [30] L. Zheng et al., "Deep belief network based nonlinear representation learning for transient stability assessment," in *Power & Energy Society General Meeting*, 2017 IEEE, 2017, pp. 1-5: IEEE.
- [31] J. Lv, M. Pawlak, and U. D. Annakkage, "Prediction of the transient stability boundary using the lasso," *IEEE Transactions on Power Systems*, vol. 28, no. 1, pp. 281-288, 2013.
- [32] A. Sharifian and S. Sharifian, "A new power system transient stability assessment method based on Type-2 fuzzy neural network estimation," *International Journal of Electrical Power & Energy Systems*, vol. 64, pp. 71-87, 2015.
- [33] Y. Xu, Z. Y. Dong, Z. Xu, K. Meng, and K. P. Wong, "An Intelligent Dynamic Security Assessment Framework for Power Systems With Wind Power," *IEEE Transactions on Industrial Informatics*, vol. 8, no. 4, pp. 995-1003, 2012.
- [34] C. Chao-Rong and H. Yuan-Yin, "Synchronous machine steady-state stability analysis using an artificial neural network," *IEEE Transactions on Energy Conversion*, vol. 6, no. 1, pp. 12-20, 1991.
- [35] S. P. Teeuwesen, I. Erlich, M. A. El-Sharkawi, and U. Bachmann, "Genetic algorithm and decision tree-based oscillatory stability assessment," *IEEE Transactions on Power Systems*, vol. 21, no. 2, pp. 746-753, 2006.
- [36] WECC Staff, "Loads and Resources Methods and Assumptions", *Wecc.org*, 2014. [Online]. Available: https://www.wecc.org/Reliability/2014LAR_MethodsAssumptions.pdf. [Accessed: 12- Apr- 2019].

- [37] J. L. Rueda and F. Shewarega, "Small Signal Stability of Power Systems with Large Scale Wind and Power Integration," *Universitat Duisberg Essen*, 28-May-2009. [Online]. Available: <https://www.uni-due.de/ean/downloads/papers/rueda2009a.pdf>. [Accessed: 12-Apr-2019].
- [38] "Fortieth Annual Report on the Electric Property of the Puerto Rico Electric Power Authority," *Aeepr.com*. [Online] Available at: <https://www2.aeepr.com/Documentos/Ley57/Tarifa/03%20Attachment%20B%20-%20Schedules/I%20Schedules/I-1.pdf> [Accessed 15 Feb. 2018].
- [39] "Operational Profile," *Aeepr.com*. [Online]. Available: <https://www2.aeepr.com/INVESTORS/OperationalProfile.aspx>. [Accessed: 01-Mar-2018].
- [40] Puerto Rico Electric Power Authority, "PREPA General Overview and Challenges," *CURRENT Annual Planning Meeting*, San Juan, Puerto Rico, 2017.
- [41] "Calculate distance and bearing between two Latitude/Longitude points using haversine formula in JavaScript," *Movable Type Scripts*. [Online]. Available: <https://www.movable-type.co.uk/scripts/latlong.html>. [Accessed: 28-Feb-2018].
- [42] "Population," *Google*. [Online]. Available: https://www.google.com/publicdata/explore?ds=kf7tgg1uo9ude_&met_y=population&hl=en&dl=en#!ctype=l&strail=false&bcs=d&nselm=h&met_y=population&scale_y=lin&ind_y=false&rdim=country&idim=country:US&idim=state:43000&ifdim=country&hl=en_US&dl=en&ind=false. [Accessed: 15-Feb-2018].
- [43] *Google Maps*. [Online]. Available: <https://www.google.com/maps>. [Accessed: 16-Mar-2018].
- [44] D. E. Whitehead, K. Owens, D. Gammel and J. Smith, "Ukraine cyber-induced power outage: Analysis and practical mitigation strategies," *2017 70th Annual Conference for Protective Relay Engineers (CPRE)*, College Station, TX, 2017, pp. 1-8.
- [45] E-ISAC (Electricity Information Sharing and Analysis Center), "Analysis of the Cyber Attack on the Ukrainian Power Grid," Washington, D.C., 2016.
- [46] "Who We Are," *Who We Are | Dominion Energy*. [Online]. Available: <https://www.dominionenergy.com/about-us/who-we-are>. [Accessed 19 Feb. 2019].
- [47] S. Kumar, N. Gaur and A. Kumar, "Developing a Secure Cyber Ecosystem for SCADA Architecture," *2018 Second International Conference on Computing Methodologies and Communication (ICCMC)*, Erode, 2018, pp. 559-562.
- [48] CNN, "What's an electromagnetic pulse attack?," *YouTube*, 25-Nov-2011. [Online]. Available: <https://www.youtube.com/watch?v=vurpNu84seU>. [Accessed 28 Feb. 2019].

- [49] "Geomagnetic Disturbances," *ISO New England*. [Online]. Available: <https://www.iso-ne.com/about/what-we-do/in-depth/geomagnetic-disturbances>. [Accessed 19 Feb. 2019].
- [50] C. Ten, K. Yamashita, Z. Yang, A. V. Vasilakos and A. Ginter, "Impact Assessment of Hypothesized Cyberattacks on Interconnected Bulk Power Systems," in *IEEE Transactions on Smart Grid*, vol. 9, no. 5, pp. 4405-4425, Sept. 2018.
- [51] C. Ten, A. Ginter and R. Bulbul, "Cyber-Based Contingency Analysis," in *IEEE Transactions on Power Systems*, vol. 31, no. 4, pp. 3040-3050, July 2016.

APPENDIX

A.1 Python and MATLAB Scripts Used to Generate Test Cases in Machine Learning Project

A.1.1 Python Scripts for 23-Bus System

A.1.1.1 Steady-State Saved Case Generation

#This script creates steady-state PSS/E saved cases for the 23-bus example system (savnw).
#Load data for each zone is based off of balancing authority data, and values are scaled to fit the 23-bus system.
#Line outages are scheduled based on probability, and generators are scheduled for maintenance during light-load periods.
#To schedule line outages, outage probability was taken from the .prb file. A separate MATLAB script was used to create
#the generator outage schedule.

```
psspy.lines_per_page_one_device(1,60)
psspy.progress_output(2,r"""Log""",[0,0])
```

```
import csv
import random
```

```
#Import load data for each zone from csv file, and scale to fit 23-bus system
```

```
datetime = [];
AESOload = [];
PACWload = [];
TEPload = [];
with open('Load_RT_hourly.csv', 'rb') as csvfile:
    spamreader = csv.reader(csvfile, delimiter=',', quotechar='')
    rowCount = 1;
    for row in spamreader:
        if(rowCount != 1):
            datetime.append(row[0]);
            AESOload.append(float(row[1]));
            PACWload.append(float(row[20]));
            TEPload.append(float(row[33]));
            rowCount = rowCount + 1;
```

```
AESOavg = sum(AESOload)/float(len(AESOload))
PACWavg = sum(PACWload)/float(len(PACWload))
TEPavg = sum(TEPload)/float(len(TEPload))
```

```
Area1Avg = 200.0-((max(AESOload)-AESOavg)/max(AESOload))*200.0
Area2Avg = 2500.0-((max(PACWload)-PACWavg)/max(PACWload))*2500.0
Area5Avg = 500.0-((max(TEPload)-TEPavg)/max(TEPload))*500.0
```

```
AESOdev = [];
PACWdev = [];
TEPdev = [];
```

```
for i in range(len(datetime)):
    AESOdev.append((AESOload[i] - AESOavg)/AESOavg)
    PACWdev.append((PACWload[i] - PACWavg)/PACWavg)
    TEPdev.append((TEPload[i] - TEPavg)/TEPavg)
```

```
#Schedule out-of-service machines
```

```
f = open("machineOutages.py", "w")
generatorMaintenance = [[3011,2037],[206,6593],[101,1052],[102,2709],[211,3400],[3018,350]]
generatorMaintenanceSchedule = []
```

```

startingHour = 0
for j in range(len(generatorMaintenance)):
    for i in range(len(datetime)):
        if((i+1) == generatorMaintenance[j][1]):
            startingHour = i
            machStatus = 0
        elif(i <= (startingHour+671) and startingHour != 0):
            machStatus = 0
        else:
            machStatus = 1
            startingHour = 0
        generatorMaintenanceSchedule.append([generatorMaintenance[j][0],(i+1),machStatus])
f.write(str(generatorMaintenanceSchedule))

#Schedule out-of-service branches using probability
reactance138kV = 0.762
reactance230kV = 0.746
reactance500kV = 0.746

fmt138kV = 0.1
fmt230kV = 0.1
fmt500kV = 0.1

ft138kV = 0.1
ft230kV = 0.1
ft500kV = 0.1

dt138kV = 10
dt230kV = 10
dt500kV = 10

dmt138kV = 7
dmt230kV = 10
dmt500kV = 10

fromBuses = psspy.abrnint(-1,1,1,1,1,'FROMNUMBER')[1][0]
toBuses = psspy.abrnint(-1,1,1,1,1,'TONUMBER')[1][0]
IDs = []
reactances = []
lengths = []
frequencies = []
durations = []
failureTimes = []

for i in range(len(fromBuses)):
    if((fromBuses[i] == fromBuses[i-1]) and (toBuses[i] == toBuses[i-1])):
        IDs.append('2')
    else:
        IDs.append('1')

for i in range(len(fromBuses)):
    reactances.append(psspy.brndt2(fromBuses[i],toBuses[i],IDs[i],'RX')[1].imag)

for i in range(len(fromBuses)):
    if(psspy.busdat(fromBuses[i],'BASE')[1] == 138):
        length = reactances[i]/reactance138kV
        lengths.append(length)
    elif(psspy.busdat(fromBuses[i],'BASE')[1] == 230):
        length = reactances[i]/reactance230kV

```

```

lengths.append(length)
elif(psspy.busdat(fromBuses[i], 'BASE')[1] == 500):
    length = reactances[i]/reactance500kV
    lengths.append(length)

for i in range(len(fromBuses)):
    if(psspy.busdat(fromBuses[i], 'BASE')[1] == 138):
        frequency = lengths[i]*fmt138kV+ft138kV
        duration = (fmt138kV*dmt138kV*lengths[i]+ft138kV*dt138kV)/frequency
        failureTime = (frequency*duration)/9528/10
    elif(psspy.busdat(fromBuses[i], 'BASE')[1] == 230):
        frequency = lengths[i]*fmt230kV+ft230kV
        duration = (fmt230kV*dmt230kV*lengths[i]+ft230kV*dt230kV)/frequency
        failureTime = (frequency*duration)/9528/10
    elif(psspy.busdat(fromBuses[i], 'BASE')[1] == 500):
        frequency = lengths[i]*fmt500kV+ft500kV
        duration = (fmt500kV*dmt500kV*lengths[i]+ft500kV*dt500kV)/frequency
        failureTime = (frequency*duration)/9528/10
    frequencies.append(frequency)
    durations.append(duration)
    failureTimes.append(failureTime)

HourlyStatus = []

f = open("lineOutages.py", "w")
outageStart = 0
status = 1
for j in range(len(fromBuses)):
    for i in range(len(datetime)):
        randomNumber = random.uniform(0,1)
        if(randomNumber <= failureTimes[j]):
            status = 0
            outageStart = 1
            elif((i+) >= 1 and HourlyStatus[i-1+(j*len(datetime))][3] == 1 and HourlyStatus[i-1+(j*len(datetime))][0]
== [fromBuses[j],toBuses[j],IDs[j]]):
                status = 0
                outageStart = 0
                elif((i+) >= 2 and HourlyStatus[i-2+(j*len(datetime))][3] == 1 and HourlyStatus[i-2+(j*len(datetime))][0]
== [fromBuses[j],toBuses[j],IDs[j]]):
                    status = 0
                    outageStart = 0
                    elif((i+) >= 3 and HourlyStatus[i-3+(j*len(datetime))][3] == 1 and HourlyStatus[i-3+(j*len(datetime))][0]
== [fromBuses[j],toBuses[j],IDs[j]]):
                        status = 0
                        outageStart = 0
                        elif((i+) >= 4 and HourlyStatus[i-4+(j*len(datetime))][3] == 1 and HourlyStatus[i-4+(j*len(datetime))][0]
== [fromBuses[j],toBuses[j],IDs[j]]):
                            status = 0
                            outageStart = 0
                            elif((i+) >= 5 and HourlyStatus[i-5+(j*len(datetime))][3] == 1 and HourlyStatus[i-5+(j*len(datetime))][0]
== [fromBuses[j],toBuses[j],IDs[j]]):
                                status = 0
                                outageStart = 0
                                elif((i+) >= 6 and HourlyStatus[i-6+(j*len(datetime))][3] == 1 and HourlyStatus[i-6+(j*len(datetime))][0]
== [fromBuses[j],toBuses[j],IDs[j]]):
                                    status = 0
                                    outageStart = 0
                                    elif((i+) >= 7 and HourlyStatus[i-7+(j*len(datetime))][3] == 1 and HourlyStatus[i-7+(j*len(datetime))][0]
== [fromBuses[j],toBuses[j],IDs[j]]):
                                        status = 0
                                        outageStart = 0

```

```

        status = 0
        outageStart = 0
        elif((i+) >= 8 and HourlyStatus[i-8+(j*len(datetime))][3] == 1 and HourlyStatus[i-8+(j*len(datetime))][0]
== [fromBuses[j],toBuses[j],IDs[j]]):
            status = 0
            outageStart = 0
            elif((i+) >= 9 and HourlyStatus[i-9+(j*len(datetime))][3] == 1 and HourlyStatus[i-9+(j*len(datetime))][0]
== [fromBuses[j],toBuses[j],IDs[j]]):
                status = 0
                outageStart = 0
            else:
                status = 1
                outageStart = 0
        hour = i+1
        HourlyStatus.append([[fromBuses[j],toBuses[j],IDs[j]],hour,status,outageStart])
f.write(str(HourlyStatus))

```

#For each time step, scale loads, set machines and branches in and out of service, perform economic dispatch, perform power flow, and create saved case file

```

for k in rangelen(datetime):
    psspy.case(r""savnw.sav"")
    #Scale loads
    psspy.bsys(0,0,[ 13.8, 500.],1,[1],0,[],0,[],0,[])
    psspy.scal_2(0,0,1,[0,0,0,0,0],[0.0,0.0,0.0,0.0,0.0,0.0,0.0,0.0])
    psspy.scal_2(0,1,2,[i,1,0,1,0],[ (1+PACWdev[k])*Area1Avg, 1500.0,0.0,-600.0, 300.0,-.0, 100.0])
    psspy.bsys(0,0,[ 13.8, 500.],1,[2],0,[],0,[],0,[])
    psspy.scal_2(0,0,1,[0,0,0,0,0],[0.0,0.0,0.0,0.0,0.0,0.0,0.0,0.0])
    psspy.scal_2(0,1,2,[i,1,0,1,0],[ (1+AESOdev[k])*Area2Avg, 1400.0,0.0,-.0, 650.0,-.0, 1650.0])
    psspy.bsys(0,0,[ 13.8, 500.],1,[5],0,[],0,[],0,[])
    psspy.scal_2(0,0,1,[0,0,0,0,0],[0.0,0.0,0.0,0.0,0.0,0.0,0.0,0.0])
    psspy.scal_2(0,1,2,[i,1,0,1,0],[ (1+TEPdev[k])*Area5Avg, 358.66,0.0,-.0,0.0,-.0, 200.0])

    #Set machines in and out of services
    for i in range(len(generatorMaintenanceSchedule)):
        if(generatorMaintenanceSchedule[i][1] == (k+1)):
            machine = generatorMaintenanceSchedule[i][0]
            mStatus = generatorMaintenanceSchedule[i][2]

    psspy.machine_chng_2(machine,r""1""",[mStatus,_i,_i,_i,_i,_i],[_f,_f,_f,_f,_f,_f,_f,_f,_f,_f,_f,_f,_f,_f,_f])

```

```

    #Set branches in and out of service
    for i in range(len(HourlyStatus)):
        if(HourlyStatus[i][1] == (k+1)):
            fromBus = HourlyStatus[i][0][0]
            toBus = HourlyStatus[i][0][1]
            ID = HourlyStatus[i][0][2]
            branchStatus = HourlyStatus[i][2]

    psspy.branch_chng(fromBus,toBus,ID,[branchStatus,_i,_i,_i,_i],[_f,_f,_f,_f,_f,_f,_f,_f,_f,_f,_f,_f,_f,_f,_f])

```

```

###Perform economic dispatch
totalLoad = (1+PACWdev[k])*Area1Avg + (1+AESOdev[k])*Area2Avg + (1+TEPdev[k])*Area5Avg
psspy.ecdi(0,1,1,r""C:\Users\sfabus\Documents\Machine Learning Project\EXAMPLE PSSE System - Changing Power Flow\EXAMPLE\savnw.ecd""",0,[ 0.0,0.0])
psspy.ecdi(0,1,2,r""C:\Users\sfabus\Documents\Machine Learning Project\EXAMPLE PSSE System - Changing Power Flow\EXAMPLE\savnw.ecd""",0,[ 0.0,0.0])

```

```

psspy.ecdi(0,1,3,r"C:\Users\sfabus\Documents\Machine Learning Project\EXAMPLE PSSE System -
Changing Power Flow\EXAMPLE\savnw.ecd",0,[ totalLoad,0.0])
psspy.ecdi(0,1,4,r"C:\Users\sfabus\Documents\Machine Learning Project\EXAMPLE PSSE System -
Changing Power Flow\EXAMPLE\savnw.ecd",0,[ 0.0,0.0])
##perform OPF
psspy.nopf(0,1)
## solve power flow without Var limit
psspy.fdns([0,0,0,1,1,0,-1,0])
#psspy.save(r"C:\Users\sfabus\Documents\Machine Learning Project\EXAMPLE PSSE System -
Changing Power Flow\EXAMPLE\GeneratedCases\savnw_"" + ""Hour_"" + str(k+1) + ""_sav""")

##Solve power flow
# psspy.fdns([0,0,0,1,1,0,99,0])
#Check for convergence
ival = psspy.solved()
if(ival == 0):
    psspy.save(r"C:\Users\sfabus\Documents\Machine Learning Project\EXAMPLE PSSE System -
Changing Power Flow\EXAMPLE\GeneratedCases\savnw_"" + ""Hour_"" + str(k+1) + ""_sav""")
else:
    psspy.save(r"C:\Users\sfabus\Documents\Machine Learning Project\EXAMPLE PSSE System -
Changing Power Flow\EXAMPLE\UnconvergedGeneratedCases\savnw_"" + ""Hour_"" + str(k+1) +
""_sav""")

```

A.1.2 Python Scripts for 18-Bus System

A.1.2.1 Steady-State Saved Case Generation

#This script creates the saved cases for different generator outputs and load values at each time step in the Input_24hr_PV_GEN.csv file for the 18-bus systems.

#Currently only 5-minute data is used, even though the csv file has data for every 4 seconds.

```

import csv

#Import generation data
time_GEN = []
NORTH_G1 = []
WEST_G1 = []
SOUTH_G1 = []
EAST_G1 = []
EAST_PV = []
with open('Input_24hr_PV_GEN.csv', 'rb') as csvfile:
    spamreader = csv.reader(csvfile, delimiter=',', quotechar='|')
    rowCount = 0
    for row in spamreader:
        #Only get data every 5 minutes
        if(rowCount != 0 and (rowCount == 1 or ((rowCount-1)%75 == 0))):
            time_GEN.append(float(row[0]))
            NORTH_G1.append(float(row[1]))
            WEST_G1.append(float(row[2]))
            SOUTH_G1.append(float(row[3]))
            EAST_G1.append(float(row[4]))
            EAST_PV.append(float(row[5]))
            rowCount = rowCount + 1
#Import load data
time_LOADS = []
NORTH_02 = []
NORTH_03 = []
WEST_02 = []
WEST_03 = []

```



```

SOUTH_01_1 = []
SOUTH_01_2 = []
SOUTH_03 = []
EAST_01 = []
with open('Input_24hr_PV_LOADS.csv', 'rb') as csvfile:
    spamreader = csv.reader(csvfile, delimiter=',', quotechar='')
    rowCount = 0
    for row in spamreader:
        #Only get data every 5 minutes
        if(rowCount != 0 and (rowCount == 1 or ((rowCount-1)%75 == 0))):
            time_LOADS.append(float(row[0]))
            NORTH_02.append(float(row[1]))
            NORTH_03.append(float(row[2]))
            WEST_02.append(float(row[3]))
            WEST_03.append(float(row[4]))
            SOUTH_01_1.append(float(row[5]))
            SOUTH_01_2.append(float(row[6]))
            SOUTH_03.append(float(row[7]))
            EAST_01.append(float(row[8]))
            rowCount = rowCount + 1

#Based on base case PGen of NORTH_G1
NORTH_G1_H1_PERCENT = 159.6729/(159.6729 + 141.5969)
NORTH_G1_H2_PERCENT = 1 - NORTH_G1_H1_PERCENT

for i in range(12*24):
    #Load base case
    psspy.case(r"t3ps_v33_PV_time_00_00_bus111_2mach.sav")
    #Set generation
    psspy.machine_chng_2(101,r"H1",[_i,_i,_i,_i,_i],[
NORTH_G1[i]*NORTH_G1_H1_PERCENT,_f,_f,_f,_f,_f,_f,_f,_f,_f,_f,_f,_f,_f])
    NORTH_G1_H2 = NORTH_G1[i] - (NORTH_G1[i]*NORTH_G1_H1_PERCENT)
    print NORTH_G1[i]*NORTH_G1_H1_PERCENT
    psspy.machine_chng_2(101,r"H2",[_i,_i,_i,_i,_i],[
NORTH_G1_H2,_f,_f,_f,_f,_f,_f,_f,_f,_f,_f,_f,_f,_f])
    WEST_G1[i] = WEST_G1[i] - 70.0
    psspy.machine_chng_2(111,r"1",[_i,_i,_i,_i,_i],[
WEST_G1[i],_f,_f,_f,_f,_f,_f,_f,_f,_f,_f,_f,_f,_f])
    psspy.machine_chng_2(231,r"1",[_i,_i,_i,_i,_i],[
SOUTH_G1[i],_f,_f,_f,_f,_f,_f,_f,_f,_f,_f,_f,_f,_f])
    psspy.machine_chng_2(311,r"1",[_i,_i,_i,_i,_i],[
EAST_G1[i],_f,_f,_f,_f,_f,_f,_f,_f,_f,_f,_f,_f,_f])
    psspy.machine_chng_2(312,r"PV",[_i,_i,_i,_i,_i],[
EAST_PV[i],_f,_f,_f,_f,_f,_f,_f,_f,_f,_f,_f,_f,_f])
    #Set loads
    psspy.load_chng_4(2,r"1",[_i,_i,_i,_i,_i],[ NORTH_02[i],_f,_f,_f,_f])
    psspy.load_chng_4(3,r"1",[_i,_i,_i,_i,_i],[ NORTH_03[i],_f,_f,_f,_f])
    psspy.load_chng_4(12,r"1",[_i,_i,_i,_i,_i],[ WEST_02[i],_f,_f,_f,_f])
    psspy.load_chng_4(13,r"1",[_i,_i,_i,_i,_i],[ WEST_03[i],_f,_f,_f,_f])
    psspy.load_chng_4(21,r"1",[_i,_i,_i,_i,_i],[ SOUTH_01_1[i],_f,_f,_f,_f])
    psspy.load_chng_4(21,r"2",[_i,_i,_i,_i,_i],[ SOUTH_01_2[i],_f,_f,_f,_f])
    psspy.load_chng_4(23,r"1",[_i,_i,_i,_i,_i],[ SOUTH_03[i],_f,_f,_f,_f])
    psspy.load_chng_4(31,r"1",[_i,_i,_i,_i,_i],[ EAST_01[i],_f,_f,_f,_f])
    hour = i/12
    minutes = (i - (hour*12))*5
    #Solve power flow
    psspy.fdns([0,0,0,1,1,0,99,0])
    #Check for convergence and save to file
    ival = psspy.solved()

```

```

if(ival == 0):
    psspy.save(r""Generated Cases\t3ps_v33_PV_hour_"" + str(hour+1) + ""_min_"" + str(minutes) +
""_bus111_2mach.sav""")
else:
    psspy.save(r""UnconvergedGeneratedCases\t3ps_v33_PV_hour_"" + str(hour+1) + ""_min_"" +
str(minutes) + ""_bus111_2mach.sav""")

```

A.1.2.2 Frequency Stability Assessment Dynamic File Generation

This script creates individual dynamic files for each time step, based on input from the Input_24hr_PV_GEN_7Mach.csv file for the 18-bus system.
This file was created using the generator outputs from the previously generated saved cases for each time step.
Inertia is scaled linearly with generation output.

```
import csv
```

```
#Import generation data
```

```
time_GEN = []
```

```
total_GEN = []
```

```
with open('Input_24hr_PV_GEN_7Mach.csv', 'rb') as csvfile:
```

```
    spamreader = csv.reader(csvfile, delimiter=',', quotechar='|')
```

```
    rowCount = 0
```

```
    for row in spamreader:
```

```
        #Only get data every 5 minutes
```

```
        if(rowCount != 0):
```

```
            time_GEN.append(float(row[0]))
```

```
            total_GEN.append(float(row[9]))
```

```
            rowCount = rowCount + 1
```

```
max_GEN = max(total_GEN)
```

```
min_GEN = min(total_GEN)
```

```
Sid=-1 # All machines
```

```
Flag=1 # Only in-service machines at in-service plants
```

```
ierr, Nmach = psspy.amachcount(Sid, Flag) # get no of machines in the subsystem
```

```
ierr, iMbus = psspy.amachint(Sid, Flag, 'NUMBER') # get machine bus numbers
```

```
ierr, cMids = psspy.amachchar(Sid, Flag, 'ID') # get machine IDs
```

```
iMbus=iMbus[0]
```

```
cMids=cMids[0]
```

```
H=[]
```

```
D=[]
```

```
Mbase=[]
```

```
P=[]
```

```
Q=[]
```

```
psspy.dyre_new([1,1,1,1],r""C:\Users\sfabus\Documents\Machine Learning Project\18 Bus System from NREL\t3ps_PV_bus312_db1_bus111_2mach.dyr""", "", "", "")
```

```
#Get base inertia and machine parameters
```

```
for iM in range(0,(Nmach-1)): # iterate through the list of machines except for PV machine
```

```
    ibus = iMbus[iM]
```

```
    genId = cMids[iM]
```

```
ierr, busN = psspy.notona(ibus) # return the bus 18-character extended bus name for a specified bus number
```

```
    iH = 0 # resetting the inertia value index
```

```
    iD = 0 # resetting the speed damping value index
```

```
    ierr, icon0 = psspy.mdlind(ibus, genId, 'GEN', 'CON') # get initial CON address (index)
```

```
    ierr, genMdl = psspy.mdlnam(ibus, genId, 'GEN') # get generator model name
```

```
    print genMdl
```

```

genMdl = genMdl.strip()          # remove blanks
# Find absolute index iH in CONS array using relative CON index in the generator model and
# previously found starting CON index of the generator model
# (here shown only for the three most common models)
if genMdl=='GENCLS': iH=icon0
if (genMdl=='GENSAL'))(genMdl=='GENSAE'): iH=icon0+3
if (genMdl=='GENROU'))(genMdl=='GENROE'): iH=icon0+4
# Find absolute index iD in CONS array using relative CON index in the generator model and
# previously found starting CON index of the generator model
# (here shown only for the three most common models)
if genMdl=='GENCLS': iD=icon0+1
if (genMdl=='GENSAL'))(genMdl=='GENSAE'): iD=icon0+4
if (genMdl=='GENROU'))(genMdl=='GENROE'): iD=icon0+5
# Get value from CONS array corresponding to the generator inertia
H.append(psspy.dsval('CON', iH)[1])
D.append(psspy.dsval('CON', iD)[1])
# Get MBASE value
MBASE.append(psspy.macdat(ibus, genId, 'MBASE')[1])
P.append(psspy.macdat(ibus, genId, 'P')[1])
Q.append(psspy.macdat(ibus, genId, 'Q')[1])

#Change inertia of each machine based on total generation at each time step
slope = (1-0.2)/(max_GEN-min_GEN)
intercept = 1-(max_GEN*slope)
inertiaScaleFactor = 1
inertias = []
for i in range(12*24):
    #Load base dynamic case each time so all inertia levels are set to base value
    psspy.dyre_new([1,1,1,1],r"C:\Users\sfabus\Documents\Machine Learning Project\18 Bus System from
NREL\t3ps_PV_bus312_db1_bus111_2mach.dyr","", "", "")
    # Linear equation was derived by using (0.2, min total gen over 24-hour period) and (1, max total gen over
24-hour period)
    # Throughout the 24-hour period inertia is scaled between 0.2-1 times the base inertia value
    inertiaScaleFactor = slope*total_GEN[i]+intercept
    for iM in range(0,(Nmach-1)):
        print "-----"
        print H[iM]
        # flag = 1
        ibus = iMbus[iM]
        genId = cMids[iM]
        ierr,busN = psspy.notona(ibus) # return the bus 18-character extended bus name for a specified bus
number
        iH = 0 # resetting the inertia value index
        iD = 0 # resetting the speed damping value index
        ierr, icon0 = psspy.mdlind(ibus, genId, 'GEN', 'CON') # get initial CON address (index)
        ierr, genMdl = psspy.mdlnam(ibus, genId, 'GEN') # get generator model name
        print genMdl
        genMdl = genMdl.strip()          # remove blanks
        # Find absolute index iH in CONS array using relative CON index in the generator model and
        # previously found starting CON index of the generator model
        # (here shown only for the three most common models)
        if genMdl=='GENCLS': iH=icon0
        if (genMdl=='GENSAL'))(genMdl=='GENSAE'): iH=icon0+3
        if (genMdl=='GENROU'))(genMdl=='GENROE'): iH=icon0+4
        # Find absolute index iD in CONS array using relative CON index in the generator model and
        # previously found starting CON index of the generator model
        # (here shown only for the three most common models)
        if genMdl=='GENCLS': iD=icon0+1
        if (genMdl=='GENSAL'))(genMdl=='GENSAE'): iD=icon0+4

```

```

if (genMdl=='GENROU')|(genMdl=='GENROE'): iD=icon0+5
# Check the generator output
if ((P[iM]<999999999)&(P[iM]>-999999999))&((Q[iM]<999999999)&(Q[iM]>-999999999)):
print '*** A zero output generator is found.***'
print(ibus)
print(genId)
if genMdl=='GENCLS':
ibus
genId
ierr = psspy.change_con(iH, H[iM]*inertiaScaleFactor)
print(ibus)
print(genId)
print(iH)
print(H[iM]/10)
print '*** End ***'
if (genMdl=='GENSAL')|(genMdl=='GENSAE'):
ibus
genId
ierr = psspy.change_con(iH, H[iM]*inertiaScaleFactor)
print(ibus)
print(genId)
print(iH)
print(H[iM]/10)
print '*** End ***'
if (genMdl=='GENROU')|(genMdl=='GENROE'):
ibus
genId
ierr = psspy.change_con(iH, H[iM]*inertiaScaleFactor)
print(ibus)
print(genId)
print(iH)
print(H[iM]/10)
print '*** End ***'
hour = i/12
minutes = (i - (hour*12))*5
psspy.dyda(0,1,[2,1,1],0,r"C:\Users\sfabus\Documents\Machine Learning Project\18 Bus System from
NREL\Frequency Stability\Dynamic Cases\t3ps_PV_bus312_db1_hour_"" + str(hour+1) + ""_min_"" +
str(minutes) + ""_bus111_2mach.dyr""")
inertias.append(inertiaScaleFactor)
print inertias

```

A.1.2.3 Frequency Stability Assessment Generation Trip Batch Simulations

This script takes each converted saved case file and dynamic file (with scaled inertia) at each time period.
A generation trip is performed at each time step, with the same amount of generation (70 MW) tripped each time.

#Load base cases

```

ierr = psspy.case("C:\Users\sfabus\Documents\Machine Learning Project\18 Bus System from
NREL\t3ps_v33_PV_time_00_00_bus111_2mach.sav")
psspy.dyre_new([1,1,1],r"C:\Users\sfabus\Documents\Machine Learning Project\18 Bus System from
NREL\t3ps_PV_bus312_db1_bus111_2mach.dyr","","")

```

Generator Bus Number - MachBus

```
ierr, MachBus = psspy.amachint(-1, 1, 'NUMBER')
```

Generator ID - MachID

```
ierr2, MachID = psspy.amachchar(-1, 1, 'ID')
```

```
psspy.dynamics_solution_param_2([50,_i,_i,_i,_i,_i,_i],[_f,_f, 0.004,_f,_f,_f,_f])
```

```

psspy.bsys(0,0,[ 0.12, 999.],0,[],len(MachBus[0]),MachBus[0],0,[],0,[])

#Monitor machine speed deviation
psspy.chsb(0,0,[-1,-1,-1,1,7,0]);
psspy.set_chnfil_type(0)

#Convert loads and generators in saved cases
for i in range(12*24):
    hour = i/12
    minutes = (i - (hour*12))*5
    #Load saved case for each time
    ierr = psspy.case(r""t3ps_v33_PV_hour_""+str(hour+1)+""_min_""
+str(minutes)+""_bus111_2mach.sav""")
    psspy.cong(0)
    psspy.conl(0,1,1,[0,0],[0.0,0.0,0.0,0.0])
    psspy.conl(0,1,2,[0,0],[0.0,0.0,0.0,0.0])
    psspy.conl(0,1,3,[0,0],[0.0,0.0,0.0,0.0])
    psspy.save(r""C:\Users\sfabus\Documents\Machine Learning Project\18 Bus System from
NREL\Converted Saved Case
Files\t3ps_v33_PV_hour_""+str(hour+1)+""_min_""+str(minutes)+""_bus111_2mach_conv.sav""")

#Trip generation for each case at each time step
for i in range(12*24):
    hour = i/12
    minutes = (i - (hour*12))*5
    #Load converted file
    ierr = psspy.case(r""C:\Users\sfabus\Documents\Machine Learning Project\18 Bus System from
NREL\Converted Saved Case
Files\t3ps_v33_PV_hour_""+str(hour+1)+""_min_""+str(minutes)+""_bus111_2mach_conv.sav""")
    #Load dynamic file
    psspy.dyre_new([1,1,1,1],r""C:\Users\sfabus\Documents\Machine Learning Project\18 Bus System from
NREL\Frequency Stability\Dynamic Cases\t3ps_PV_bus312_db1_hour_"" + str(hour+1) + ""_min_"" +
str(minutes) + ""_bus111_2mach.dyr"" , , , ,)
    if((hour+1) < 10):
        if(minutes < 10):
            psspy.strt(1,r""C:\Users\sfabus\Documents\Machine Learning Project\18 Bus System from
NREL\Frequency Stability\Output Files\t3ps_v33_PV_hour_0"" + str(hour+1) + ""_min_0"" + str(minutes)
+""_bus111_2mach_Trip70MW.out""")
        else:
            psspy.strt(1,r""C:\Users\sfabus\Documents\Machine Learning Project\18 Bus System from
NREL\Frequency Stability\Output Files\t3ps_v33_PV_hour_0"" + str(hour+1) + ""_min_"" + str(minutes)
+""_bus111_2mach_Trip70MW.out""")
        else:
            if(minutes < 10):
                psspy.strt(1,r""C:\Users\sfabus\Documents\Machine Learning Project\18 Bus System from
NREL\Frequency Stability\Output Files\t3ps_v33_PV_hour_"" + str(hour+1) + ""_min_0"" + str(minutes)
+""_bus111_2mach_Trip70MW.out""")
            else:
                psspy.strt(1,r""C:\Users\sfabus\Documents\Machine Learning Project\18 Bus System from
NREL\Frequency Stability\Output Files\t3ps_v33_PV_hour_"" + str(hour+1) + ""_min_"" + str(minutes)
+""_bus111_2mach_Trip70MW.out""")
    psspy.run(0,1,0,1,1)
    #Trip 70 MW of generation
    psspy.dist_machine_trip(111,2)
    psspy.run(0,20.0,0,1,1)

```

A.1.2.4 Transient Stability Assessment 3-Phase Fault Batch Simulations

This script loads each converted saved case file at each time period and the base dynamic file.
A 3-phase fault is performed on the same branch at each time step. Clearing times are adjusted, and results are saved to individual files.

```
#Load base cases
ierr = psspy.case("C:\Users\sfabus\Documents\Machine Learning Project\18 Bus System from
NREL\Transient Stability\t3ps_v33_PV_hour_1_min_0_bus111_2mach.sav")
psspy.dyre_new([1,1,1,1],r"C:\Users\sfabus\Documents\Machine Learning Project\18 Bus System from
NREL\Transient Stability\t3ps_PV_bus312_db1_bus111_2mach.dyr","","")

# Generator Bus Number - MachBus
ierr, MachBus = psspy.amachint(-1, 1, 'NUMBER')
# Generator ID - MachID
ierr2, MachID = psspy.amachchar(-1, 1, 'ID')

psspy.dynamics_solution_param_2([50, _i, _i, _i, _i, _i, _i],[_f, _f, 0.004, _f, _f, _f, _f])
psspy.bsys(0,0,[ 0.12, 999.],0,[],len(MachBus[0]),MachBus[0],0,[],0,[])

#Monitor machine rotor angle
psspy.chsb(0,0,[-1,-1,-1,1,0]);
psspy.set_chnfil_type(0)

clearingTimes =
[0.096,0.098,0.100,0.120,0.140,0.160,0.180,0.200,0.220,0.240,0.260,0.280,0.300,0.320,0.340,0.360,0.380,
0.400,0.420,0.440,0.460,0.480,0.500,0.520,0.540,0.560,0.580,0.600,0.620,0.640,0.660,0.680,0.700]

for i in range(12*24):
    hour = i/12
    minutes = (i - (hour*12))*5
    #Load converted file
    ierr = psspy.case(r"C:\Users\sfabus\Documents\Machine Learning Project\18 Bus System from
NREL\Transient
Stability\t3ps_v33_PV_hour_""+str(hour+1)+""_min_""+str(minutes)+""_bus111_2mach_conv.sav")
    #Load dynamic file
    psspy.dyre_new([1,1,1,1],r"C:\Users\sfabus\Documents\Machine Learning Project\18 Bus System from
NREL\Transient Stability\t3ps_PV_bus312_db1_bus111_2mach.dyr","","")
    for j in range(len(clearingTimes)):
        clearingTimeName = str(clearingTimes[j])
        if(clearingTimes[j] == 0.5 or clearingTimes[j] == 0.6 or clearingTimes[j] == 0.7):
            clearingTimeName = clearingTimeName + '00'
        else:
            clearingTimeName = clearingTimeName + '0'
        if((hour+1) < 10):
            if(minutes < 10):
                psspy.str(1,r""t3ps_v33_PV_hour_0"" + str(hour+1) + ""_min_0"" + str(minutes)
+ ""_bus111_2mach_Fault_CT_0_"" +clearingTimeName[2:5]+ ""_out""")
            else:
                psspy.str(1,r""t3ps_v33_PV_hour_0"" + str(hour+1) + ""_min_"" + str(minutes)
+ ""_bus111_2mach_Fault_CT_0_"" +clearingTimeName[2:5]+ ""_out""")
            else:
                if(minutes < 10):
                    psspy.str(1,r""t3ps_v33_PV_hour_"" + str(hour+1) + ""_min_0"" + str(minutes)
+ ""_bus111_2mach_Fault_CT_0_"" +clearingTimeName[2:5]+ ""_out""")
                else:
                    psspy.str(1,r""t3ps_v33_PV_hour_"" + str(hour+1) + ""_min_"" + str(minutes)
+ ""_bus111_2mach_Fault_CT_0_"" +clearingTimeName[2:5]+ ""_out""")
    psspy.run(0,1,0,1,1)
```

```
#Apply 3-phase fault
psspy.dist_branch_fault(21,32,'1',1,0.0,[0.0,-2.0E11]) # apply fault
psspy.run(1,1+clearingTimes[j],0,1,1)
psspy.dist_clear_fault(1) # clear fault after specified clearing time
psspy.run(0, 20.0,0,1,1)
```

A.2 Power Plant and Machine Modeling Consideration for PREPA Transmission Model

In the developed base case model, each generation plant was modeled as a separate machine with its rated real power output set as each plant's capacity. For example, the Aguirre Power Complex has a gas turbine plant, steam turbine plant, and a combined cycle plant. The three plants were modeled as three individual machines connected to one bus. The same process was followed for the Costa Sur steam and turbine plants and the San Juan steam and combined cycle plants, with two machines at each location connected to a single bus. Palo Seco also has two machines at a single bus, one steam and the other combustion-turbine. All other plants were modeled as a single machine connected to a single bus. (If necessary for specific studies, further modifications could be made to show individual units at each plant and their capacities.)

A.3 Development of High PV Models of PREPA System Using 2019 Day-Peak Model

The PREPA 2019 day-peak model, provided by DOE, contains 1,237 buses, including transmission and distribution levels. In this model, there are 133 total machines, with 62 of the machines online.

The purpose of the study was to analyze system dynamic frequency response, after a set contingency, when non-renewable machines in the system are replaced with solar. First, generator models for each machine specified in the dynamics (.dyr) file, were used to determine whether or not a machine was renewable or non-renewable. During this study, the real power output of online machines was used to calculate the percentage of renewable machine output to total generation output. The total real power output of all online machines is approximately 2,698.43 MW, and the total capacity of online machines is 13,973.46 MW. In the base case, the percentage of renewable machine output to total online generation was calculated to be approximately 15%, with the real power output of renewable machines totaling 408.19 MW. At each penetration level studied including the base case, a machine at San Juan Steam Plant, outputting 80 MW, was tripped. In each scenario, the speed deviation of all machines in the system was monitored and converted to frequency. The frequency response of tripping 80 MW in the base case, is shown in Figure A.1.

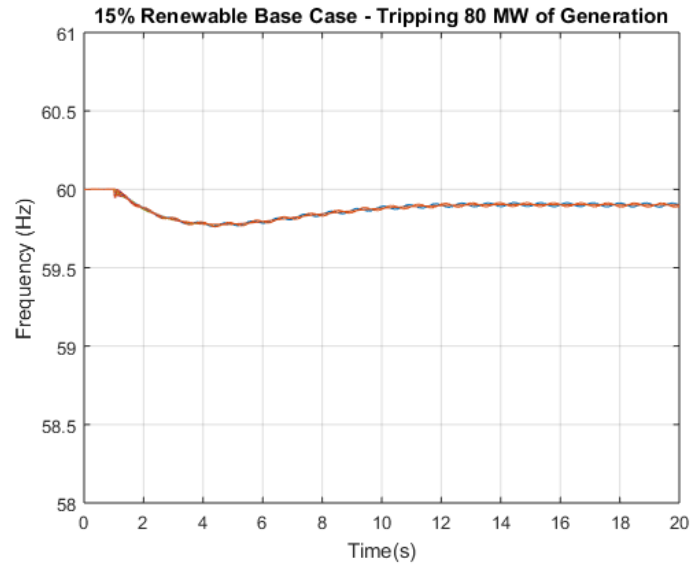


Figure A.1. Frequency response of tripping 80 MW of generation in 15% renewable case

Simulations of this contingency were also performed at the 30%, 50%, 70%, 80%, and 90% renewable penetration levels. Table A.1 contains the online non-renewable machines, including their bus number, bus name, ID, and real power output. To obtain certain levels of renewable penetration, combinations of machines listed in Table A.1 were replaced with solar machines. To do this, the machine's generator model, governor model, and exciter models were deleted in the dynamic file. The generator model was then replaced with the GEPVG model, and the exciter model was replaced with the GEPVE model. The parameters for the GEPVG model are included in Table 3.9. The PRATE parameter, or rated power the generator, varied depending on the capacity of the individual machine. Typical parameters for the GEPVE model are included in Table 3.10.

The renewable penetration levels studied include 30%, 50%, 70%, 80%, and 90% of online renewable machine output to system total generation output. After the dynamic models of the substituted machines were modified for each penetration case, dynamic simulations were performed. For each penetration level, the system frequency response while tripping 80 MW of generation is plotted (Figure A.2- Figure A.8). As solar penetration increases, the frequency nadir, or minimum post-contingency frequency, decreases, and it takes the system frequency a longer time to settle.

Once the renewable penetration level reached 80%, the UFLT relays in the system began to actuate. Further explanation about the UFLT relay settings and operation is provided in Section 3.1.4. With line relays included in the model for the 80% renewable case, the frequency sharply increases after reaching approximately 58.5 Hz, rises to about 60.3 Hz, and then begins to decrease and settle. The rise in frequency above 60 Hz is due to several load buses islanded, as a result of under-frequency line trips, without any in-service machines. Without line relays in the model, the frequency response is smoother and more closely follows the shape of the 70% case but with lower frequency nadir.

Line relays also trip in the 90% renewable case. Comparing Figure A.7 to Figure A.5, the frequency initially dropped at a faster rate than the 80% case. Frequency also increased at a faster rate after reaching a frequency nadir of about 58.5 Hz.

When removing line relays, the frequency of the 90% case continued to drop. This is because several machines dropped off of the system due to their under-frequency protection trip settings.

Table A.1. Online non-renewable machines

Bus Number	Bus Name	ID	PGen (MW)
805	C.S.5 23.000	1	250
806	C.S.6 23.000	1	250
809	AG.1 24.000	1	230.5284
810	AG.2 23.000	1	230
819	P.SECO3 20.000	1	170
820	P.SECO4 20.000	1	170
871	AES 1 21.000	1	166
872	AES 2 21.000	1	166
856	SJREPG1 13.800	1	139.5
860	ECOSTEAM 17.100	1	98
858	ECOGT1 17.100	1	88
859	ECOGT2 17.100	1	88
813	SANJUAN7 13.800	1	80
814	SANJUAN8 13.800	1	80
811	SJREPST1 13.800	1	56

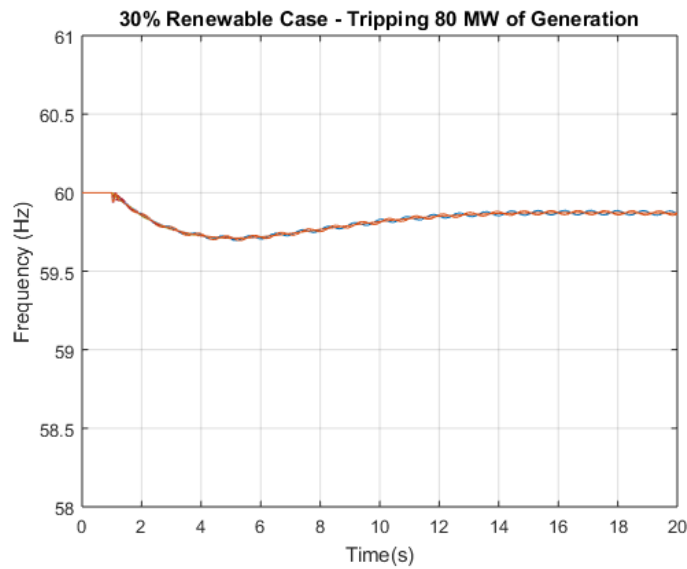


Figure A.2. Frequency response of tripping 80 MW of generation in 30% renewable case

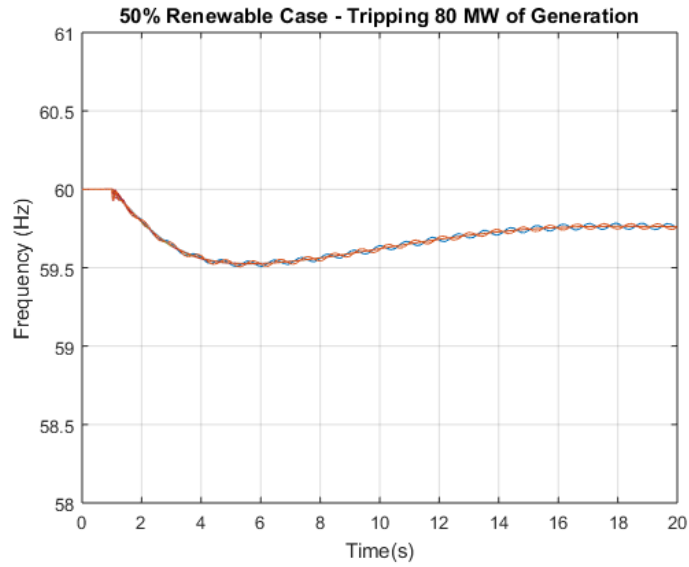


Figure A.3. Frequency response of tripping 80 MW of generation in 50% renewable case

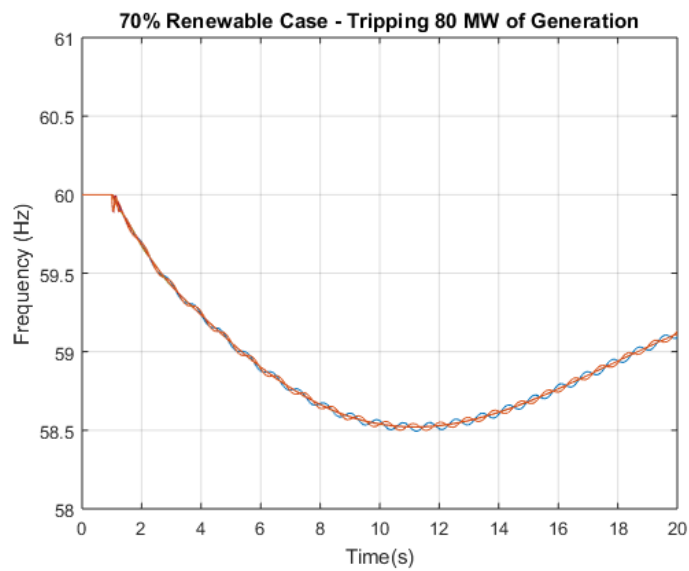


Figure A.4. Frequency response of tripping 80 MW of generation in 70% renewable case

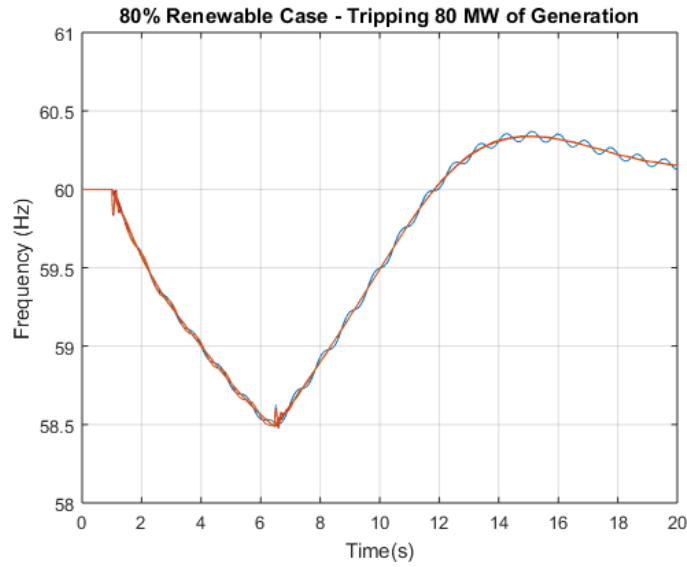


Figure A.5. Frequency response of tripping 80 MW of generation in 80% renewable case

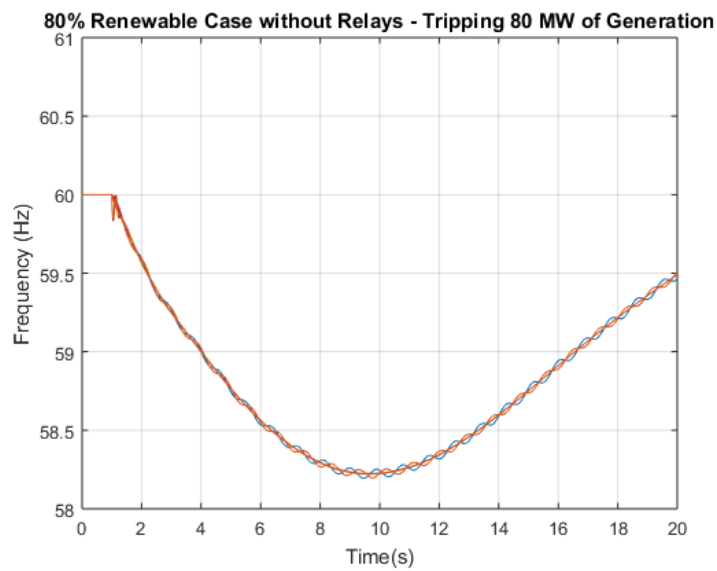


Figure A.6. Frequency response of tripping 80 MW of generation in 80% renewable case without relays included

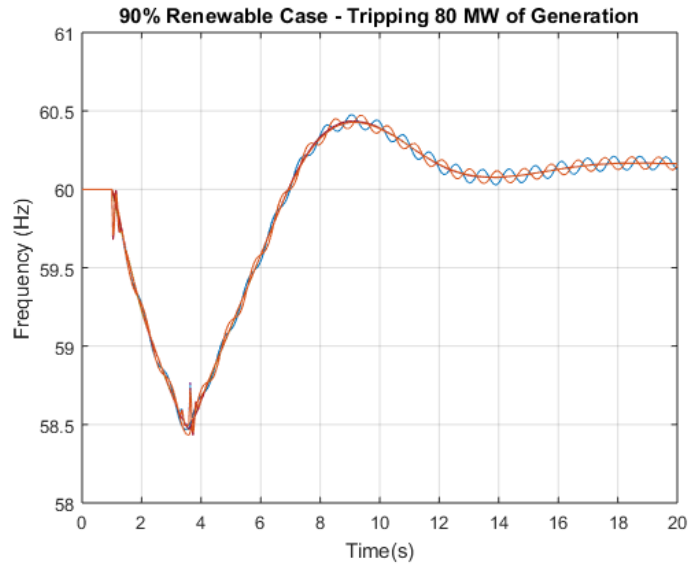


Figure A.7. Frequency response of tripping 80 MW of generation in 90% renewable case

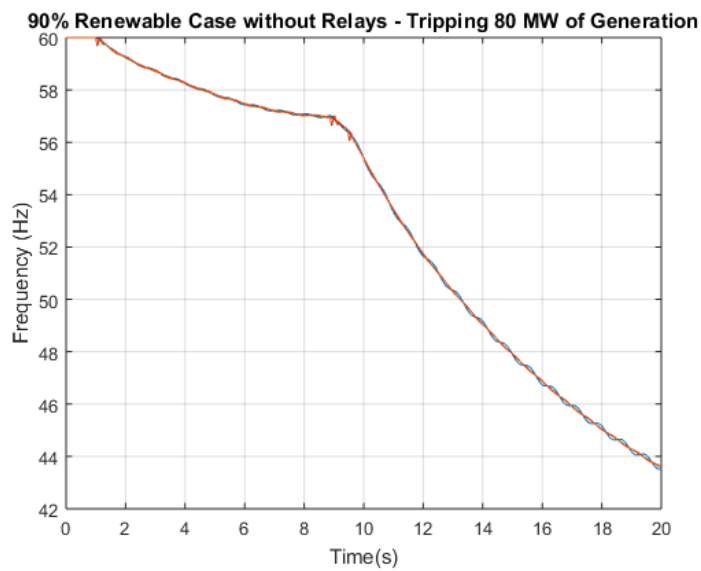


Figure A.8. Frequency response of tripping 80 MW of generation in 90% renewable case without relays included

A.4 How to Use the PGST Tool

This section describes how to use Dr. Pan's PGST tool for mapping PSS®E-developed models. This tool involves using PSSE_Data_Interface software to import PSS®E system data and export this data into text files the PSGT can read.

1. Open the PSSE_Data_Interface software. A screenshot of the software interface can be seen in Figure A.9.
2. Select the "Open raw" button, and locate your PSS®E raw file. After the file has been opened, hit "Export." These options are indicated in Figure A.10. Several text files will be generated: area, branch, bus, load transformer, and zone.
3. Open the PGST software. Click "File" -> "New" to create a new PSSE_Interface file. Select "Bus" -> "Load" and then the "bus.txt" document generated by the PSSE_Data_Interface software. Buses should be clustered in a configuration similar to Figure A.11.
4. Import branch data by selecting "Branch" -> "Load" and then the "branch.txt" file generated by the PSSE_Data_Interface software. Branches can now be seen connecting the buses in the PSSE_Interface file, such as the system seen in Figure A.12.
5. To load GPS data, create two text files: "bus_location.txt" and "bus_sub.txt." The "bus_sub.txt" file should contain all of the buses in the system pasted into a column twice with no header. The "bus_location.txt" file should contain the GPS coordinates, one column for latitude and another for longitude, with coordinates given in decimal degrees. There should be no headers in the file, and the order of the coordinate pairs should follow the order of the buses as they are listed in the "bus_sub.txt" file.
6. In PSGT, click "Bus" -> "Load Sub-Bus GPS" to import the "bus_location.txt" and "bus_sub.txt" files. Once GPS data has been added, buses should be spread out according to their location data. The previous example with GPS coordinates included is shown in Figure A.13.
7. The map can also be color-coded based on voltage level, area, and zone. This can be done by going to "View" -> "Color Mode" and then selecting one of the color level options.

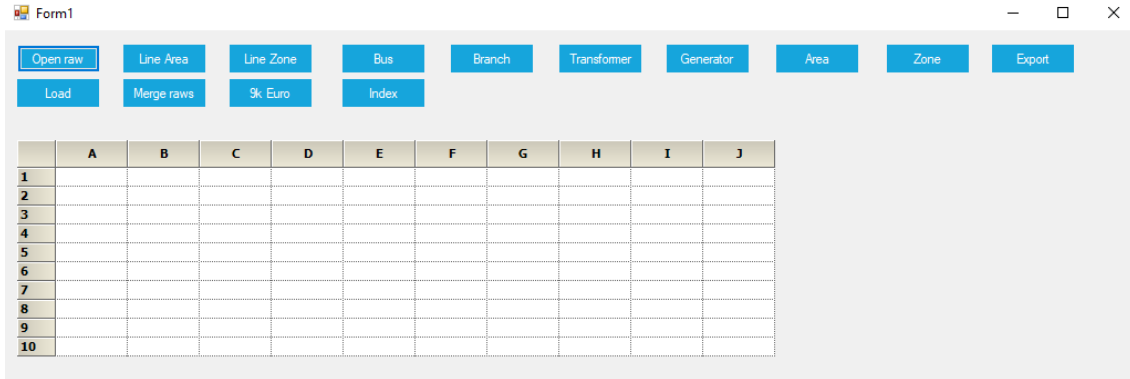


Figure A.9. PSSE_Data_Interface software user interface

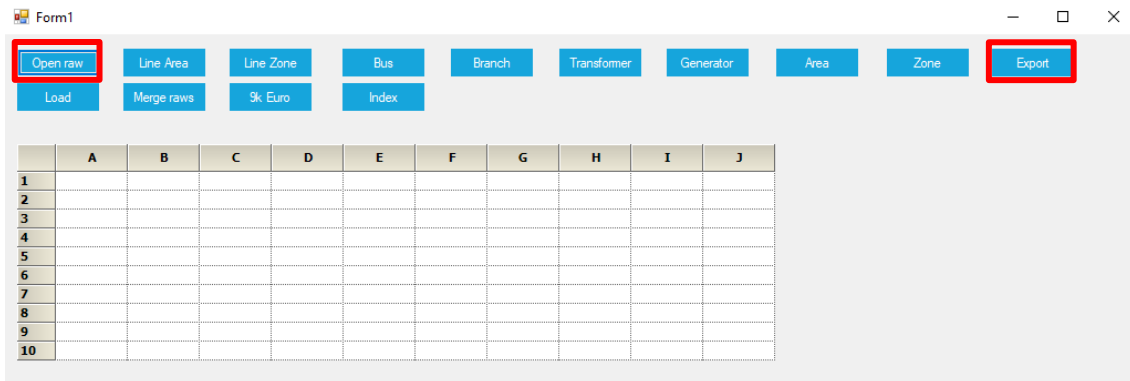


Figure A.10. PSSE_Data_Interface software user interface with PSS®E raw file import buttons highlighted

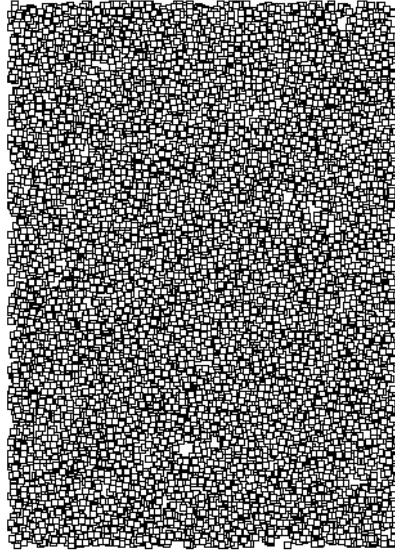


Figure A.11. Example of PSS@E model bus data imported into PSGT software

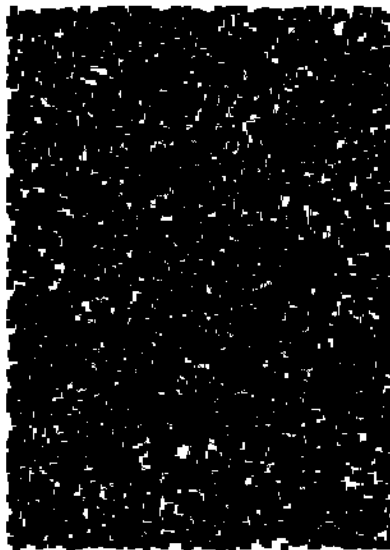


Figure A.12. Example of PSS@E model bus and branch data imported into PSGT software



Figure A.13. Example of PSS®E model imported into PSGT software with bus, branch, and GPS data

VITA

Summer Fabus is originally from Johnson City, Tennessee where she attended Science Hill High School. She graduated with a Master of Science in Electrical Engineering and Master of Business Administration from University of Tennessee Knoxville in May 2019. Previously, she obtained a Bachelor of Science in Electrical Engineering from University of Tennessee Knoxville in May 2017. As a graduate student, she worked under Dr. Yilu Liu in a group focused on power grid modeling and monitoring. Throughout her education, Summer acquired experience in many areas of the power industry including transmission, distribution, product development, and technical research at the CURENT (Center for Ultra-Wide-Area Resilient Electric Energy Transmission Networks). The companies she interned with include Tennessee Valley Authority (TVA), Eaton Corporation, and BrightRidge utility. After completing her master's degrees, Summer began working at Electric Power Research Institute (EPRI) as part of the Distributed Energy Resources (DER) team.